Université d'Ottawa · University of Ottawa

À Pop,

pour toutes les fois que tu m'as dit que j'avais la tête dure,

en voici les résultats!

À ma belle maman et à mon 'tit frère.

We will be known forever by the tracks we leave.

— *Native American Dakota Tribe*

Abstract

Non-steroidal anti-inflammatory drug (NSAID) photo-induced DNA damage in human peripheral blood mononuclear cells measured using the alkaline comet assay is presented. Whereas Tiaprofenic Acid photo-induced DNA damage is promptly produced (*i.e.,* observed at low radiation doses), Ketoprofen (KP) photo-induced DNA damage is delayed (observed at relatively higher radiation doses). This prompt and delayed effect is observed with UVA (320-400 nm), UVB (290-320 nm) and solar simulated radiation and is attributed to the NSAIDs' different photochemical properties. The results from these experiments mark the first account of NSAID photo-induced DNA damage in living cells. The neutral version of the comet assay, carried out using HL60 cells, revealed that KP photo-induced DNA damage did not lead to apoptosis, indicating that HL60 cells can sustain and possibly recover from this damage.

A new technique for measuring DNA damage based on the time-resolved fluorescence decay measurements of PicoGreen®-DNA complexes is also presented. PicoGreen® exhibits a longer fluorescence lifetime when complexed to double-stranded DNA compared single-stranded DNA. This discovery allows for the quantification of single-stranded DNA in a given sample. This technique, which also incorporates key concepts such as alkaline unwinding buffers and higher unwinding rates of damaged DNA compared to non-damaged DNA, was able to reproducibly measure and differentiate DNA damage from 0-100 Gray of gamma radiation. The results presented include experiments carried out using CT-DNA as well as DNA isolated from sheep white blood cells, suggesting its potential use with isolated DNA from any eukaryotic cell.

Acknowledgments

There are many people who are responsible for making this thesis become a reality for me. Few words can express how grateful I am to you Tito, for believing in me at a time when I thought no one else did and for giving me the opportunity to experience scientific research without borders. I thank you from the bottom of my heart and I hope I haven't disappointed you. And to Elda, thank you for always making me feel at home and an important part of your extended (chemistry) family.

I would like to extend my sincere gratitude to everyone at Health Canada for taking me in and showing me the ropes from a biologist's point of view, for putting up with my incessant questions and for giving me your time throughout my research. I am ever so grateful to have had the opportunity to work alongside Dr. Jack McLean. My heartfelt appreciation goes out to you for always being so optimistic, for your endless stream of new and exciting ideas and for all our fascinating and entertaining conversations. I am indebted to Dr. James McNamee and Pascale Bellier for sharing with me their knowledge as well as their ideas which were real driving forces behind the success of this project. I would also like to thank Dr. Diana Wilkinson for introducing me to sterile molecular biology techniques and for being there for my first successful 'baby' crop; Catherine Ferrarrotto for her vampire expertise; Dr. Pascale Reinhardt-Poulin and Michelle Cybulski for all their help with the solar simulator; Luc Periard for helping me again and again with the cell scoring which by far, has got to be the most boring task on the planet; Dr. Ruth Wilkins, Barb Kutzner and Susan Miller for all your help and support. A sincere thanks to all you guys at Health Canada for truly making this a memorable experience.

I want to thank Dr. Gonzalo Cosa for pushing me as hard as I pushed him to make our project finally work, for being my trusted sounding board over the years as well as a wonderful friend. With the endless renewal of the Spanish connection within the group, I was fortunate enough to make the acquaintance of two striking individuals, Dr. Carolina Aliaga and Dr. Alexis Aspée, who made the last stretch of my graduate career particularly enjoyable. Many thanks go to past members of the group, including Dr. Salvo Sortino for all his practical advice on NSAIDs; Dr. Fausto Ortica who is a true icon of determination; Dr. Tanya Hancock-Chen, my office mate, for all the great conversation topics and for providing me with an infinite amount of kindness and babies! and Annie Shaw, the infamous third musketeer, who was a tireless source of treasured entertainment. My thanks are also extended to other members of the group, past and present, who have contributed to my graduate life in some way, shape or form. Special thanks go out to Betty Yakimenko, Cheryl Cole and Anita Bouwman for their relentless patience and good humor as well as André Simard and Gerry Charette for their expertise; thank you all for making things run as smooth as can be.

Good friends are hard to come by and I was lucky enough to form many special friendships over these past few years; thanks to Dr. Helen Clark & Ian Clapp, Nicole Crutcher & Gyro Inman, you all hold a very special place in my heart. My heartfelt thanks go out to Dr. Pat Forgione (Fat-Ass) who has never tired of being at the butt of my jokes (yes, even here!) and for being a true friend. I am tremendously thankful for Dr. Christopher Coenjarts who has provided me with nothing but fun and laughter from the first day I met him. I am forever grateful for his generous supply of patience, help and guidance right from the start; only he truly knows how much of an accomplishment this is for me, thanks Mister.

Mom et Richard Jr., le support et l'encouragement que vous m'avez démontré pendant toutes mes études m'ont donné le courage et la force de persévérer jusqu'au bout. Je vous admire pour votre patience et votre force d'esprit, merci infiniment. Oui! J'ai finallement fini!!!

Table of Contents

Chapter 4

Chapter 5

List of Figures

List of Schemes

List of Tables

List of Equations

List of Abbreviations

ALS	alkali labile sites
BER	base excision repair
°C	Celcius degree
cm^2	square centimeter
CO_2	carbon dioxide
COX_1	cyclooxygenase isoenzyme 1
COX_2	cyclooxygenase isoenzyme 2
CT-DNA	calf thymus DNA
ddH_2O	distilled deionized water (18 MΩ)
DMSO	dimethyl sulfoxide
DNA	deoxyribonucleic acid
DSB	double-strand break
dsDNA	double-stranded DNA
ε	extinction coefficient
E	energy
EDTA	sodium tetra ethylene diamine tetraacetic acid
EtBr	ethidium bromide
FAPy-G	2,6-diamino-5-formamido-4-hydroxypyrimidine
FC	footcandle
FCS	fetal calf serum
γ radiation	gamma radiation
g/dL	gram per deciliter

g/mL	gram per milliliter
Gy	Gray (γ radiation), equivalent to one joule per kilogram
Gy/min	Gray per minute
h	hour
H•	hydrogen atom
H_2O_2	hydrogen peroxide
HBSS	Hanks balanced salt solution
HL60	human promyelocytic leukemia cell line
hν	photon
HO•	hydroxyl radical
HO^-	hydroxide anion
HO_2•	perhydroxyl radical
ISC	intersystem crossing
kJ/mol	kilojoule per mole
KP	Ketoprofen
LMP	low melting point (agarose)
LOOH	lipid hydroperoxide
μg	microgram
μg/mL	microgram per milliliter
μL	microliter
μM	micromolar
μs	microsecond
mA	milliampere
MED	minimal erythemal dose

mg/mL	milligram per milliliter
mJ	millijoule
mJ/cm^2	dose
mL	milliliter
M^{-1}·cm^{-1}	per molar per centimeter
mm	millimeter
mW/cm^2	dose rate
n	non-bonding molecular orbital
NaCl	sodium chloride
NaOH	sodium hydroxide
NER	nucleobase excision repair
nm	nanometer
ns	nanosecond
NSAID	non-steroidal anti-inflammatory drug
O_2^{-2}	peroxide anion
$O_2^{\bullet-}$	superoxide radical anion
$^1O_2$	singlet oxygen
8-oxoG	7,8-dihydro-8-oxoguanine
π	π bonding molecular orbital
π^*	π anti-bonding molecular orbital
PBMC	peripheral blood mononuclear cells
PBS	phosphate buffered saline
PER	photoenzymatic repair
pg	picogram

PG	PicoGreen® (nucleic acid dye)
ps	picosecond
R•	alkyl radical
RBC	red blood cell
RH	alkyl with abstractable hydrogen atoms
RO•	alkoxyl radical
RO•⁻	alkyl radical anion
ROO•	alkyl peroxyl radical
ROOH	alkyl peroxide
ROS	reactive oxygen species
rpm	revolution per minute
S_1	lowest singlet excited state
SCGE	single cell gel electrophoresis
SDS	sodium dodecyl sulfate
SLS	sodium lauryl sarcosine
SSB	single-strand break
ssDNA	single-stranded DNA
SSR	solar simulated radiation
T_1	lowest triplet excited state
τ	lifetime
TAE buffer 10X	0.4 M Tris acetate, 0.2 M glacial acetic acid, 0.1 M EDTA, pH 8.4
TP	Tiaprofenic Acid
Tris base	trishydroxymethylaminomethane
Triton X-100	iso-octylphenoxypolyethoxyethanol

UVA	ultraviolet A (320-400 nm)
UVB	ultraviolet B (290-320 nm)
UVC	ultraviolet C (200-290 nm)
V/cm	voltage (volt per centimeter)
Vis	visible light (400-700 nm)
W	watt
WB	whole blood
WBC	white blood cell

Chapter 1

Introduction

DNA is the blueprint of life. It encodes all the vital genetic information necessary for the development of an organism by commanding the incredible design and engineering of the simple cell. DNA has fascinated scientists all over the world for more than a century and in less than 50 years from the discovery of its double helical structure by James Watson and Francis Crick in 1953, the complete human genome was ultimately decoded.[1,2] The few billion nucleotides (3×10^9) that compose more than the 1 meter of DNA, contained in a typical animal cell, fits inside the cell nucleus that is no more than 6 μm in diameter.[3] DNA nucleotides as well as their numbering are shown in Figure 1.1.

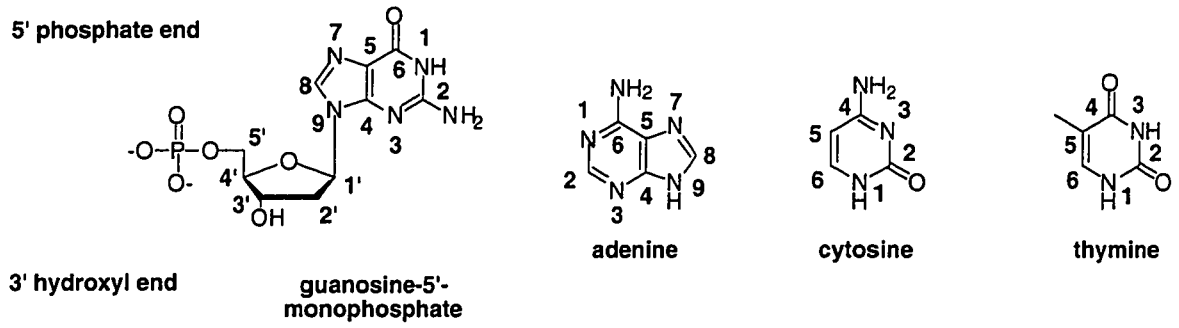

Figure 1.1: Numbering of nucleobases and nucleotides; sugar atoms bear primes (*i.e.*, 2'), heterocyclic atoms are unprimed and exocyclic atoms bear superscripted numbers (*i.e.*, N^6) (refer to text).

DNA remains unchanged throughout the life of an organism unless it becomes damaged in some way. Approximately 10 000 measurable DNA modification events occur in 1 hour (or *ca.* 7×10^7/year) in each mammalian cell due to intrinsic causes which include depurination, depyrimidination, deamination, single-strand breaks (SSBs), double-strand breaks (DSBs), base modification and protein-DNA crosslinks.[4] These events are caused by metabolic processes which lead to free radicals such as hydroxyl radicals (HO•), peroxides and other reactive oxygen species (ROS).[4] Other external forces such as UV radiation (200-400 nm), photosensitizers and free radical species can

also cause DNA damage. Following exposure to radiation, most cultured cells have the ability to rapidly rejoin the DNA strand breaks which are produced.[5] Dividing and non-dividing cells can also repair DNA stand breaks rapidly.[6]

Two techniques for detecting and quantifying DNA damage will be presented. Both take advantage of the concept that when exposed to moderately alkaline solutions, hydrogen bonds of double-stranded DNA (dsDNA) are broken and both strands unwind, creating single-stranded DNA (ssDNA).[6] The comet assay was used to assess non-steroidal anti-inflammatory drug (NSAID) photo-induced DNA damage in living cells and a new time-resolved fluorescence measurement technique was also developed to detect the difference in the lifetime of dye-DNA complexes when bound to ssDNA compared to dsDNA. In order to appreciate the value of this work, it is important to understand the mechanisms that lead to DNA damage as well as the detrimental effect it has on living organisms.

1.1 Radiation-Induced DNA Damage

Before reaching the earth's surface, most solar radiation is filtered out due to the absorption properties of ozone and other atmospheric gases which only allow transmission of wavelengths from 290-380 nm in the UV region.[7] UVA radiation constitutes *ca.* 8% of the total sunlight spectrum and UVB radiation makes up less than 0.3%. The advent of artificial UV sources as well as the thinning of the ozone layer extend the possibility of exposure to higher energy wavelengths down to 190 nm.[7] DNA bases absorb in the UV region, especially from 220-320 nm with a maximum occurring at 260 nm.[8] This region of the electromagnetic spectrum is therefore, deemed particularly relevant to photobiology

1.1.1 UVB (290-320 nm) and UVC (200-290 nm)

At wavelengths from 250-320 nm, where DNA itself is the chromophore, pyrimidine photoadducts and [2+2] pyrimidine cyclobutane dimers are the principle photoproducts formed following radiation absorption by DNA, although photooxidation also occurs (Scheme 1.1).

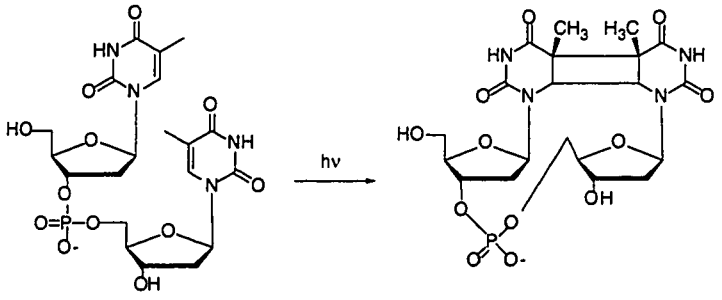

Scheme 1.1: Formation of [2+2] thymine<>thymine cyclobutane dimer following UVB radiation absorption by DNA.

The pyrimidine cyclobutane dimers are formed preferentially by thymine<>thymine, thymine<>cytosine and cytosine<>cytosine pairs and are not alkali labile sites (ALS), but repaired by enzymes.[9] The pyrimidine(6-4)pyrimidone adduct (Scheme 1.2) however, is an alkali labile lesion[10] and is formed *ca.* 50% less often than cyclobutane dimers.[11]

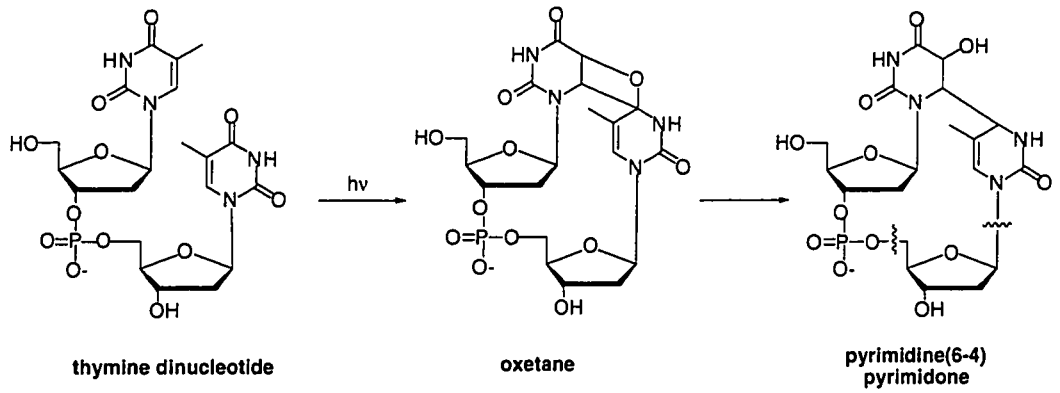

Scheme 1.2: Formation of pyrimidine(6-4)pyrimidone following UVB radiation absorption by DNA; slash indicates site of alkali-induced cleavage.

Left unrepaired or misrepaired, the photodamage suffered by DNA from the absorption of UVB radiation can pose serious problems during DNA transcription which could potentially lead to mutagenesis *via* the transcription of a damaged gene.[12] Recent results also demonstrate that UVB radiation leads to both the induction of delayed apoptosis (> 20 h)[13] as well as the stimulation of the p53 gene in human keratinocytes[14] which is potentially related to the generation of HO•.[15] Overall, pyrimidine cyclobutane dimers are the most common type of direct DNA damage, constituting *ca.* 70% of the total damage.[16] UVB radiation is responsible for most of the damage inflicted on DNA by sunlight and it is also known to be the major cause of UV-induced cancers.[7]

1.1.2 UVA (320-400 nm)

Although UVA radiation is only weakly absorbed by DNA bases, it is, however, considered to be a generator of intracellular oxidative stress. Cell death as a result of exposure to UVA radiation, can be linked to causes other than DNA damage (*i.e.,* cell components other than DNA succumbing to oxidative stress). At wavelengths longer than 320 nm, UVA radiation can cause cellular DNA damage through photosensitization reactions as opposed to a direct reaction with DNA.[7] Photosensitization occurs when cellular sensitizers (endogeneous: porphyrins, NADH, NADPH, riboflavins, melanin, hemoglobin, carotenes, keratin or exogeneous: pigments and drugs) absorb UVA radiation. The resulting photoexcited sensitizer can potentially mutate DNA or kill cells through direct interaction with cellular DNA or, more commonly, through an energy transfer to molecular oxygen, generating singlet oxygen ($^1O_2$), which can then react with cellular DNA.[7]

1.1.3 Gamma Radiation (γ Radiation)

γ radiation consists of energetic photons emitted from the nucleus of radioisotopes during radioactive decay. This is a very penetrating form of ionizing radiation which can generate *ca.* 1040 SSBs/Gray (Gy) in cellular DNA[17,18] (refer to Appendix I for calculation of SSBs/DNA base pairs). Ionizing radiation exposure in an aqueous environment leads to the radiolysis of water, generating HO$^\bullet$ as well as hydrogen atoms (H$^\bullet$) (Equation 1.1a).[9] These radicals are thought to add to the thymine base 5, 6 double bond generating either 5-yl or 6-yl reactive nucleobase species[19] which leads to deoxyribosyl hydrogen abstraction and, in turn, direct strand scission.[9]

1.2 Reactive Oxygen Species (ROS) and DNA Damage

ROS can be generated by one of two mechanisms, both involving initial radiation absorption by a sensitizer; the type I mechanism generates radical oxygen species while the type II mechanism generates $^1O_2$.

In the presence of oxygen, the type I mechanism can follow one of three pathways. In the first pathway, an electron transfer between the photosensitizer and a substrate results in the formation of anionic radicals which can donate an electron to oxygen to produce the superoxide radical anion ($O_2^{\bullet-}$) (Equation 1.1b).[20] The spontaneous dismutation of $O_2^{\bullet-}$ can lead to the formation of hydrogen peroxide (H_2O_2) (Equation 1.1c)[21]

a) $H_2O \xrightarrow{h\nu} HO^{\cdot} + H^{\cdot}$

b) $O_2 \xrightarrow{e^-} O_2^{\cdot-}$

c) $2\,O_2^{\cdot-} + 2\,H^+ \longrightarrow H_2O_2 + O_2$

d) $O_2^{\cdot-} \xrightarrow{e^-} O_2^{-2}$

e) $O_2^{-2} + 2H^+ \longrightarrow H_2O_2$

f) $H_2O_2 \longrightarrow 2HO^{\cdot}$

g) $H_2O_2 + O_2^{\cdot-} \longrightarrow HO^{\cdot} + HO^{-} + O_2$

h) (i) $Fe(III) + O_2^{\cdot-} \longrightarrow Fe(II) + O_2$

(ii) $Fe(II) + H_2O_2 \longrightarrow Fe(III) + HO^{-} + HO^{\cdot}$

i) $O_2^{\cdot-} + RH \longrightarrow HO_2^{\cdot} + R^{\cdot}$

j) $HO_2^{\cdot} + HO_2^{\cdot} \longrightarrow H_2O_2$

k) $R^{\cdot} + O_2 \longrightarrow ROO^{\cdot}$

l) $ROO^{\cdot} + RH \longrightarrow ROOH + R^{\cdot}$

m) $ROOH \longrightarrow RO^{\cdot} + HO^{\cdot}$

Equation 1.1: Reactions generating ROS.

A peroxide ion (O_2^{-2}) can be formed from the addition of another electron to $O_2^{\bullet-}$ (Equation 1.1d) which in turn forms H_2O_2 (Equation 1.1e) that can split homolytically to form HO$^\bullet$ (Equation 1.1f).[7] H_2O_2 can react with $O_2^{\bullet-}$ *via* the Haber-Weiss process (Equation 1.1g)[22] or the iron-catalyzed Fenton reaction (Equation 1.1h)[12] to generate HO$^\bullet$ and hydroxide anion (HO$^-$). Hydrogen abstraction by $O_2^{\bullet-}$ forms the perhydroxyl radical ($HO_2^\bullet$) (Equation 1.1i) which in turn can react with another $HO_2^\bullet$ to form H_2O_2 (Equation 1.1j). In the second pathway, an interaction between the sensitizer and the substrate leads to hydrogen abstraction with the formation of radicals (R$^\bullet$) which can further abstract hydrogens from other substrates or follow the first pathway. These radicals can also react with oxygen to form alkyl peroxyl radicals (ROO$^\bullet$) (Equation 1.1k) which, upon addition of hydrogen, generate alkyl peroxides (ROOH) (Equation 1.1l) leading to a homolytic cleavage to form alkoxyl radicals (RO$^\bullet$) and HO$^\bullet$ (Equation 1.1m). In the third pathway, the excited sensitizer dissociates generating radicals which can follow either of the first two reaction pathways.

The type II mechanism involves an energy transfer from the photosensitizer to molecular oxygen, forming $^1O_2$. This species can decay by either phosphorescence, non-radiative deactivation *via* collision with solvent molecules, physical quenching through the formation of a charge transfer complex or by energy transfer, photooxidation of a substrate including 1-2 and 1-4 addition to unsaturated compounds with formation of peroxides (Scheme 1.3) or by reacting with heteroatom-containing compounds (*i.e.,* DNA nucleobases and leading to DNA damage).

As evidenced by the type I and type II mechanisms, many ROS can be generated by photosensitization. Their presence in cells, known as oxidative stress, can have a detrimental effect on cellular DNA and other macromolecules and membranes, by

promoting oxidative damage to the nucleobases and the deoxyribose moiety. ROS as well as their role in DNA damage will be discussed.

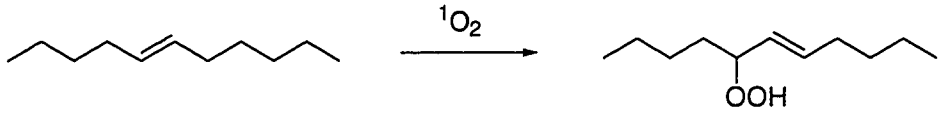

Scheme 1.3: Schenk reaction of $^1O_2$ addition to double bonds.

1.2.1 Hydroxyl Radicals (HO•)

It is estimated that over half of the DNA damage caused by HO• occurs by their action on nucleobases.[23] They are also involved in direct strand scission as a result of sugar oxidation.[23] In the presence of reductants such as Fe(II), oxidized nucleobases may be reduced back to undamaged species;[11] therefore, the probability of sugar chemistry (hydrogen abstraction) from free HO• generated by the Fenton reaction increases.[24] Alkali labile intermediates resulting from a HO• attack on guanine (Scheme 1.4) are 7,8-dihydro-8-oxoguanine (8-oxoG) (obtained under oxidative conditions) and 2,6-diamino-5-formamido-4-hydroxypyrimidine (FAPy-G) (obtained under reductive conditions). The chemistry of adenine with HO• is similar to that of guanine; however, oxidative adenine lesions are less prevalent in DNA damage[9] where HO• attacks at adenine involve addition to C4 or C8.[25] Thymine reactions with HO• can lead to direct strand scission as well as the generation of alkali labile products. The chemistry of cytosine with HO• usually generates adducts to the 5, 6 double bond leading to an increased probability of hydrolytic deamination of the N^4 amino group.[26]

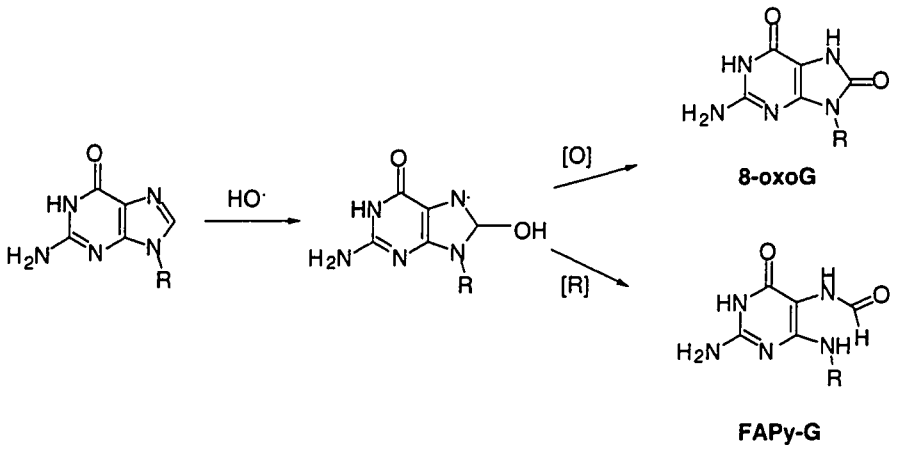

Scheme 1.4: Addition of HO• to guanine and the generation of alkali labile products.

1.2.2 Alkoxyl Radicals (RO•)

Since RO• are usually generated from ROOH, the interpretation of this DNA damage is somewhat obscured by the presence of ROO• and HO•, which are also causing damage. For RO•, nucleobase chemistry predominates over the sugar chemistry; however, the regiochemistry differs from that of HO•, where RO• generally forms adducts at the C5 position of the nucleobases.[9]

1.2.3 Alkylperoxyl Radicals (ROO•)

Lipid hydroperoxides (LOOH) are a common result of cellular exposure to oxidative stress; therefore, the potential chemistry of ROO• with nucleobases is particularly relevant. It is proposed that ROO• adds to C8 of guanine leading to 8-oxoG, and some reactivity towards thymine and cytosine has been evidenced leading to ALS.[9]

1.2.4 Superoxide Radical Anions ($O_2^{\bullet-}$)

Since $HO_2^{\bullet}$ has a pK_a of 4.8, the conjugate base $O_2^{\bullet-}$ is the major species at physiological pH;[27] however, it is very reactive and rapidly forms H_2O_2 and O_2 *via* the Haber-Weiss process.[28] Direct strand scission mediated by $O_2^{\bullet-}$ can be attributed to hydrogen abstraction from C5' of the deoxyribose.[29] Earlier conflicting results indicate that $O_2^{\bullet-}$ is not able to abstract hydrogen from lipids but that the more reactive protonated radical $HO_2^{\bullet}$ is present at only 1/500 of the concentration of $O_2^{\bullet-}$ at pH 7.4.[30] Since $HO^{\bullet}$ are much stronger oxidants than $O_2^{\bullet-}$ and they are also side products of this type of chemistry, $HO^{\bullet}$ DNA damage should also be expected wherever $O_2^{\bullet-}$ is generated.

1.2.5 Singlet Oxygen ($^1O_2$)

$^1O_2$ is formed when a triplet excited state photosensitizer transfers its energy to the triplet ground state of molecular oxygen promoting it to a singlet excited state. This noxious species reacts rapidly and indiscriminately with various electrophilic substrates such as, unsaturated lipids leading to lipid peroxidation (Scheme 1.4), proteins and nucleic acids thus generating DNA damage.[7] $^1O_2$ selectively reacts with the guanine base moiety in nucleosides generating oxidation products including 8-oxoG and FAPy-G, known ALS, and potentially leading to SSBs.[9]

1.2.6 Guanine Oxidation by Reactive Oxygen Species (ROS)

Nucleobases are preferentially oxidized by ROS due to their redox potentials, where guanine is the most easily oxidized nucleobase followed by adenine, cytosine and

thymine.[9] A guanine radical cation can be formed by direct loss of an electron due to chemical oxidation by ROS leading to the formation of 8-oxoG by hydration followed by one-electron oxidation.[11] Studies suggest that *ca.* 1 in 40 000 guanines in the genome is present as 8-oxoG under normal conditions[31] meaning that > 30 000 8-oxoG may exist at any given time in the genome of a human cell. This is formally due to the production of ROS during the course of normal metabolic processes.[32] It is; therefore, not surprising that the most common product of DNA damage is 8-oxoG, since is it also formed from UVA and UVB radiation, ROS adduct formation and hydrogen abstraction from excited-state photosensitizers. SSBs are the general outcome of 8-oxoG formation since it generates an ALS.

1.3 Alkali Labile Sites (ALS)

Early studies revealed that guanine alkylation and oxidation led to depurination of the nucleobase and ultimately strand scission at that site[33,34] as a result of the creation of an ALS. The electron-rich purine and pyrimidine heterocycles are prime targets for reactions with electrophiles; however, these reagents rarely lead to direct strand scission, but require a second chemical step such as heat or alkaline conditions to speed up this process.[9] Alkaline conditions are more commonly used since nucleobases are relatively stable to these conditions unless they have been chemically modified; this allows for unmodified nucleobases to remain intact while strand scission occurs only at specific modified sites. Strand scission occurs through a deglycosylation followed by β-elimination of the 3'-phosphate on the DNA polymer (Scheme 1.5).

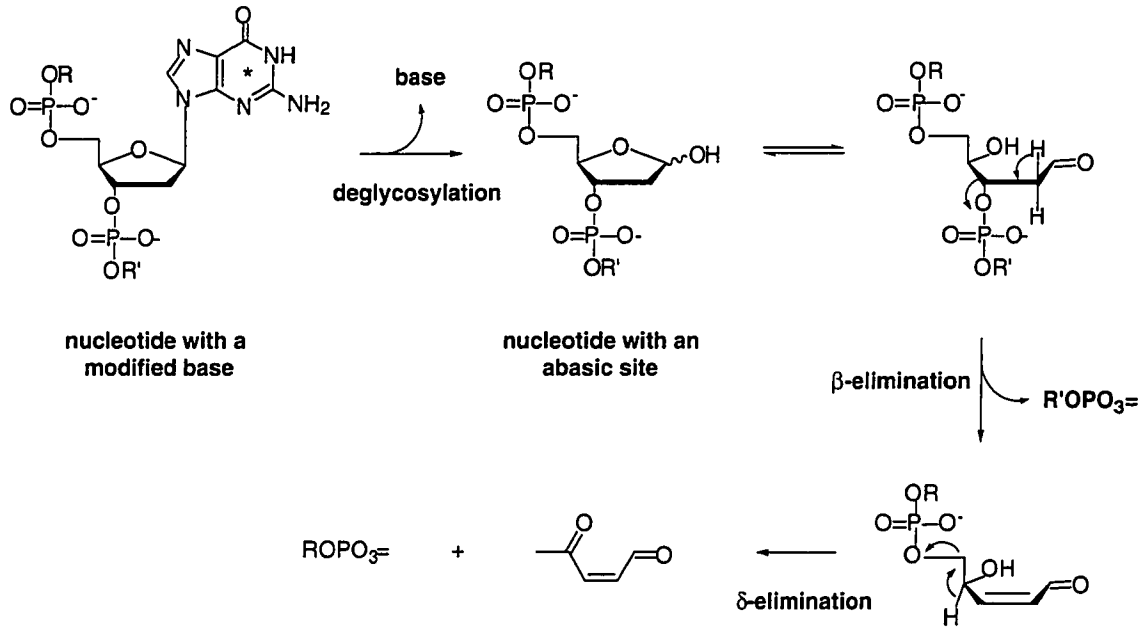

Scheme 1.5: Mechanism for DNA strand scission.

A second phosphate elimination may occur (δ-elimination) due to the acidity of $H^{4'}$, leaving behind the sugar fragment as a keto aldehyde and the 5' fragment of the original strand that now terminates with a 3' phosphate. In general, oxidation and alkylation reagents acting on nucleobases will remove electron density from the heterocycle, making the modified nucleobase a better leaving group in order to form an abasic site.[9] There are varying degrees of lability which depend on the nature as well as the site of the modification (Figure 1.2). For example, oxidation of guanine at the C8 position leads to 8-oxoG which is alkali labile while the same lesion on adenine is stable.[35]

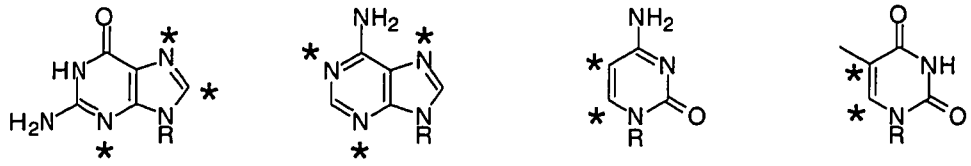

Figure 1.2: Sites of nucleobase modification leading to alkali lability.

Oxidation of C1' on the sugar moiety also generates an alkali-labile lesion, through hydrogen abstraction generating a radical which in turn can react with oxygen to give an unstable peroxyl radical leading to the formation of 2'-deoxyribonolactone (Scheme 1.6). The direct irradiation of DNA with UV radiation leads to a variety of lesions, many of which are centered on the nucleobases and are alkali labile;[36] the wavelength and radiation intensity determines to some extent the type of lesions obtained (refer to Section 1.1).

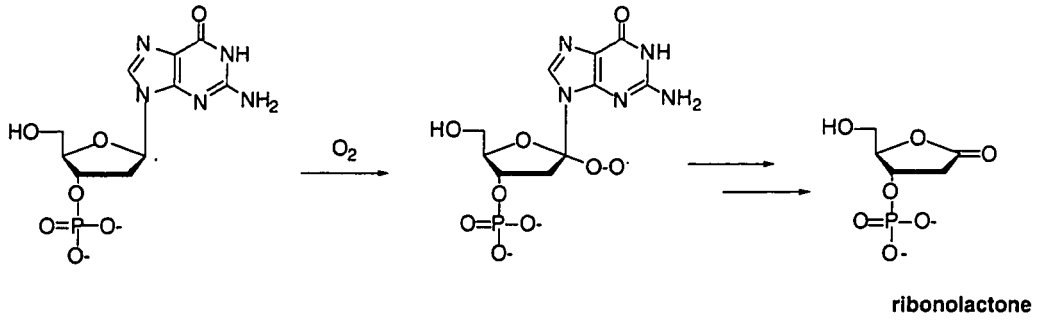

Scheme 1.6: Formation of ribonolactone after hydrogen abstraction at C1' on the sugar moiety.

For example, UVA irradiation of DNA generates alkali labile 8-oxoG either through direct oxidation of a guanine base, from hydrogen abstraction by a photosensitizer or *via* $^1O_2$. UVB irradiation of DNA, on the other hand, generates 8-oxoG as well as the pyrimidine(6-4)pyrimidone dimer, both of which are ALS.

1.4 DNA Repair

DNA damage interferes with the primary DNA functions, including transcription and replication, which can lead to mutations or cell death. The mutations or persisting lesions may lead to carcinogenesis, genetic disorders, and apoptosis. DNA nucleobases are constantly subjected to chemical modifications by environmental toxins; fortunately, an elaborate system of DNA repair enzymes recognize and excise the damaged bases.[37] Mechanisms for restoring the damaged DNA developed early in the evolutionary process, they include nucleotide excision repair (NER),[9] base excision repair (BER),[38] photoenzymatic repair (PER),[39] mismatch repair and recombinational repair. DNA is usually unwound at the site of damage or disassociated from nucleosomal proteins allowing for repair enzymes to locate and access the damaged site. While a strand scission does not necessarily occur with BER, almost all of the enzymes involved in the NER cleave the damaged DNA strand.[9] The scission event typically occurs by hydrolysis of the N-glycosyl bond of the 5'-pyrimidine base, initiated by DNA glycosylases, leaving an abasic site, followed by the excision, *via* a cleavage 3' to the site, by an endonuclease, and subsequent resynthesis of the DNA around the damaged site. Ligation of the SSB occurs once the DNA polymerase complex has released the DNA strand. Evidence has evolved that NER, a repair system originally thought to repair only bulky DNA lesions, can also repair some oxidative DNA damages (*i.e.,* thymine glycol and abasic sites). PER involves a small enzyme, photolyase, which specifically locates and binds to a cyclobutane dimer whereupon absorption of a photon (UVA-Vis radiation) catalyses the reversal of the dimerization.[39] Base damage is generally repaired with much slower kinetics than SSBs; half-lives of

ca. 30 min compared to 3-5 min respectively.[40] The overall effect of DNA damage on living organisms greatly depends on the type of lesion incurred and its genomic location. If the damage is repaired correctly, the DNA is restored to its original state and cell function resumes after a short delay. If the damage is not repaired, cell proliferation will cease (necrosis) or if the damage is located on a gene required for metabolic function, the cell will die (apoptosis).[39] In the event that a DNA polymerase should come across a non-repaired lesion, an incorrect complementary base will be produced, hence the creation of a mutation.

1.5 References

(1) Zubay, G. L.; Parson, W. W.; Vance, D. E., *Principles of Biochemistry, Molecular Genetics*, Sievers, E. M., Wm. C. Brown Communications Inc., Dubuque, 1995, Vol. 3.

(2) International Human Genome Sequencing Consortium, Initial Sequencing and Analysis of the Human Genome, *Nature*, **2001**, 409, 860-921.

(3) Rhoades, R.; Pflanzer, R., *Human Physiology*, Second Edition, Saunders College Publishing, Fort Worth, 1992.

(4) Billen, D., Spontaneous DNA Damage and its Significance for the "Negligible Dose" Controversy in Radiation Protection, *Radiat.Res.*, **1990**, 124, 242-245.

(5) Ormerod, M. G., *Radiation-Induced Strand Breaks in the DNA of Mammalian Cells*, In: Biology of Radiation Carcinogenesis, Yuhas, J. M., Tennant, R. W. and Regan, J. D., Raven Press, New York, 1976, 67-92.

(6) Birnboim, H. C.; Jevcak, J. J., Fluorometric Method for Rapid Detection of DNA Strand Breaks in Human White Blood Cells Produced by Low Doses of Radiation, *Cancer Res.*, **1981**, 41, 1889-1892.

(7) Peak, M. J.; Peak, J. G., *Photosensitized Reactions of DNA*, In: CRC Handbook of Organic Photochemistry and Photobiology, Horspool, W. M. and Song, P. S., CRC Press, Inc., Kentucky, 1995, 1318-1325.

(8) Coohill, T. P., *Action Spectroscopy: Ultraviolet Radiation*, In: CRC Handbook of Organic Photochemistry and Photobiology, Horspool, W. M. and Song, P. S., CRC Press, Inc., Kentucky, 1995, 1267-1275.

(9) Burrows, C. J.; Muller, J. G., Oxidative Nucleobase Modifications Leading to Strand Scission, *Chem. Res.*, **1998**, 98, 1109-1151.

(10) Franklin, W. A.; Lo, K. M.; Haseltine, W. A., Alkaline Lability of Fluorescent Photoproducts Produced in Ultraviolet Light-Irradiated DNA, *J.Biol.Chem*, **1982**, 257, 13535-13543.

(11) Cadet, J., *Identification and Biological Significance*, In: DNA Adducts, Hemminki, A., Dipple, A., Shuker, D. E. G., Kadlubar, F. F., Segerback, D. and Bartsch, H., IARC Scientific, Lyon, 1994.

(12) Pourzand, C.; Tyrrell, R., M., Apoptosis, the Role of Oxidative Stress and the Example of Solar UV Radiation, *Photochem.Photobiol.*, **1999**, 70, 380-390.

(13) Godar, D. E.; Miller, S. A.; Thomas, D. P., Immediate and Delayed Apoptotic Cell Death Mechanisms: UVA Versus UVB and UVC Radiation, *Cell Death Differ.*, **1994**, 1, 59-66.

(14) Cotton, J.; Spandu, D. F., Ultraviolet B-Radiation Dose Influences the Induction of Apoptosis and p53 in Human Keratinocytes, *Radiat.Res.*, **1997**, 147, 148-155.

(15) Gorman, A.; McGowan, A.; Cotter, T. G., Role of Peroxide and Superoxide Anion During Tumor Cell Apoptosis, *FEBS Lett.*, **1997**, 40, 27-33.

(16) Woollons, A.; Clingen, P. H.; Price, M. L.; Arlett, C. F.; Green, M. H. L., Induction of Mutagenic DNA Damage in Human Fibroblasts After Exposure to Artificial Tanning Lamps, *Br. J. Dermatol.*, **1997**, 137, 687-692.

(17) Ward, J. F., *DNA Damage Produced by Ionizing Radiation in Mammalian Cells: Identities, Mechanisms of Formation, and Reparability*, In: Nucleic Acid Research and Molecular Biology, Academic Press Inc., New York, 1988, Vol. 35, 95-125.

(18) Goodhead, D. T., Initial Events in the Cellular Effects of Ionizing Radiations: Clustered Damage in DNA, *Int.J.Radiat.Biol*, **1994**, 65, 7-17.

(19) von Sonntag, C., *The Chemical Basis of Radiation Biology*, Taylor and Francis, London, 1987.

(20) Condorelli, G.; Costanzo, L. L.; De Guidi, G.; Giuffrida, S.; Miano, P.; Sortino, S.; Velardita, A., Photosensitization Induced by Non Steroidal Anti Inflammatory Drugs: An Overview of Molecular Mechanisms in Biological Systems, *Newsletter*, **1996**, 58, 66-77.

(21) Halliwell, B.; Gutterridge, J. M. C., *Free Radicals in Biology and Medicine*, Clarendon Press, Oxford, 1985.

(22) Haber, F.; Weiss, J., The Catalytic Decomposition of Hydrogen Peroxide by Iron Salts, *Proc.Roy.Soc. London (A)*, **1934**, 147.

(23) Breen, A. P.; Murphy, J. A., Reactions of Oxyl Radicals with DNA, *J.A.Free Radic. Biol.Med.*, **1995**, 18, 1033-1077.

(24) Pogozelski, W. K.; McNeese, T. J.; Tullius, T. D., What Species is Responsible for Strand Scission in the Reaction of [FeIIEDTA]2- and H2O2, *J.Am.Chem.Soc.*, **1995**, 117, 6428-6433.

(25) Vieira, A. J. S. C.; Steeken, S., Pattern of Hydroxy Radical Reactions with Adenine and its Nucleosides and Nucleotides. Characterization of Two Types of Isomeric Hydroxy Adduct and Their Unimolecular Transformation Reactions, *J.Am.Chem.Soc.*, **1990**, 112, 6986-6994.

(26) Setlow, R. B.; Carrier, W. L.; Bollum, F. J., Pyrimidine Dimers in Ultraviolet-Irradiated Polydeoxyinosinic Acid-Polydeoxycitidylic Acid, *J.Proc.Natl.Acad.Sci.U.S.A.*, **1965**, 53, 1111-1118.

(27) Bielski, B. H. J.; Cabelli, D. E.; Arudi, R. L.; Ross, A. B., Reactivity of Perhydroxyl/Superoxide Radicals in Aqueous Solution, *J.Phys.Chem.Ref.Data*, **1985**, 14, 1041-1100.

(28) Van Eden, M. E.; Aust, S. D., The Consequences of Hydroxyl Radical Formation on the Stoichiometry and Kinetics of Ferrous Iron Oxidation by Human Apoferritin, *Free Radic.Biol.Med.*, **2001**, 31, 1007-1017.

(29) Dix, T. A.; Hess, K. M.; Medina, M. A.; Sullivan, R. W.; Tilly, S. L.; Webb, T. L. L., Mechanism of Site-Selective DNA Nicking by the Hydrodioxyl (Perhydroxyl) Radical, *Biochemistry*, **1996**, 35, 4578-4583.

(30) Tien, M.; Svingen, B. A.; Aust, S. D., Superoxide Dependent Lipid Peroxidation, *Fed,Proc.*, **1981**, 40, 179-182.

(31) Shigenaga, M. K.; Park, J.-W.; Cundy, K. C.; Gimeno, C. J.; Ames, B. N., In Vivo Oxidative DNA Damage Measurement of 8-Hydroxy-2'-Deoxyguanosine in DNA and Urine by High-Performance Liquid Chromatography with Electrochemical Detection, *Methods Enzymol.*, **1990**, 186, 521-530.

(32) Fehér, J.; Csomòs, G.; Vereckei, A., *Free Radical Reactions in Medicine*, Springer- Verlag, Berlin, 1985.

(33) Tamm, C.; Shapiro, H. S.; Lipshitz, R.; Chargaff, E., Distribution Density of Nucleotides Within a Deoxyribonucleic Acid Chain, *J.Biol.Chem.*, **1953**, 203, 673-688.

(34) Lawley, P. D., Hydrolysis of Methylated Deoxyguanylic Acid at pH 7 to Yield 7-Methylguanine, *Proc.Chem.Soc.*, **1957**, , 290-291.

(35) Chung, M.-H.; Kiyosawa, H.; Ohtsuka, E.; Nishimura, S.; Kasai, H., DNA Strand Cleavage at 8-Hydroxyguanine Residues by Hot Piperidine Treatment, *Biochem.Biophys.Res.Commun.*, **1992**, 188, 1-7.

(36) Cadet, J.; Vigny, P., *Bioorganic Photochemistry*, Morrison, H., Wiley, New York, 1990, Vol. 1.

(37) Davis, S. S.; Williams, S. D., Chemistry of Glycosylases and Endonucleases Involved in Base-Excision Repair, *Chem. Rev.*, **1998**, 98, 1221-1261.

(38) Hickson, I. D., *Base Excision Repair of DNA Damage*, Chapman and Hall, New York, 1997.

(39) Mitchell, D. L., *DNA Damage and Repair*, In: CRC Handbook of Organic Photochemistry and Photobiolgy, Horspool, W. M. and Song, P. S., CRC Press, Inc., Kentucky, 1995, 1326-1331.

(40) Banáth, J. P.; Wallace, S. S.; Thompson, J.; Olive, P. L., Radiation-Induced DNA Base Damage Detected in Individual Aerobic and Hypoxic Cells with Endonuclease III and Formamidopyrimidine-Glycosylase, *Radiat.Res.*, **1999**, 151, 550-558.

Chapter 2

Prompt and Delayed NSAID Photo-Induced DNA Damage in Living Cells

2.1 Introduction

Non-steroidal anti-inflammatory drug (NSAID) photo-induced DNA damage has been evidenced by numerous accounts in the literature over the past 30 years.[1-4] However, these studies were usually not conducted *in vivo* or on cultured cells, but almost exclusively on DNA in solution. The results are nonetheless biologically relevant as many experiments were carried out on supercoiled Φ_{χ}-174 DNA, calf thymus DNA or pBR 322 plasmid DNA in phosphate buffered saline (PBS) at physiological pH (7.0-7.4). The goal of this project is to investigate whether DNA damage photo-induced by NSAIDs occurs in living cells, despite ongoing metabolic functions. Initial experiments were conducted with an HL60 cell line, but were eventually replaced by peripheral blood mononuclear cells (PBMC) isolated from human whole blood (WB) (*vide infra*). Ketoprofen (KP) and Tiaprofenic Acid (TP) (Figure 2.1), both 2-arylpropionic acid derivatives, were the drugs of choice for quantifying NSAID photo-induced DNA damage in cells due to their well-known phototoxicity.

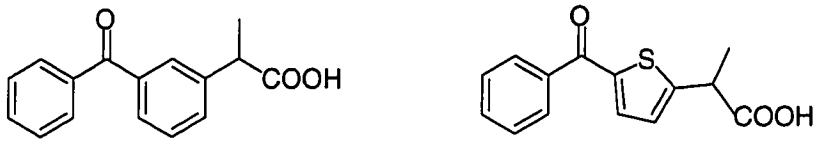

Figure 2.1: Structures of Ketoprofen and Tiaprofenic Acid.

The comet assay was used to express the DNA damage photo-induced by NSAIDs. This damage can arise from a variety of pathways, such as sugar or base modifications leading to alkali labile sites (ALS). The expression of damage inflicted on DNA is enhanced during the comet assay by means of converting ALS to single-strand breaks (SSBs) through the use of an alkaline unwinding buffer. Repair experiments were also

carried out; however, due to the increase in sources contributing to DNA damage once cells are given a chance to repair (*i.e.,* non-ALS damage), final experiments were conducted without repair times. Without repair, the DNA damage expressed is that of direct interaction between the photoexcited NSAIDs and DNA leading to either ALS or direct strand breaks. Different radiation sources, such as UVA (320-400 nm), UVB (290-320 nm) and solar simulated radiation (SSR), were employed in order to investigate their influence on NSAID photo-induced DNA damage.

2.2 Non-Steroidal Anti-Inflammatory Drugs (NSAIDs)

NSAIDs are a large class of compounds which inhibit cyclooxygenase isoenzymes 1 and 2 (COX_1 and COX_2). These enzymes are responsible for catalyzing the rate-limiting step in prostaglandin synthesis from arachidonic acid.[5] In light of their pharmacological significance, NSAIDs have seen world-wide popularity as anti-inflammation therapeutics. Over the past 30 years, NSAIDs have also undergone critical scrutiny, from a pharmacological point of view, concerning their photostability, photochemistry and potential phototoxicity.[6] Since solar radiation (UVB, UVA, Vis) of wavelengths longer than 310 nm is able to penetrate the subcutaneous layers of the skin, thereby reaching the blood vessels, NSAIDs present in the blood stream can absorb the incident radiation and initiate noxious reactions (Figure 2.2).[7]

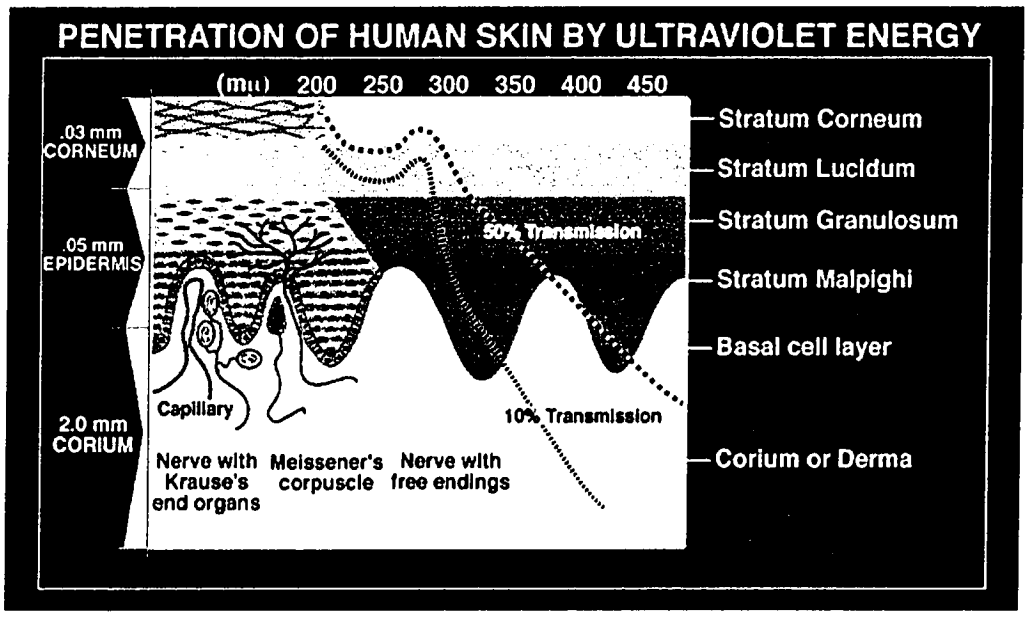

Figure 2.2: Penetration of UV radiation into the skin layers.[8]

Whether NSAIDs are administered orally or applied topically, they are susceptible to exposure to UV radiation; after which, they can act as a photosensitizer with DNA as their substrate. Both KP and TP are known to elicit phototoxic and photoallergic reactions. TP in particular has been found to be the most potent photosensitizer out of 32 tested drugs and chemicals in a multicentre photopatch test.[9] Phototoxicity is more common than photoallergy and regresses upon discontinuation of drug treatment or radiation exposure. Photoallergy is a delayed T cell-mediated hypersensitivity response involving immunological responses and requires a previous sensitization and a latency period.[10]

KP (2-[3-benzoylphenyl]propionic acid) is a potent non-steroidal anti-inflammatory agent which also has analgesic and antipyretic activity; it has been widely used for the treatment of rheumatoid arthritis as well as osteoarthritis.[11] In general, KP is safe and effective; however, owing to its widespread use, cutaneous side effects have been reported, especially after topical application.[12] These include the induction of allergic and photoallergic contact dermatitis, particularly in countries such as those bordering the Mediterranean, where the use of topical NSAIDs is widespread and exposure to sunlight is intense.[13] Although it is well adsorbed following oral administration, its use has also been associated with a number of undesirable side effects on the stomach as well as the kidneys.[11] KP is known to promote the photohemolysis of erythrocytes *via* free radicals, superoxide radical anion ($O_2^{\bullet-}$) and other generated photoproducts.[12,14,15] KP is also able to induce lipid photoperoxidation involving radical intermediates[12,16] which inevitably leads to cell damage.[15,17,18] In terms of protein damage, photobinding of KP, as well as its major photoproduct, 3-ethylbenzophenone (EB), to human serum

albumine has been observed.[19,20] Following irradiation, KP has demonstrated its ability to cause SSBs in supercoiled $\Phi_{\chi}174$ DNA as well as promote pyrimidine photodimerization.[2,21-24]

TP (2-[4-(2-benzoyl)thiophenyl]propionic acid) is the most phototoxic non-steroidal anti-inflammatory agent in terms of photosensitizing.[3] TP has been known to elicit photocontact dermatitis;[25] furthermore, its phototoxicity has been clinically proven and confirmed by *in vivo* and *in vitro* laboratory tests.[7] TP is also known to induce lipid peroxidation and evidence strongly suggests the involvement of both type I and type II mechanisms.[4] It has been shown that TP (and its major photoproduct) can photooxidize specific amino acids through a type I mechanism (tyrosine) as well as a type II mechanism (histidine and tryptophan).[26] Further investigation has demonstrated the formation of higher-molecular weight protein aggregates (protein photo-crosslinking) by means of a covalent bond between the drug (or photoproduct) and the protein (photobinding).[27,28] When DNA is irradiated with low concentrations of TP, photooxidative damage occurs as opposed to the production of SSBs.[4] The involvement of both type I and type II mechanisms are thought to be responsible for purine and pyrimidine oxidation.

2.2.1 Photochemistry and Photophysical Properties

2.2.1.1 Ketoprofen (KP)

The benzophenone-derived structure of KP (Scheme 2.1) allows for the absorption of photons in the UVC-UVB region of the electromagnetic spectrum (200-320 nm), with the weak π,π^* transition extending through most of the UVA region (refer to Figure

2.16). Upon absorption of a photon, KP reaches a singlet excited state (KP1) (energy of lowest n,π^* excited singlet state in ethanol is 323.4 kJ/mol[29]) and undergoes rapid decarboxylation from the singlet manifold to form a ground state carbanion (KP2).[6] This transient is primarily formed when the carboxylate form of KP, almost exclusively present in aqueous solutions under physiological conditions (pH 7.0-7.4), is irradiated. Subsequent protonation of the ground state carbanion leads to the formation of EB as the major photoproduct.

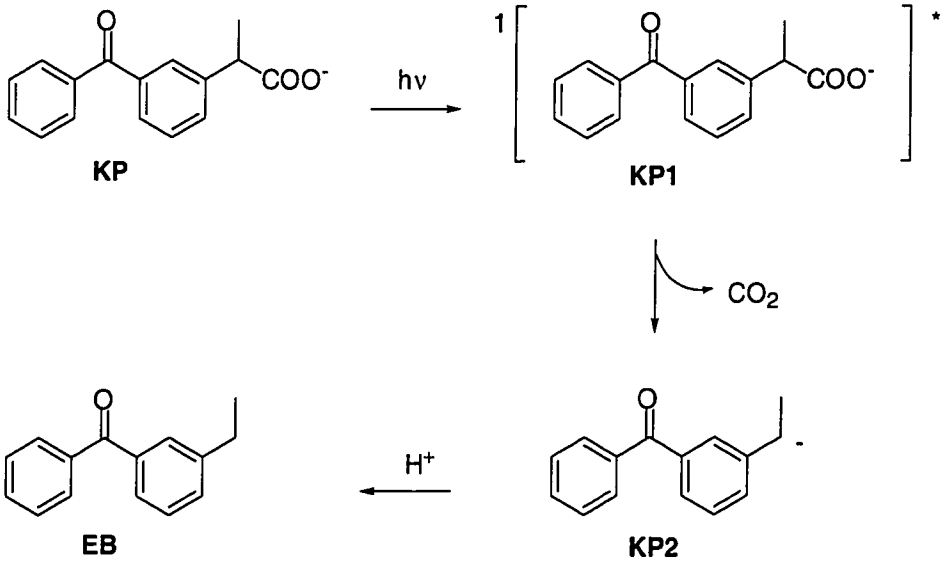

Scheme 2.1: Photochemistry of Ketoprofen.

Some studies indicate the formation of a triplet excited state of KP (τ_{KP} = 250 ps[30]) (energy of lowest n,π^* triplet excited state in ethanol is 289.9 kJ/mol[29]); however, it is believed that decarboxylation to the ground state carbanion (KP2) (τ_{KP2} = 200 ns in water[6]) does not occur from the triplet manifold.[6,31] EB having retained the benzophenone chromophore, can in turn absorb another photon and is known to

generate a triplet excited state (EB1) leading to a ketyl radical (EB2) following hydrogen abstraction (Scheme 2.2).

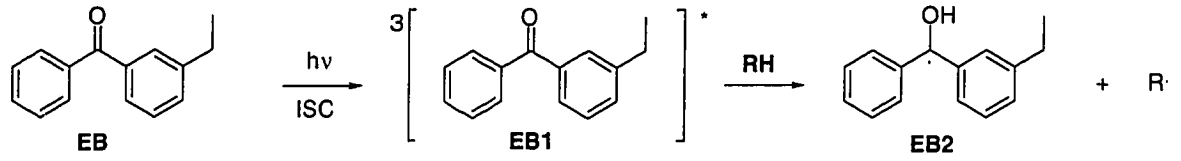

Scheme 2.2: Photochemistry of 3-ethylbenzophenone.

Photoproducts other than EB have been observed under non-aqueous conditions; however, these were generated using long irradiation times (1 h) and KP concentrations above 100 μM.[15,16] These experimental conditions are not representative of physiological conditions; therefore, the *only* photoproduct anticipated within the scope of this project is EB (*vide infra*).

Excited KP in its anionic form decays mainly through decarboxylation in less than 6 ns (typical laser pulse duration) with 75% efficiency;[6] therefore competing pathways, such as hydrogen abstraction or energy transfer to molecular oxygen, are not likely to occur. As a result of a short singlet excited state lifetime, KP1 itself is not capable of generating noxious species (*i.e.*, photosensitization). These are only produced upon absorption of a second photon by EB, the major photoproduct. This should cause a delay in the onset of generated noxious species upon KP irradiation, requiring higher radiation doses to be used in order to induce their appearance.

2.2.1.2 Tiaprofenic Acid (TP)

The 2-benzoylthiophene-derived structure of TP (Scheme 2.3) allows for the absorption of photons in the UVC-UVA region of the electromagnetic spectrum (200-400 nm) (refer to figure 2.16). Upon absorption of a photon, TP reaches a singlet

excited state (energy of lowest n,π^* singlet excited state in water is 338.9 kJ/mol) and quickly undergoes intersystem crossing (ISC) to a triplet excited state (TP1) (energy of lowest π,π^* triplet excited state in water is 242.7 kJ/mol) with 90% efficiency.[32] The promotion to an n,π^* triplet excited state (TP2) by thermal activation over a 41.8 kJ/mol energy barrier results in decarboxylation with 25% efficiency[33] to form a triplet biradical (TP3) and then a ground state enolate (TP4), both of which are in equilibrium with their conjugate acids.[32] Subsequent protonation of TP4 leads to the formation of the major photoproduct (TP5).

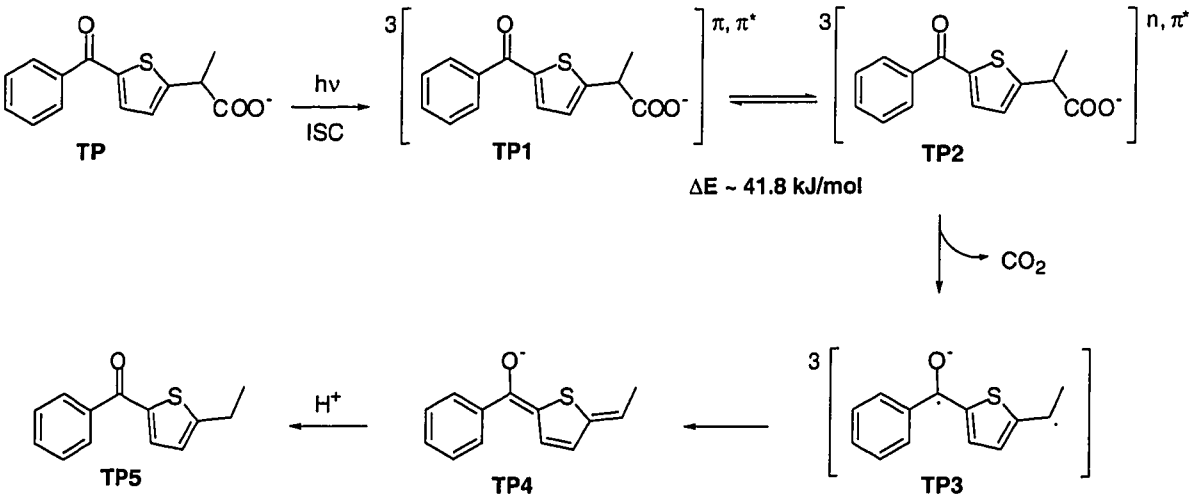

Scheme 2.3: Photochemistry of Tiaprofenic Acid.

The mechanism for the formation of the other photoproducts obtained from the irradiation of TP (Scheme 2.4), is trapping of the benzylic radical (TP3) by oxygen leading to two TP derivatives, an alcohol (TP6) and a ketone (TP7).[34]

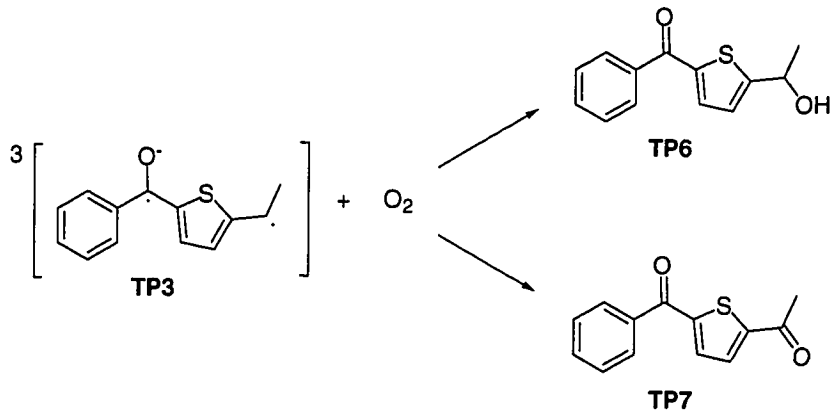

Scheme 2.4: Formation of Tiaprofenic Acid photooxidation products.

Unlike KP, TP is believed to generate noxious species (TP1, TP2 and TP3) upon absorption of a single photon, thus eliminating the need for higher radiation doses to be used in order to induce their appearance. Owing to their long lived triplet excited states (τ_{TP1} = 0.8 μs, τ_{TP2} = 1.5 μs and τ_{TP3} ~ ms),[4] hydrogen abstraction as well as energy transfer to molecular oxygen quickly become likely decay pathways for these noxious species (*vide infra*). Along with TP1, TP2 and TP3, TP5 is also able to undergo the same type of photochemistry as TP,[33] hence increasing the incidence of generated noxious species.

2.2.2 Pathways Leading to DNA Damage

Based on the photochemistry of KP and TP, it is possible to speculate which noxious species will be generated and by what pathways they cause DNA damage. Hydrogen abstraction by EB1, EB2 and TP3 can occur (type I mechanism), leading to nucleobase and/or ribosyl radicals resulting in subsequent direct DNA strand scission.[35] Adduct formation can also occur from these species generating sugar or base modifications resulting in ALS.[35] The formation of a guanine radical cation is only

possible through EB1 and TP3. This process involves an electron transfer from the nucleobase to the triplet excited state of the photosensitizer, leading to a nucleotide radical cation, and subsequent rapid deprotonation to give a neutral radical (*i.e.*, the generation of 8-oxoG).

The major photoproducts EB and TP5, generated following decarboxylation of KP and TP respectively, have retained their chromophoric moiety allowing for subsequent absorption of photons and the possibility of generating more noxious species. Studies have shown that EB and TP5 are even more effective in causing photohemolysis through lipid peroxidation of cell membranes than either KP or TP themselves. Due to the lack of the carboxylate moiety, rendering these compounds highly lipophilic, resulting in preferential location in cell membranes,[36] they could accumulate in the hydrophobic membrane of cells therein initiating lipid peroxidation *via* a type I mechanism.[25] The latter mechanism could potentially be detrimental to DNA owing to the known affinity of ROS for heteroatom-containing compounds.

TP and TP5 can act as photosensitizers (type II mechanism), thereby transferring their energy to molecular oxygen and generating $^1O_2$. Quantum yields for $^1O_2$ generation have been reported to be 0.22 and 0.58 for TP and TP5, respectively, in PBS.[37] However, KP and EB are not known to generate significant amounts of $^1O_2$.[37]

Studies have shown that KP and TP could potentially be involved in the photosensitized formation of DNA pyrimidine dimers.[21] This process requires an energy transfer from the triplet excited state of the drug to a DNA nucleobase (Figure 2.3). Thymine is the nucleotide with the lowest triplet energy (305.4 kJ/mol) requiring the triplet excited state energy of the photosensitizer to be at least as high for efficient sensitization. However, triplet excited state energies of benzophenone-derived

NSAIDs are considered to be too low (E_{KP} = 289.9 kJ/mol) rendering KP and TP poor candidates for energy transfer-induced dimerization of DNA.

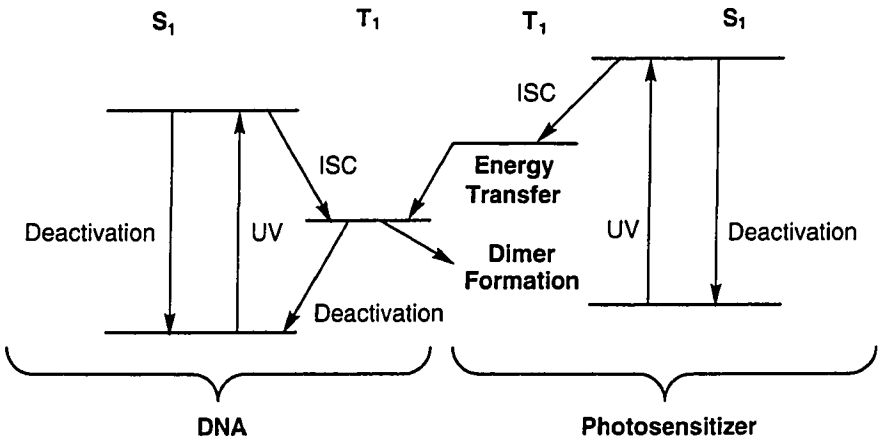

Figure 2.3: Formation of DNA pyrimidine dimers by energy transfer from the triplet excited state of NSAIDs to DNA.

A more recent study shows strong evidence implicating KP in the formation of DNA cyclobutane thymine dimers *via* a triplet-triplet energy transfer from KP to a poly-thymine oligonucleotide in PBS;[38] however, these results have yet to be achieved under biological conditions.

2.3 Radiation Sources

Three different radiation sources were tested, at biologically relevant doses (refer to Table 2.1), in order to investigate their ability to induce differences in the expression of NSAID photo-induced DNA damage (also refer to Appendix A, B and C for UVA, UVB and SSR lamps specifications, respectively). The UVA radiation was used at a dose rate of 1.34 mW/cm^2 (equivalent to $mJ/cm^2 \cdot s$) and irradiation times were between 0-15 min resulting in doses of 0-1206 mJ/cm^2. The UVB radiation was used at a dose rate of 1.54 mW/cm^2 and irradiation times were between 0-60 sec resulting in doses of 0-92.4 mJ/cm^2. SSR, which is a combination of UVA (98.17%) and UVB (1.83%) radiation, was used at a dose rate of 1.07 mW/cm^2 from UVA radiation (320-400 nm) and 0.019 mW/cm^2 from UVB radiation (290-320 nm), for a total dose rate of 1.09 mW/cm^2; irradiation times were between 0-17.5 min resulting in doses of 0-1149 mJ/cm^2. Radiation sources were compared using the total actual irradiance values. Refer to Appendix F for calculations of the minimal erythemal dose (MED) and Appendix G for all relevant values for each radiation source.

2.4 The Comet Assay

The comet assay, also known as single cell gel electrophoresis (SCGE), is a DNA damage quantification technique that gets its name from the comet-shaped DNA migration pattern obtained upon completion of the assay. This technique is recognized as a sensitive, reliable, and moderately rapid method for detection of DNA double-strand breaks (DSBs) and SSBs, ALS and delayed repair sites. Its strength lies in the fact that observations are made at the single cell level, allowing the technique to be used with virtually any eukaryotic cell. In comparison with other sensitive methods, the comet assay is relatively robust and economical in its use of materials since only a small number of cells are required and data can be obtained within a few hours of sampling. The DNA damage detected by the comet assay can arise through various mechanisms, including DNA DSBs, SSBs, DNA interstrand cross-linking, ALS, and incompletely repaired excision sites present at the time of lysis. A positive response in the assay means that the above events have been detected.[39]

Rydberg and Johanson were the first group of researchers to quantify DNA damage in individual cells.[40] They embedded the cells in agarose and lysed them under mild alkali conditions allowing partial unwinding of the DNA. After neutralization, acridine orange was used to visualize the extent of DNA damage using fluorescence detection with a photometer to quantify the ratio of double-stranded DNA (dsDNA) to single-stranded DNA (ssDNA).

Ostling and Johanson sought to improve the sensitivity of detecting DNA damage in single cells by developing a microgel electrophoresis technique known today as the comet assay.[41] In their technique, the cells were cast into an agarose gel and placed

onto a microscope slide where DNA was isolated from the nucleus by subjecting the cells to a lysis buffer as well as a high salt treatment. The DNA was subsequently electrophoresed under neutral conditions; no separation of DNA strands occurred after electrophoresis. Ethidium bromide (EtBr) was used with fluorescence microscopy to visualize the cell's nucleus, which had developed into a comet-like morphology. The shortcomings of this, so far, primitive assay was that it only detected DSBs and that the presence of RNA lead to potential artifact measurements.

Two versions of the comet assay were introduced by Singh *et. al.*[42] and Olive and co-workers.[43] The first group used alkaline electrophoresis, with a pH > 13, to analyze DNA damage after treatment with X-rays or hydrogen peroxide (H_2O_2). This version, which is currently in use, is known as the SCGE technique and it is capable of detecting DNA SSBs and ALS in individual cells. Olive and co-workers[44] originally developed a neutral technique which involved lysis by alkali treatment followed by electrophoresis at either neutral or mild alkaline (pH 12.3) conditions to detect DSBs. The alkaline version is normally used to detect SSBs and ALS while a modified version of the neutral assay can be used to detect the late stages of apoptosis.

Over the years, the comet assay has been used for various applications, including genetic toxicology as well as oncology, and has been adapted for various purposes never straying far from the original neutral or alkaline versions. It is only possible to achieve an appreciation for this novel technique by explaining the role of each of the steps of the assay (Figure 2.4).

The first step of the assay, after having induced damage and cast the cells (embedded in agarose) onto a solid support, involves exposing the cells to a high salt lysis buffer (pH 10). The detergents in the lysis buffer break up the cellular membrane as well as

the nuclear membrane leaving naked DNA embedded in the agarose gel (proteinase K can also be added to remove any residual proteins). This process relies on the effect of subjecting the cells to a hypertonic environment whereby forcing the flux of water outwards until the cell ruptures. At this point, all cellular components have been removed and the DNA is left naked within the agarose gel.

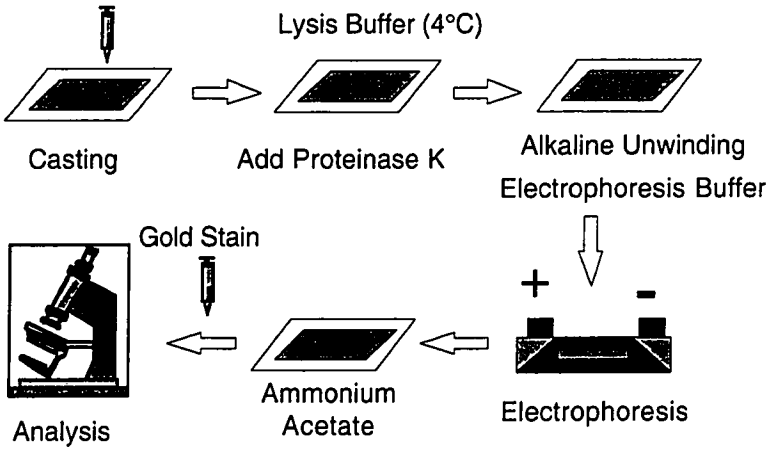

Figure 2.4: Steps of the comet assay.

For the alkaline version of the comet assay, the gels are then subjected to an alkaline unwinding buffer at a pH > 12.3 allowing the DNA to unwind. The high alkalinity of the buffer reduces the hydrogen bonding between the nucleobases of DNA; therefore, forcing them apart and creating ssDNA. The ALS, as a result of DNA attack by noxious species, will also be converted to SSBs under the effect of the unwinding buffer. The amount of ssDNA formed is directly proportional to the unwinding time used. Eventually, if left to unwind for long enough, all the DNA will become single-stranded. The SSBs formed during unwinding will have created shorter ssDNA which will migrate faster than its longer counterparts during electrophoresis. This forces the damaged DNA to migrate away from the bulk of the DNA, creating comet-shaped structures.

Therefore, to be consistent and to obtain reproducible results, the unwinding time must be kept constant.

Electrophoresis is carried out in the same alkaline unwinding buffer using a fresh solution. Many of the variations of the comet assay are found during the electrophoresis step. The desired voltage and time of electrophoresis are related to the levels of DNA damage expressed in the cells studied. Since DNA is required to migrate only a fraction of a millimeter for microscopic observation, significant DNA migration, which leads to comet formation, is possible with very short electrophoresis runs (5-30 min) and with very low voltages (0.5-5 V/cm) as compared to most conventional DNA electrophoretic techniques. The unwinding time and the duration of the electrophoresis are variables that depend on the cell type being assessed.

For the neutral version of the comet assay, the gels are subjected to a neutral buffer after cell lysis; therefore, no unwinding occurs and ALS are not converted to SSBs. The shape of the DNA remains that of an outward scattering about a center point. Electrophoresis for the modified version of the neutral assay is very brief (2 min) since only a short migration distance is enough for the discrimination between apoptotic and non-apoptotic cells.

After electrophoresis, the gels are neutralized in an ammonium acetate buffer, then dried in ethanol. The last two steps create permanent slides which can be kept for an indefinite period of time.

2.5 DNA Damage Quantification Parameters

"There are almost as many methods for quantifying DNA damage by the comet assay as there are scientists using the technique...".[39] The most flexible approach for collecting comet assay data involves the application of an image analysis technique to individual cells; several commercially available software programs have been developed specifically for collecting such data. To visualize the damaged DNA, the gels are individually stained with a fluorescent nucleic acid dye (SYBRGold®) which intercalates into the DNA strands and comets are observed through a fluorescent microscope (Figure 2.5).

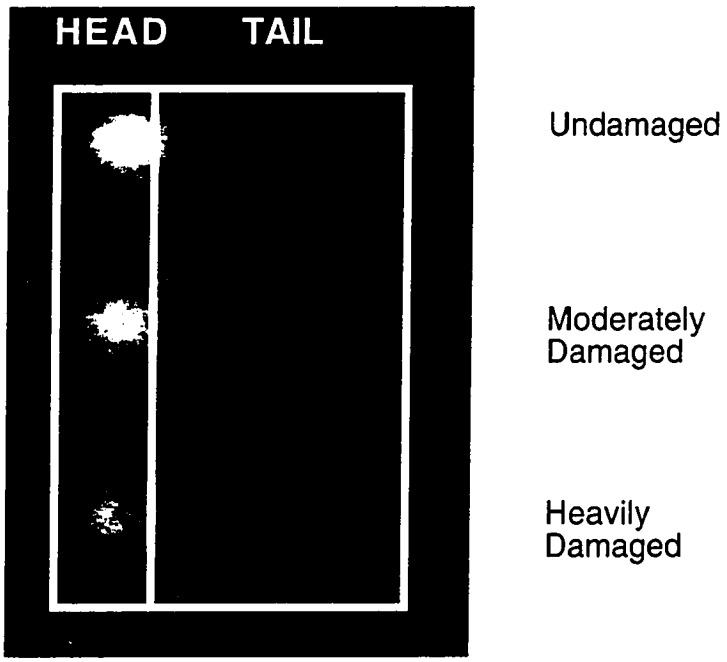

Figure 2.5: Typical comets produced from NSAID photo-induced DNA damage following the alkaline comet assay.

The microscope is interfaced with image analysis software allowing for the visualization of the comets on a computer monitor. The software is designed to allow the selection of

the head and the tail of the comet. Subjectivity is the technique's major drawback; however, it can be overcome by using semi-automated analysis software, analyzing many comets (> 50 for a single sample), blinding the samples to be analyzed as well as repeating the same experiment several times.

The selected cells are then analyzed according to four parameters designed to represent the amount of DNA damage. Comet length (the distance from the head to the tip of the comet, given in μm) and tail length (the distance from the end of the head to the tip of the tail also given μm) were the first two parameters used to quantify DNA damage with the comet assay technique since it was obvious that the greater the damage, the more SSBs would be present, resulting in longer comets. Therefore, in the early stages of the technique, larger, longer comets were assumed to be due to greater amounts of DNA damage. Since it was later determined that long electrophoresis times could also cause longer, larger comets (even with the controls), a measure of the DNA density and distribution in different regions of the comet was needed to better assess the damage. Olive and Durand discounted the use of the length of DNA migration as a parameter for DNA damage on the basis that it reaches a plateau while the percentage of migrated DNA continues to increase.[45] This resulted in the use of the head-to-tail ratio (measure of the ratio of fluorescence in the tail over the total fluorescence of the comet) and tail moment (product of the head-to-tail ratio and the distance between the center of gravity in the head and the center of gravity in the tail of the comet) parameters which further increased the sensitivity of the comet assay by quantitating the amount of migrated DNA fragments as well as taking into account the variations in DNA distribution throughout the comet.

2.6 Results and Discussion

The process of constructing a reliable protocol for quantifying NSAID photo-induced DNA damage using the comet assay was arduous. The many different conditions used were part of a necessary learning process which led to the optimization of this technique. Initial comet assay experiments were carried out very differently than the protocol stipulated in Section 2.8; therefore, variations on that protocol will be discussed before the presentation of each experimental result.

The results of NSAID photo-induced DNA damage on living cells are reported using the tail moment parameter because this is an indicator of damage that is proportional to the number of strand breaks in a cell.[46] To provide a reference, a tail moment value of 20 is equivalent to *ca.* 75% of the DNA in the comet tail. Refer to Appendix D for the dose rate determination of the UVA lamps for Sections 2.6.1 and 2.6.2. Refer to Appendix C for the dose rate determination of SSR applicable in Section 2.6.3. For Section 2.6.4, refer to Appendix A, B and C for determination of dose rate of UVA lamps, UVB lamps and SSR respectively. The dose is calculated by multiplying the dose rate by the irradiation time (in sec) in order to obtain a value in mJ/cm^2.

2.6.1 Preliminary Experiments with HL60 Cells

The HL60 cell line was chosen for experiments using the comet assay since this mammalian cell line proliferates indefinitely so long as viable culture conditions are maintained. This condition is important as it reduces the chance of external forces acting on the cells that would prevent the effect of experimental conditions from being detected. It was important to demonstrate that the individual damaging agents used in the actual experiments did not harm the cells. For this reason, preliminary experiments

consisting of exposing the cell cultures to the individual damaging agents were conducted. Cell cultures at 1 X 10^5 cells/mL confluence were exposed to either various concentrations of KP or various doses of UVA radiation and allowed to grow for five days without any manipulation.

The blood plasma concentration of KP after a typical oral dose of 100 mg is *ca.* 3 μg/mL.[47] The KP concentrations used in this preliminary experiment were in the range of biologically relevant concentrations. The growth curve of HL60 cells incubated with 0, 1, 10 and 100 μM KP (Figure 2.6 A) shows no apparent differences in the growth patterns of the cells regardless of the KP concentration, indicating that KP alone has no effect on HL60 cell proliferation. For biological relevance, the physiological concentration of 10 μM (equivalent to 3 μg/mL) was chosen for future comet assay experiments.

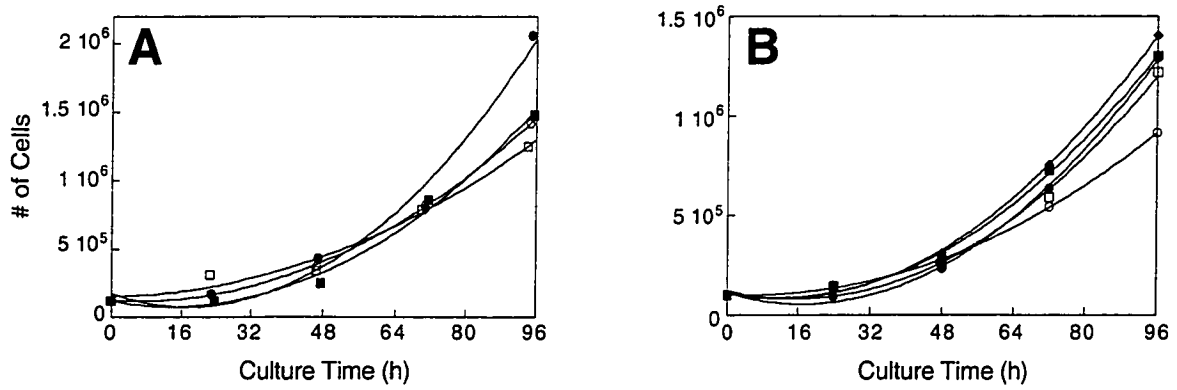

Figure 2.6: (A) Growth curve of HL60 cells incubated with 0 (○), 1 (●), 10 (□) and 100 (■) μM KP. (B) Growth curve of HL60 cells after exposure to 0 (◆), 771 (■), 1052 (●), 1541 (□) and 2105 (○) mJ/cm² of UVA radiation.

To verify the effects of UVA radiation on HL60 cells, cell cultures at 1 X 10^5 cells/mL confluence were exposed to a one-time dose of 771, 1052, 1541 or 2105 mJ/cm² of UVA radiation and allowed to grow for a period of five days. Differences in the cell proliferation patterns between the conditions become apparent only after 48 h into the

growth curve (Figure 2.6 B). At this time, higher UVA radiation doses caused a small reduction in cell proliferation. With the exception of the 2105 mJ/cm^2 UVA radiation dose, which demonstrates a notable decrease in cell proliferation, at all other UVA radiation doses cells are considered to have proliferated at a normal rate. It was expected that the UVA radiation doses administered in this experiment would hinder the growth of the HL60 cells due to the oxidizing capability of UVA radiation;[48] however, this allowed the determination of an experimental UVA radiation dose at which cells would still be viable. From these results, it was concluded that the UVA radiation range for conducting experiments should be between 1052 and 1541 mJ/cm^2. In order to establish the upper limits of resistance of HL60 cells to damaging agents, cells were exposed to what is considered to be lethal doses of KP and UVA radiation and cultured over five days. The growth curve of HL60 cells incubated with no KP as well as a lethal dose of 200 μM (Figure 2.7 A) shows that cells incubated with KP were less viable as soon as 24 h into the growth curve and continued to deteriorate throughout the five day incubation period. From the growth curve of HL60 cells exposed to no UVA radiation and to a lethal dose of 3827 mJ/cm^2 (Figure 2.7 B), it is apparent that HL60 cells did not tolerate this dose of UVA radiation since no viable cells were found as soon as 24 h into the growth curve. The cells most likely suffered from heat damage leading to necrosis or UVA-induced apoptosis.[48]

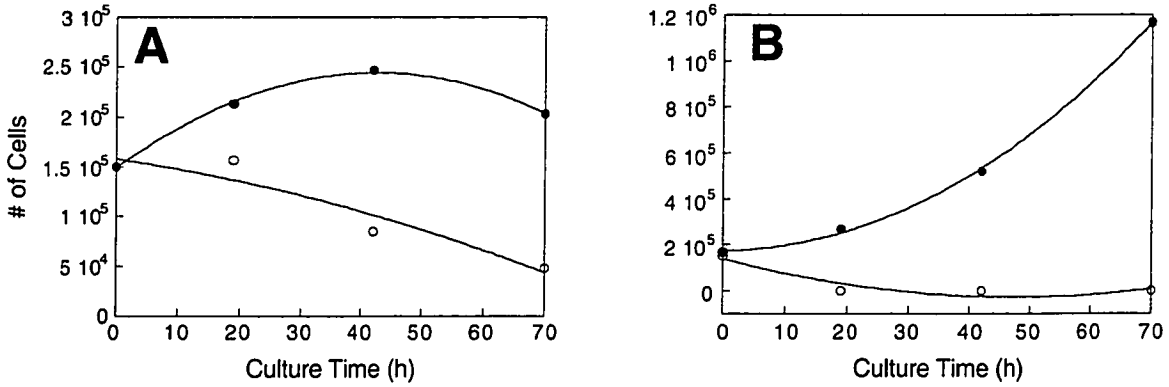

Figure 2.7: (A) Growth curve of HL60 cells incubated with 0 (●) and 200 (lethal dose) (O) μM KP. (B) Growth curve of HL60 cells after exposure to 0 (●) and 3827 (lethal dose) (O) mJ/cm² of UVA radiation.

These simple, yet important, experiments revealed the tolerances of the HL60 cell line to KP and UVA radiation; results onto which future experiments were based.

2.6.2 HL60 Cell Line Experiments

Both the neutral and the alkaline versions of the comet assay were carried out with HL60 cells. The end-point measurement for the neutral version of the comet assay is apoptosis, conversely, that of the alkaline version is DNA damage. It was of interest to use both techniques to elucidate the possible outcomes of KP photo-induced DNA damage. The major difference between the neutral and alkaline versions of the comet assay resides in the equilibration step prior to electrophoresis. In the neutral assay, a TAE buffer (pH 8.4, refer to Section 2.8 for description) is used so that no DNA unwinding occurs while in the alkaline assay, a sodium hydroxide (NaOH) buffer at pH 13.1 is used, converting all ALS to SSBs. If the alkaline version gave positive results, speculations as to how the different types of DNA damage were caused could be

made. If the neutral version gave positive results, it could be hypothesized that the DNA damage incurred by the cells was lethal resulting in apoptosis.

The neutral comet assay experiment was carried out as follows: four sets of HL60 cell cultures were diluted or concentrated to 5 X 10^5 cells/mL. For the control, 100 μL of the blank solution (no KP) were added to one cell culture plate. To two other culture plates, 100 μL of a 1 mM solution of KP were added to achieve a final concentration of 10 μM of KP. No incubation time was allotted for KP to equilibrate with the cells. The contents of each plate was transferred to a centrifuge tube and centrifuged for 8 min at 1500 revolutions per minute (rpm). The supernatant was discarded and the HL60 cell pellets were resuspended in PBS while maintaining the same cell concentration. Cell suspensions were then transferred to clean 100 mm petri dishes, checked for viability, and allowed to equilibrate for 15 min.

The control plate and the plate that received KP were placed inside the photoreactor for 15 min with the lamps off. The remaining two plates were placed, one at a time, into the photoreactor and received 1156 mJ/cm^2 of UVA radiation. For each culture plate, an aliquot of 100 μL was mixed with 900 μL of 0.75% low melting point (LMP) agarose, in a 1:10 dilution, to obtain 5 X 10^4 cells/mL in one gel. A duplicate volume of 120 μL was dispensed into the casting chamber previously attached to the Gelbond® film (refer to Section 2.8.7 for the description and casting technique). Once the gels were solidified, the casters were removed and the gels were treated following the protocol for the neutral comet assay as stipulated in Section 2.8.9. HL60 cells were assayed with the neutral comet assay after 0, 24 and 48 h. Analysis of the 24 and 48 h time points were important since the cells had a chance to repair the damage inflicted on them by the damaging agents and express necrosis/apoptosis if need be. The percentage of

apoptotic fraction expressed at different repair times is considered insignificant since it remains well below 5% (Figure 2.8). There is also no apparent trend in apoptosis expression between the presence or absence of KP; therefore, the results are a good indication that the damage inflicted onto the cells from the action of photoexcited KP does not lead to apoptosis. It does not, however, preclude the possibility of KP photo-induced DNA damage but implies that HL60 cells can sustain and possibly recover from this damage.

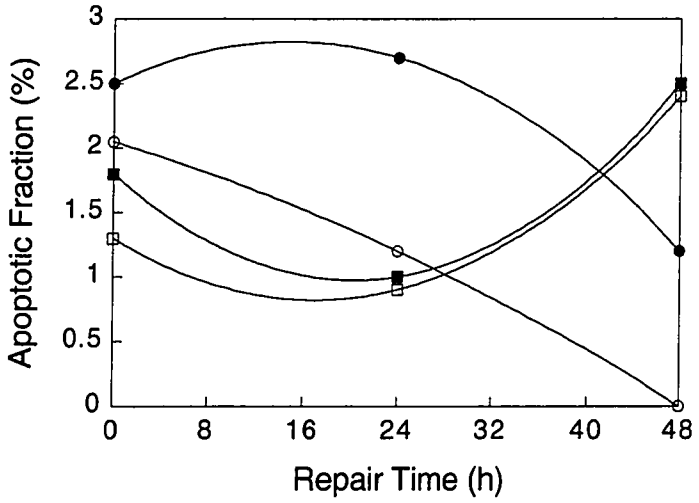

Figure 2.8: Percentage of apoptotic fraction of HL60 cells after 0, 24 and 48 h repair time following the neutral comet assay under experiment conditions of control (O), 10 μM KP (●), 1156 mJ/cm² of UVA radiation (■) and 10 μM KP + 1156 mJ/cm² of UVA radiation (□).

The alkaline version of the comet assay was performed on HL60 cells with the following experimental conditions: control (no KP or UVA radiation), 10 μM KP, 1156 mJ/cm² of UVA radiation and 10 μM KP + 1156 mJ/cm² of UVA radiation. HL60 cells were exposed to the damaging agents in the same fashion as the previous experiment and subsequently treated with the alkaline comet assay as follows. Once the gels were solidified, the casters were removed and the gels were submerged into 50 mL of

complete media (contained in a 150 mm culture plate) and incubated at 37°C for 1 h. After 60 min, the gels were rinsed with distilled deionized water (ddH_2O) and submerged into 50 mL of ice cold lysis A buffer and kept at 4°C for 30 min. After 30 min, the lysis A buffer was discarded and the gels were rinsed with ddH_2O and submerged into 50 mL of lysis B buffer. A volume of 1 mL of the proteinase K solution was added and the plates were incubated at 37°C for 60 min. After 60 min, the lysis B buffer was discarded and the gels were rinsed with ddH_2O, submerged into 50 mL of alkaline unwinding/electrophoresis buffer and incubated at 37°C for 30 min. The buffer was discarded and the gels were electrophoresed for 20, 40 and 60 min in fresh unwinding/electrophoresis buffer. Different electrophoresis times were carried out in order to optimize the detection of DNA damage.

KP photo-induced DNA damage on HL60 cells following the alkaline comet assay using 20, 40 and 60 min electrophoresis times is shown in Figure 2.9. The results were plotted to clearly indicate the increase in tail moment with increasing electrophoresis time; this phenomenon being expressed at all experimental conditions. Longer electrophoresis times express higher tail moment values because more of the ssDNA is able to migrate into the tail. This fact does not imply that more DNA damage is incurred at longer electrophoresis times, but that the DNA damage incurred is better expressed. Most accounts of the alkaline comet assay in the literature employ 20 min electrophoresis times; therefore, for purposes of comparison and saving time, subsequent alkaline comet assays were carried out with a 20 min electrophoresis time.

In analyzing these results for KP photo-induced DNA damage, the cells are considered to have suffered minimal damage, possibly due to the 1 h incubation period after

irradiation and before the casting step, during which the cells would have had the time to repair some of the DNA damage inflicted on them.[49]

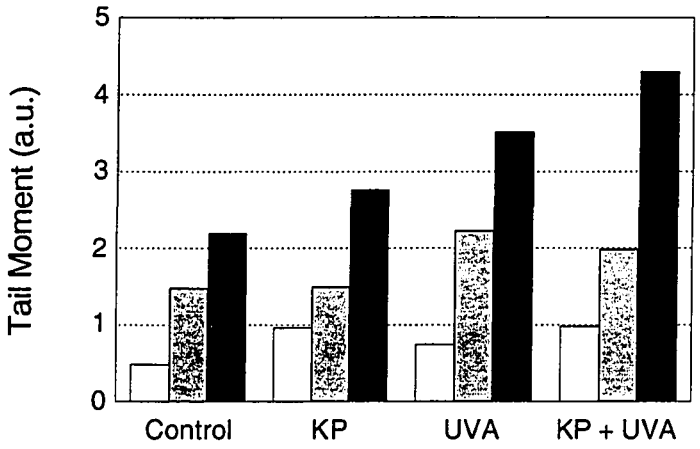

Figure 2.9: DNA damage photo-induced by 10 μM KP + 1156 mJ/cm² of UVA radiation in HL60 cells following the alkaline comet assay with 20 (white), 40 (gray) and 60 (black) min electrophoresis times.

A subsequent experiment using the alkaline version of the comet assay was performed on HL60 cells following the same experimental conditions as the previous one. The only protocol variations were, the elimination of the 1 h incubation prior to casting and the use of 20 min electrophoresis time. Eliminating the 1 h incubation time prevents the formation of SSBs from cellular repair of DNA damage (Section 1.4); therefore, the only DNA damage expressed is that of direct strand scission and ALS converted to SSBs. The results of this experiment proved to be less fruitful than anticipated; nevertheless, it uncovered many underlying problems with the current protocol. In examining the results (Figure 2.10), it quickly becomes obvious that something is awry. It was anticipated that photoexcited KP would produce more DNA damage than either KP or UVA radiation alone; however, the tail moment value for the control is higher than any other experimental condition.

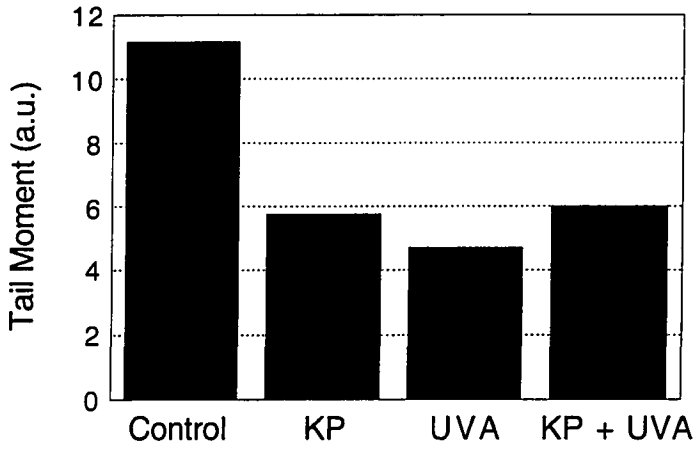

Figure 2.10: DNA damage photo-induced by 10 μM KP + 1156 mJ/cm² of UVA radiation in HL60 cells following the alkaline comet assay with 20 min electrophoresis time.

This experiment was repeated many times giving irreproducible results. One recurring problem, which turned out to be the major setback, was the overwhelming presence of 'apoptotic-looking' comets encountered during the sample analysis. When the samples are analyzed for DNA damage, 'apoptotic-looking' comets are passed (not scored) since they are not representative of a damaged DNA sample. The origins of the abnormal comets were eventually identified as being associated with assaying a rapidly proliferating cell line. During mitosis, S-phase cells contain active DNA replication forks which, following cell lysis and subsequent DNA unwinding and migration, will exhibit more DNA damage than cells in other phases of the cell cycle.[50] To rectify this problem as well as render this project more biologically relevant, the HL60 cell line was abandoned and subsequent experiments were carried on with human PBMC, which are non-dividing.

2.6.3 Peripheral Blood Mononuclear Cells (PBMC) and Solar Simulated Radiation (SSR)

The PBMC isolated from human WB encompass all the sub-cell types involved in an immune response; which include monocytes and macrophages, but primarily lymphocytes.[51] As mentioned above, PBMC are non-dividing; therefore, the presence of 'apoptotic-looking' cells found during the scoring of the samples should be greatly reduced.

The isolation of PBMC from human WB is fairly straightforward. The biggest hurdle was developing a method to expose the cells to the damaging agents while keeping the manipulations to a minimum. Many of the following experiments served mainly as verification of possible improvements to the protocol.

SSR was also implemented as a new radiation source; therefore, preliminary experiments with PBMC needed to be conducted in order to establish their tolerance to SSR. One major factor to consider is that DNA can absorb radiation in the UVB range.[52] This is relevant to the analysis of results using different radiation sources. In this case, upon absorption of radiation, DNA is modified, forming pyrimidine photoproducts, in particular pyrimidine cyclobutane dimers and [6-4]-pyrimidine adducts (an ALS).[52] Given the chance to repair, the cell will convert the pyrimidine photoproducts into SSBs resulting in an increase in DNA damage expression. In order to determine the ideal dose of SSR that would allow the expression of KP photo-induced DNA damage beyond that of UV-induced pyrimidine photoproducts, a dose-response to SSR experiment was conducted with PBMC.

The PBMC isolation was carried out in a similar fashion to the protocol described in Section 2.8.6, with the following changes. Once centrifuged through the gradient, the cell

suspension was not diluted 2:1 with complete media, it was simply re-centrifuged for 20 min at 1500 rpm. The low recovery of PBMC was due to forced centrifugation through the gradient; however, this problem was not noted until later experiments. Once the isolation was complete, cells were resuspended in PBS with a concentration of 2 X 10^6 cells/mL, checked for viability, and allowed to equilibrate for 15 min. Aliquots of 500 µL of the cell suspension were dispensed as beads in the centre of 5 separate 100 mm petri dishes. Irradiation doses of 0, 287, 574, 861 and 1149 mJ/cm^2 of SSR were carried out and 5 mL of complete media was added to each dish (1:10 dilution) to obtain 2 X 10^5 cells/mL. A volume of 100 µl of the cells suspension was added to 900 µL of 0.75% LMP agarose and 120 µL of this solution was cast onto a Gelbond® film (in duplicate); this was done for each irradiation dose.

Once the gels were solidified, the alkaline version of the comet assay was carried out as described in the previous experiment with HL60 cells. The remaining cell suspensions were incubated at 37°C for 2 and 4 h and subsequently assayed with the alkaline version of the comet assay with the same protocol as the cells that were not incubated. Repair times of 2 and 4 h were implemented in this experiment, in anticipation of exploring the effects of repair time on the expression of NSAID photo-induced DNA damage in future experiments.

DNA damage in PBMC exposed to SSR with 0, 2 and 4 h repair time following the alkaline comet assay is shown in Figure 2.11. Without the chance for pyrimidine photoproduct repair, the DNA damage expressed is minimal. When the cells are given a chance to repair the damage inflicted on their DNA, a significant increase in DNA damage expression is observed; furthermore, the expression of DNA damage is increased with the increase in repair time. From these results, a maximal dose of 230

mJ/cm^2 of SSR was chosen to conduct all subsequent experiments for KP photo-induced DNA damage requiring repair times. As an increase in DNA damage is expected from these experiments, it is important to use a SSR dose high enough to elicit a response but low enough be able to detect DNA damage above that caused by the SSR itself. SSR doses above 230 mJ/cm^2, with either 2 or 4 h repair, tend to reach a plateau in tail moment values, which would make it difficult to detect any increase in KP photo-induced DNA damage at these doses.

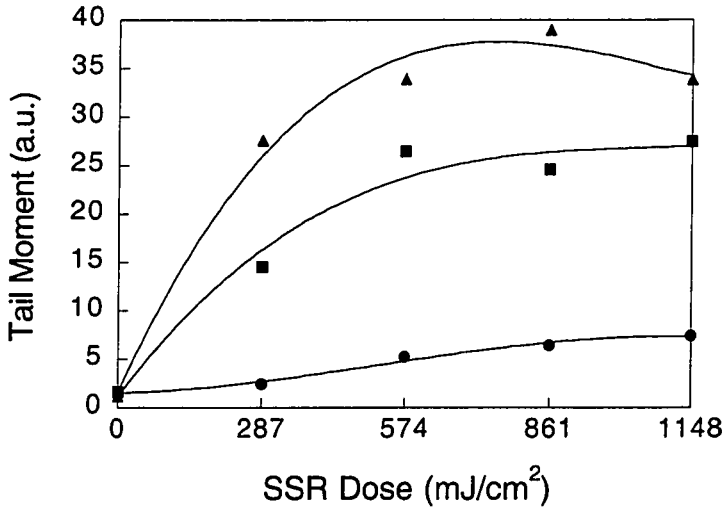

Figure 2.11: Dose-response curve of DNA damage in PBMC exposed to 0, 287, 574, 861 and 1149 mJ/cm^2 of SSR with 0 (●), 2 (■) and 4 (▲) h repair time following the alkaline comet assay.

The first experiment using the alkaline comet assay to assess KP photo-induced DNA damage in PBMC was accompanied by the following changes in the protocol. The PBMC isolation was carried out as described in the previous experiment. Once the cell suspension was obtained at 1 X 10^6 cells/mL in complete media, a volume of 1 mL was dispensed into 6 centrifuge tubes. A volume of 110 µL of KP solutions were added to the cell suspension in each centrifuge tube to obtain final concentrations of 0, 1,

5, 10, 50 and 100 μM in a 1:10 dilution of KP stock solutions. All the tubes were then incubated at 37°C for 1 h to ensure proper uptake of KP into the cells. A study of the uptake of a 2.7 mM KP solution in rabbit stomach parietal cells showed that initial uptake is very rapid, reaching 75% of the equilibrium value within 2 min and complete equilibrium at *ca.* 4 min; therefore, 1 h was considered a reasonable incubation period since lower KP concentrations exhibit a slower rate of uptake.[53] After 60 min, all the tubes were centrifuged for 3 min at 1500 rpm, to remove the excess KP solution, the pellet was resuspended into 1 mL of PBS and then the cells were checked for viability. An aliquot of 250 μL of cell suspension from each tube was dispensed as a bead in the centre of 6 separate wells of a 24-well culture plate. Irradiation doses of 0, 58, 115 and 230 mJ/cm^2 of SSR were carried out and 2.25 mL of complete media was added to each dish (1:10 dilution) to obtain 1 X 10^5 cells/mL. DNA-embedded agarose gels were cast and the alkaline version of the comet assay was carried out with the following changes. Gels remained in the lysis A buffer for 1.5 h at 4°C while treatment with the lysis B buffer was abolished thus eliminating treatment with proteinase K as well. Previous studies have shown that unless DNA-protein crosslinks are considerable, which is not the case here, treatment with proteinase K is unnecessary.[54,55] After 1.5 h, the lysis A buffer was discarded and the gels were rinsed with ddH_2O, submerged into 50 mL of alkaline unwinding/electrophoresis buffer for 30 min at room temperature and kept in the dark. The remaining cell suspensions were incubated at 37°C in complete media for 30 and 60 min, to allow expression of DNA strand breaks from DNA damage repair, and subsequently assayed with the alkaline version of the comet assay in exactly the same fashion as the cells that were not incubated.

With no repair time (Figure 2.12), there is an increase in KP photo-induced DNA damage compared to controls. Furthermore, there appears to be a dose-response relationship which increases with KP concentrations. Given that the only damage expressed at this time point is that of direct strand breaks and ALS converted to SSBs, a SSR dose higher than 230 mJ/cm^2 SSR might increase the probability of detecting more significant differences between KP doses.

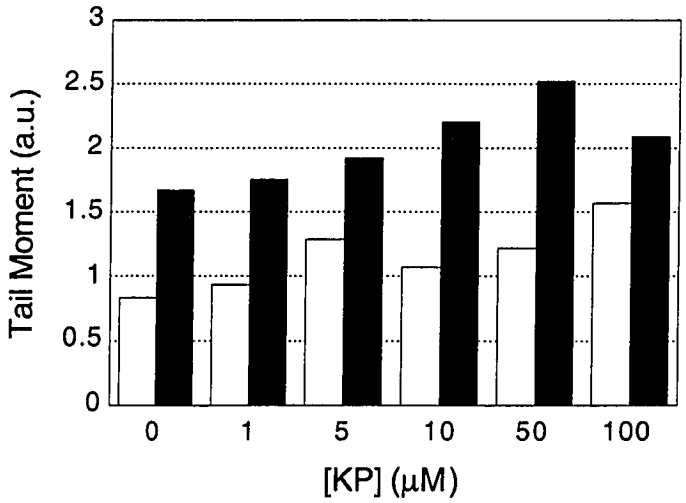

Figure 2.12: DNA damage photo-induced by 0, 1, 5, 10, 50 and 100 μM KP in PBMC exposed to 0 (white) and 230 (black) mJ/cm^2 of SSR following the alkaline comet assay with no repair time.

Given the chance to repair for 60 min (Figure 2.13), a significant increase in DNA damage is expressed well beyond that expressed by the controls. With the exception of 5 μM KP, the photo-induced DNA damage increases with increasing KP concentration. The type of DNA damage expressed after 60 min repair not only reflects ALS converted to SSBs during the unwinding step, but other types of DNA damage requiring cell repair in order to be expressed. These include UVA radiation

photosensitized damage, UVB radiation induced photoadduct formation as well as other types of base oxidation.[35]

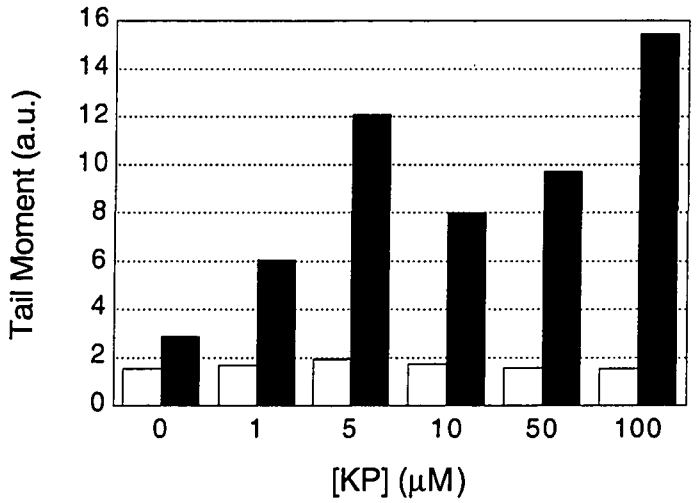

Figure 2.13: DNA damage photo-induced by 0, 1, 5, 10, 50 and 100 μM KP in PBMC exposed to 0 (white) and 230 (black) mJ/cm² of SSR following the alkaline comet assay with 60 min repair time.

No significant amounts of DNA damage or apoptotic cells were observed without repair time during the sample scoring; however, many 'apoptotic-looking' comets were found in samples with 60 min repair time. Since the neutral version of the comet assay, carried out previously on HL60 cells, had already ruled out the possibility of apoptosis as the end result, this means that the cells were possibly harmed during the manipulations leading up to their mixing with agarose and subsequent casting onto Gelbond® film.

Verification of cell viability was routinely conducted before the addition of KP and the percentage of non-viable cells was always minimal (below 5%). However, the viability test cannot reveal if the cells have sustained irreparable damage. Potential problems considered included the time the cells spent in contact with the gradient during isolation and the temperature of the agarose during cell mixing and subsequent casting.

However, since these manipulations had routinely been employed by collaborators without complications, they were ruled out as being the source of this problem.

It became apparent that the cause for the increase in 'apoptotic-looking' comets was the process of resuspending the cells in PBS for irradiation. This step was implemented into the protocol to remove the excess KP that had not penetrated the cells as well as provide an appropriate medium in which to irradiate the cells. The colour of complete media, in which the cells are most viable, is red; therefore, it absorbs most of the radiation arriving at the sample (Figure 2.14), especially in the UVB region, leaving nothing to be absorbed by the KP within the cells (refer to Figure 2.16 for the absorbance spectrum of KP). PBS, being a transparent solution, was used as a medium in which to resuspend the cells for irradiation assuming that the cells would not be harmed.

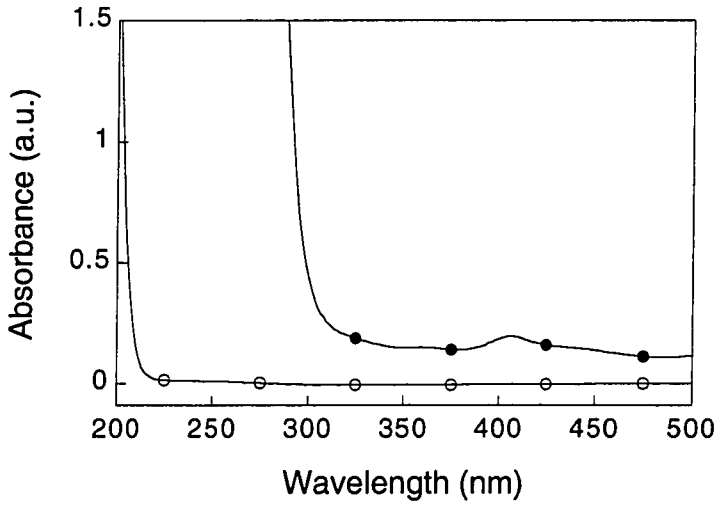

Figure 2.14: Absorbance spectra of complete media (●) and PBS pH 7.4 (O).

In order to verify whether incubation in PBS or resuspension of the cells into PBS after incubation with KP was damaging, the alkaline comet assay was performed with PBMC

following the same protocol as the previous experiment (with only 60 min repair time), implementing two key steps: the cells were incubated with KP in PBS, then half of the samples were resuspended in PBS after the incubation period while the other half were not. The alkaline version of the comet assay was carried out in exactly the same fashion as the previous experiment. However, instead of assessing DNA damage, the samples were evaluated by means of determining the percentage of apoptotic cells found in 50 cells (Figure 2.15).

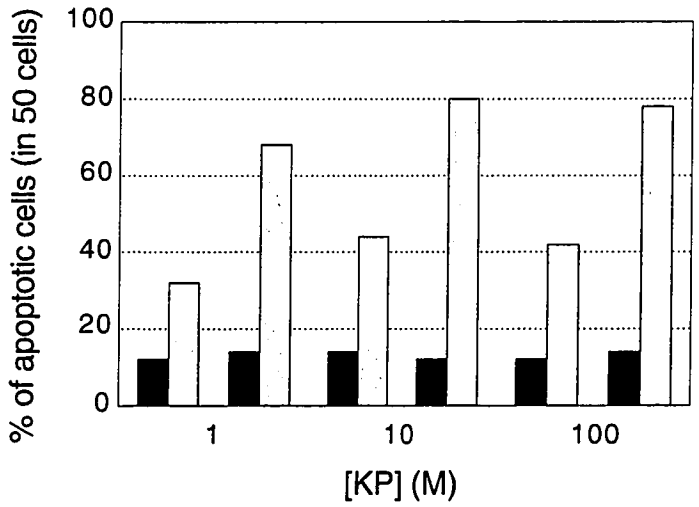

Figure 2.15: Percentage of apoptosis photo-induced by 0, 1, 10 and 100 μM KP in PBMC exposed to 230 mJ/cm² of SSR following the alkaline comet assay with no repair time (black) and 60 min repair time (gray). The first set (2 sets/concentration) was incubated in PBS pH 7.4 without resuspension and the second set was incubated in PBS 7.4 and resuspended into PBS 7.4.

Without any repair time, the percentage of apoptosis was well below 20%. This is reasonable since apoptosis is only expressed once the cells have been given the chance to repair. After 60 min repair time, a significant increase in the percentage of apoptosis is observed. The incubation in PBS (first set of bars for each KP concentration) seems to indicate that the cells are distressed since there is a 3-4-fold

increase in the percentage of apoptotic cells. This may be explained by the lack of proper nutrients in the PBS buffer for the cells to be properly maintained viable. As anticipated, the resuspension of the cells into PBS (second set of bars for each KP concentration) caused a 6-7-fold increase in the percentage of apoptotic cells. The results of this experiment indicate that both incubation in PBS and the resuspension into PBS, engender serious harm to the cells. From this point forward, cells were incubated in complete media and the resuspension step was eliminated from the protocol.

Many trials were conducted for each experiment described earlier as well as with several other experimental conditions which, so far, did not yield reproducible results. Based on some of these results (not shown), many varying theories on the role of photoexcited KP in DNA damage were proposed. However, with the lack of concrete evidence of KP photo-induced DNA damage on PBMC, serious reconsideration of the protocol was undertaken and a new protocol was developed.

2.6.4 Effect of UVA, UVB and SSR on NSAID Photo-Induced DNA Damage in PBMC

During the course of developing the new protocol for quantifying KP photo-induced DNA damage, Agapakis-Caussé *et. al.* published results confirming photo-induced DNA damage on human fibroblasts by TP as evidenced by the comet assay.[3] In order to confirm the ability of the new protocol in quantifying NSAID photo-induced DNA damage, the use of TP was implemented into the experiments as a positive control.

One major change to the protocol was the implementation of the casting step *before* irradiation. This eliminated the need for resuspension into PBS as the cells were mixed

with agarose and cast onto the Gelbond® film immediately after incubation with the drug. The implementation of this step also assured uniform irradiation of the samples from experiment to experiment and the opportunity for cells to repair before casting was basically eliminated.

Another change to the protocol was the preparation of drug-containing agarose solutions. In previous experiments, cells were centrifuged after incubation with KP and resuspended in PBS (or complete media) in order to remove the excess drug that had not been taken up by the cells. However, this most likely forced KP out of the cell in its attempt to equilibrate with the new surrounding solution. In the new protocol, aliquots were taken directly from the cell suspension incubated in complete media with the drug, and mixed with drug-containing agarose solutions, with the same drug concentration, and cast onto a Gelbond® film. This eliminated the possibility of the drug diffusing out of the cells by insuring its constant concentration within the cells. Keeping the NSAIDs in close proximity to cell components other than the cell nucleus, such as membranes, proteins, enzymes, greatly increases the chances of other types of damage occurring to those components. However, since all cell components, with the exception of DNA, are removed during cell lysis, this should have no repercussions on the expression of DNA damage.

As previously mentioned, low recovery of PBMC was observed during isolation; therefore, to facilitate their centrifugation out of the remaining gradient the PBMC fraction was diluted 2:1 with complete media.

Overnight lysis was also implemented into the protocol following results published by Banáth *et. al.* indicating that 16-24 h lysis is more reproducible in detecting DNA damage (*i.e.,* increased sensitivity) as a result of increasing the opportunity for DNA

unwinding and diffusion leading to an increase in the percentage of DNA migration during subsequent electrophoresis.[46]

Since the objective of these experiments is to establish if NSAIDs cause photo-induced DNA damage, assaying the cells immediately after exposure to the damaging agents (*i.e.*, no repair time) would confirm that the damage caused is a direct result from the effects of the photoexcited drugs. Eliminating repair time will, in turn, eliminate the expression of some of the UVB-induced DNA damage. Therefore, the rest of the experiments follow the protocol as stated in section 2.8.

Since these NSAIDs were compared in terms of their ability to cause DNA damage, it was important to determine their ability to absorb in the UV region of the electromagnetic spectrum (200-400 nm). KP and TP have very different absorption spectra (Figure 2.16).

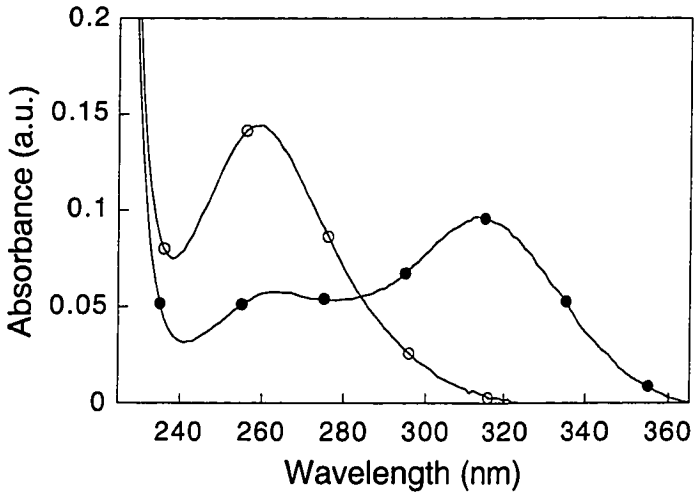

Figure 2.16: Absorbance spectra of 10 μM KP (O) and 10 μM TP (●); in PBS pH 7.4.

KP absorbs mostly in the UVC region (200-290 nm), with a maximum at around 260 nm and an extinction coefficient (ε) of 14 441 $M^{-1} \cdot cm^{-1}$, and extends all the way into the

UVB region. TP absorbs all across the UV region, from below 250 nm well into the UVA region with a maximum at 313 nm and an ε of 9 660 $M^{-1} \cdot cm^{-1}$.

For additional insight into the effect different radiation sources could have on NSAID photo-induced DNA damage in PBMC, the alkaline comet assay was carried out using SSR, UVB and UVA radiation under the same conditions for each experiment. Since no repair times were to be analyzed in these experiments, SSR doses were increased as high as 1149 mJ/cm^2 without concern of harming the cells as evidenced in a previous experiment (Figure 2.11). Preliminary experiments were conducted in order to determine the proper UVB radiation dose (results not shown); these results along with references from the literature,[21,22] led to the selection of 0, 23.1, 46.2, 69.3 and 92.4 mJ/cm^2 for UVB radiation doses. UVA radiation doses were 0, 402, 804 and 1206 mJ/cm^2; the dose rate for UVA lamps was reevaluated (refer to Appendix A). Table 2.1 shows the actual dose rate, irradiation time and dose range for each radiation source used for the experiments.

	UVA (320-400nm)	UVB (290-320nm)	SSR (UVA+UVB)
Dose rate (mW/cm^2)[a]	1.34	1.54	1.09
Irradiation Time	0-15 min	0-60 sec	0-17.5 min
Dose (mJ/cm^2)[b]	0-1206	0-92.4	0-1149

Table 2.1: Actual dose rate, irradiation time and dose range for UVA, UVB and SSR radiation. [a] Refer to Appendix A, B and C for determination of actual dose rate for UVA, UVB and SSR lamps respectively. [b] The dose is calculated by multiplying the dose rate by the irradiation time (in sec) in order to obtain a value in mJ/cm^2.

Less photo-induced DNA damage was anticipated for KP compared to TP when using a UVA radiation source since KP does not absorb in the UVA region. This effect could also be observed when a UVB radiation source is used since the absorption of TP is

maximal in the UVB region; however, KP exhibits a reasonable amount of tailing well into the UVB region of its absorption spectrum which could eliminate this phenomenon. Since SSR is a mixture of UVB as well as UVA radiation, the expected expression of photo-induced DNA damage in PBMC should be comparable between the two NSAIDs (if not considering their photochemistry).

Also, owing to their respective photochemistry, it is anticipated that the ability for TP to produce DNA damage will be immediate (*i.e.,* expressed at low doses of radiation) while that of KP will require an induction period. This phenomenon is mainly due to the fact that TP is able to generate noxious species upon absorption of a single photon, whereas KP requires subsequent photon absorption, specifically by the major photoproduct, in order to generate any noxious species. Due to the absorption properties of KP and TP, it is anticipated that prompt and delayed photo-induced DNA damage will be more apparent when the SSR or UVB radiation source is used, since both drugs absorb mostly in the UVB region.

The drug:base pairs molar ratio for the experiments was *ca.* 1 (using 10 μM drug and 6 X 10^6 cells/mL, refer to Appendix H for calculations). Results from a study on Φ_χ-174 DNA using a similar ratio, indicated that SSB formation was observed but with very little induced dimerization; furthermore, the photosensitization of pyrimidine dimers occurred only when the concentration of drug was sufficiently high (25 μM).[22] Therefore KP- or TP-photosensitized pyrimidine dimers are not anticipated to contribute to the formation of NSAID photo-induced DNA damage under the present conditions.

The following discussion is made possible with the help of Appendix A, B and C as they provide specific information regarding the different sources of radiation employed

in the experiments, namely UVA, UVB and SSR respectively. For relevant values pertaining to each radiation source, refer to Appendix G.

Using UVA radiation, drug concentrations of 5 μM did not display significant increases in DNA damage compared to the control until a UVA radiation dose of 804 mJ/cm^2 (for TP) and 1206 mJ/cm^2 (for KP) was reached (Figure 2.17A). This result is the same as that obtained by Agapakis-Caussé *et.al.*[3] confirming that this technique can, in fact, measure NSAID photo-induced DNA damage. At drug concentrations of 10 μM, a significant increase in DNA damage is observed with TP as soon as 402 mJ/cm^2 of UVA radiation while KP only exhibits significant DNA damage compared to the control at the highest dose of UVA radiation (1206 mJ/cm^2) (Figure 2.17B). Under these conditions, the DNA damage produced by TP is always higher than that of KP regardless of the UVA radiation dose. When the difference in tail moment compared to the controls is plotted (Figure 2.18A and B), the immediate onset of photo-induced DNA damage by TP is clear, whereas that of KP is considerably delayed. The output of the UVA lamps combined with the absorbance spectra of the drugs, indicate that TP is much more likely to absorb UVA than KP. Although evidence of prompt and delayed photo-induced DNA damage is definite, the inability of KP to absorb the incident radiation can account for the very low amounts of expressed DNA damage by KP. Also, the low susceptibility to harm of the cells by this source of UVA radiation is suggested by the results since DNA damage to the controls was minimal.

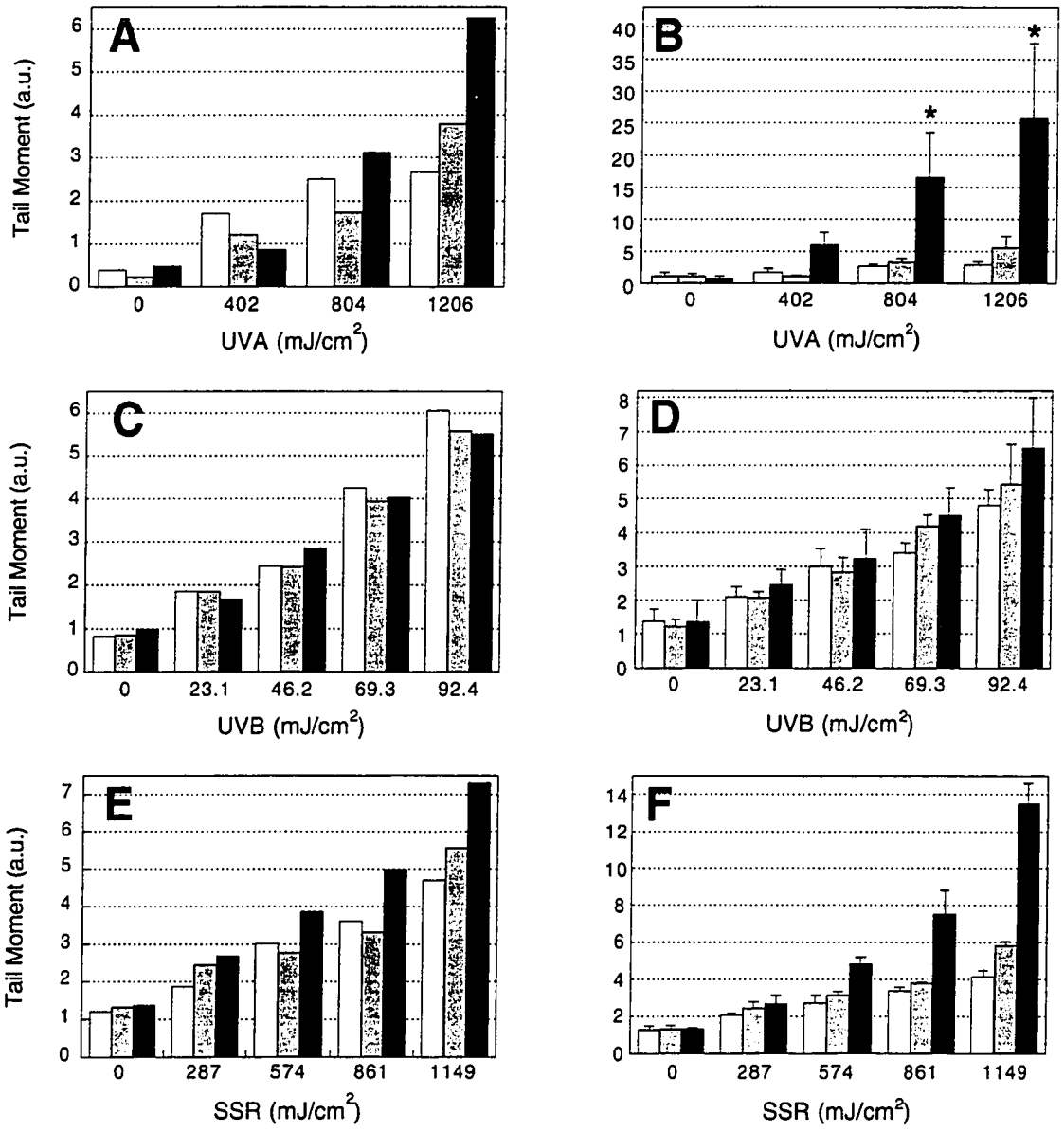

Figure 2.17: DNA damage photo-induced by no drug (white), KP (gray) and TP (black) in PBMC following the alkaline comet assay. A, C and E were exposed to 5 μM drug concentration while B, D and F were exposed to 10 μM drug concentration. Each pair of horizontal panels has been obtained with the same radiation source.

One important finding to point out is the high tail moment values obtained for TP at 10 μM following 804 and 1206 mJ/cm² of UVA radiation (black bars marked with an

asterisk in Figure 2.17B). The comets contained in these samples were mostly 'apoptotic-looking'. It was originally thought that the cells had suffered heat damage from the high radiation dose; however, preliminary results indicated that this dose of UVA radiation did not promote such damage (*vide supra*). Also, the control as well as the sample containing KP, were irradiated together with the TP sample, as they were all on the same Gelbond® film, and no signs of heat damage (or 'apoptotic-looking' cells) were observed in these samples. This led to the conclusion that TP was responsible for causing the observed DNA damage; however, the mechanism by which this damage may have caused 'apoptotic-looking' cells remains unknown.

Using UVB radiation, drug concentrations of 5 μM did not display significant increases in DNA damage compared to the control at any of the UVB radiation doses used (Figure 2.17C). This could be due to the low concentration of the drug (half that of the physiological concentration) making it impossible for the photo-induced DNA damage caused by TP or KP to exceed that photo-induced by the UVB radiation. At drug concentrations of 10 μM, an increase in DNA damage is observed with both TP and KP at UVB radiation doses of 69.3 and 92.4 mJ/cm^2, with TP exhibiting more DNA damage than KP (Figure 2.17D). When the difference in tail moment compared to the controls is plotted (Figure 2.18C and D), it becomes more evident that a 5 μM drug concentration is too low to produce DNA damage above that photo-induced by UVB radiation. However, at a drug concentration of 10 μM, the immediate onset of photo-induced DNA damage by TP is clear, whereas that of KP is considerably delayed and lower. It was anticipated that KP and TP would exhibit similar patterns of photo-induced DNA damage (if only the absorption properties were considered) as both drugs are capable of absorbing the UVB radiation, albeit TP absorbs more than KP.

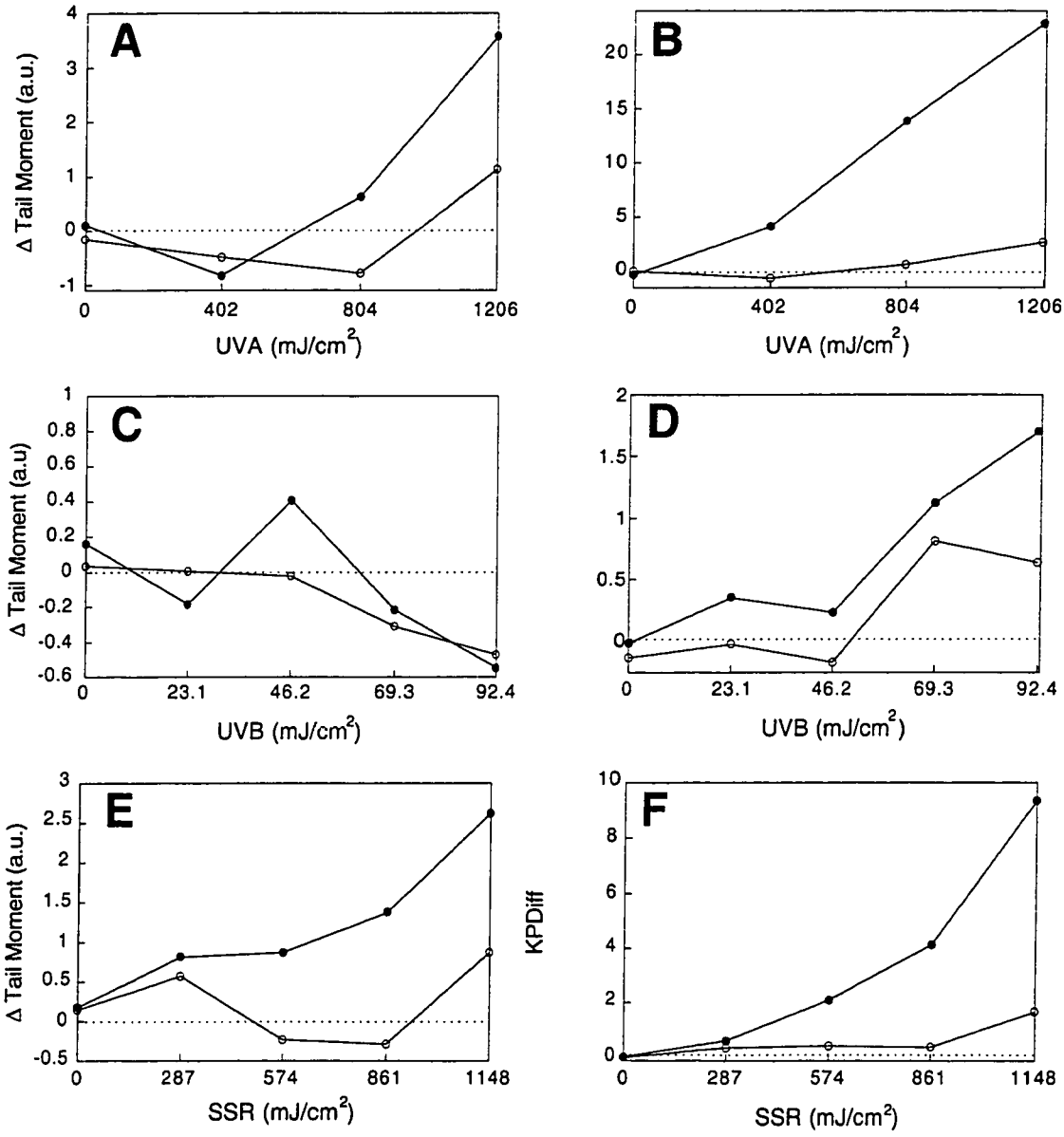

Figure 2.18: Difference in DNA damage photo-induced by KP (O) and TP (●) compared to control in PBMC following the alkaline comet assay. A, C and E were exposed to 5 μM drug concentration while B, D and F were exposed to 10 μM drug concentration. Each pair of horizontal panels has been obtained with the same radiation source.

However, in this case, it is evident that their photochemistry plays a role in the manifestation of prompt and delayed photo-induced DNA damage by these drugs. Also, the occurrence of high tail moment values for the controls confirms the great susceptibility of the cells to UVB radiation (*i.e.,* the background DNA damage is increased).

Using SSR, drug concentrations of 5 μM displayed an immediate onset of photo-induced DNA damage with TP compared to controls, while those with KP did not show significant DNA damage above controls until the highest dose of 1149 mJ/cm^2 of SSR (Figure 2.17E). At drug concentrations of 10 μM, TP repeatedly causes more DNA damage than KP at all radiation doses; furthermore, the TP photo-induced DNA damage increases at all doses whereas KP exhibits little significant DNA damage compared to the control even at the highest dose of SSR radiation (Figure 2.17F). When the difference in tail moment compared to the controls is plotted (Figure 2.18E and F), the immediate onset of photo-induced DNA damage by TP is evident at both drug concentrations, whereas that of KP is practically nonexistent. The absorbance of TP is much greater than that of KP with SSR; however, KP does exhibit the capability of absorption from this radiation source. Therefore, with longer irradiation times, the confirmation of prompt and delayed NSAID photo-induced DNA damage with SSR could potentially be confirmed. The susceptibility to harm by this source of SSR exhibited by the cells is confirmed by the constant increase in tail moment values of the controls.

It is interesting to note however, that tail moment values obtained from the experiment with the UVB radiation source are comparable (albeit still lower) to those values obtained with either SSR or UVA radiation sources even though the radiation dose is

ca. 10 times lower. The relatively lower tail moment values obtained when UVB radiation is used may be explained by the weak reduction in the electrophoretic mobility of the DNA that may be attributed to the formation of pyrimidine dimers which are UVB-induced DNA damage that did not lead to ALS. Those dimers, although not explicitly expressed as DNA damage, will still affect the shape of the comets obtained.[21]

The smallest difference in DNA damage compared to the controls is exhibited with the UVB radiation source, where TP shows a maximal difference of *ca.* 1.75 while KP shows a maximal difference of only 0.75 at the highest UVB radiation dose of 92.4 mJ/cm^2 and drug concentrations of 10 μM. This can be explained by the fact that pyrimidine(6-4)pyrimidone dimers generated as a result of UVB radiation absorption by the DNA are ALS[56] and are converted to SSBs during the unwinding step of the comet assay hereby increasing the amount of background DNA damage observed. Whereas this outcome is not as dramatic with the SSR source, this effect is virtually non-existent with the UVA radiation source owing to its UVB component of less than 2%. Therefore, UV-induced photoproduct formation is greatly reduced when conducting experiments using UVA radiation or SSR.

Experiments using 5 μM NSAID solutions (Graphs A, C, E of Figures 2.17 and 2.18) were carried out only once; therefore, each tail moment value corresponds to an average of over 50 cells (N = 1). Experiments using 10 μM NSAID solutions (Graphs B, D and F of Figures 2.17 and 2.18) were repeated three times using a different donor for each experiment; therefore, each tail moment value corresponds to an average over 150 cells (N = 3).

The use of the different radiation sources did exhibit some differences in the expression of NSAID photo-induced DNA damage; however, these differences are not believed

to be associated with the NSAIDs' absorption capacity since the same trend is observed for KP and TP with all the radiation sources. The prompt and delayed trend exhibited by TP and KP respectively is attributed entirely to their photochemical properties.

2.7 Conclusion

Results of NSAID photo-induced DNA damage in human PBMC measured using the alkaline comet assay have been presented. A protocol for detecting NSAID photo-induced DNA damage in living cells was also developed which established proper sample preparation in order to obtain reproducible results. The neutral version of the comet assay, carried out using HL60 cells, revealed that KP photo-induced DNA damage did not lead to apoptosis. For both the 24 and 48 h timepoints, the percentage of apoptosis remained below 5%, indicating that HL60 cells can sustain and possibly recover from this damage. Using different radiation sources (UVA, UVB and SSR) to conduct similar experiments, it was established that TP promptly produces DNA damage while KP produces DNA damage in a delayed fashion. This prompt and delayed mechanism of producing DNA damage was attributed to the NSAIDs' different photochemical properties. This results in the detection of TP photo-induced DNA damage at relatively low doses of UV radiation (402, 23.1 and 237 mJ/cm^2 for UVA, UVB and SSR respectively), whereas KP requires higher UV doses to produce significant amounts of DNA damage. Evidence of the PBMC susceptibility to UVB-induced DNA damage was demonstrated using the UVB and SSR radiation sources as the tail moment values for the controls were significantly increased compared to those obtained with the UVA radiation source. The results obtained from these experiments mark the first account of NSAID photo-induced DNA damage in living cells. The comet assay combined with the protocol developed within could remarkably contribute to the assessment of the phototoxicity of other NSAIDs in living cells.

2.8 Experimental

2.8.1 Introduction

No previous protocol exists on the application of the alkaline comet assay designed to measure NSAID photo-induced DNA damage in living cells. The conventional version by Singh *et. al.*[57] was; therefore, implemented as a starting point and many changes have been made in order to amplify the expression of DNA damage in living cells. The protocol described here reflects the final version of the amended alkaline comet assay, fit to analyze NSAID photo-induced DNA damage; any changes derived leading up to this version are explicitly detailed in Section 2.6. The experiments in their entirety were performed under reduced lighting.

2.8.2 Materials

HL60 cells were obtained from American Type Culture Collection (Rockville, MD, USA). Fetal calf serum (FCS) was from Immunocorp (Montréal, PQ, Canada). RPMI Medium 1640, 0.1 μm filtered without L-glutamine, L-glutamine in 85% NaCl and Hank's balanced salt solution without phenol red, 0.1 μm filtered (HBSS) were from Gibco BRL Life Technologies (Grand Island, NY, USA). Histopaque®-1077 was obtained from Sigma Diagnostics Inc. (St-Louis, MO, USA). Ketoprofen (KP), fluorescein diacetate, ethidium bromide (EtBr), N-lauryl sarcosine sodium salt (SLS) and 8-hydroxy-1-azanaphthalene (8-hydroxyquinoline) were obtained from Sigma Chemical Company (St-Louis, MO, USA). Tiaprofenic acid (TP) was a gift from Dr. Miguel Miranda (Universidad Politécnica de Valencia, Spain). SYBRGold® nucleic acid stain was obtained from Molecular Probes (Eugene, OR, USA). Agarose high strength,

analytical grade, ultra pure DNA grade (low-melting point (LMP) agarose) was obtained from Bio-Rad Laboratories (Hercules, CA, USA). Dimethyl sulfoxide (DMSO), trishydroxymethylaminomethane (Tris base), acetone, ammonium acetate, sodium hydroxide (NaOH), sodium tetra ethylene diamine tetraacetate (EDTA), sodium phosphate monobasic ($NaH_2PO_4 \cdot 2H_2O$) and sodium phosphate dibasic (Na_2HPO_4) were obtained from Fischer Scientific (Fairlawn, NJ, USA). Iso-octylphenoxypolyethoxy-ethanol (Triton X-100) and sodium chloride (NaCl) were from BDH (Toronto, ON, Canada). Anhydrous ethyl alcohol (ethanol) was obtained from Commercial Alcohols Inc. (Brampton, ON, Canada). Proteinase K was obtained from Boehringer Mannhein (Indianapolis, IN, USA). The TAE buffer (0.4 M Tris acetate, 0.2 M glacial acetic acid, 0.1 M EDTA), 10X pH 8.4 was from Roche Diagnostics (Manheim, Germany). Trend domestic bleach, containing 5.25% sodium hypochloride, was from Dutch Distributions Inc. (Weston, ON, Canada). All solvents and chemicals were used without further purification.

2.8.3 Preparation of Solutions

All solutions were prepared with 18 MΩ water (ddH_2O) (Milli-Q plus PF unit, Millipore Corp., Bedford, MA, USA). The culture media, RPMI 1640, was supplemented with 2 mM L-glutamine and 10% FCS to give complete media. Fluorescein diacetate was prepared at 5 mg/mL in acetone. The EtBr solution was prepared at 200 μg/mL in HBSS. The working viability stain was prepared by adding 50 μL of the EtBr solution and 7.5 μL of the fluorescein diacetate solution to 1.2 mL of HBSS. The freezing solution consisted of 10% 0.2 μm filtered (Acrodisc, low protein binding, Gelman Sciences, Ann Arbor, MI, USA) DMSO in complete media. The lysis A buffer

consisted of 2.5 M NaCl, 100 mM EDTA, 10 mM Tris base, 1% SLS, adjusted to pH 10 in ddH_2O, 1% Triton X-100 and 10% DMSO were added to the lysing solution immediately before use, to assist in the removal of cellular proteins. The 1X TE buffer consisted of 10 mM Tris base and 1 mM EDTA at pH 7.4. The proteinase K stock solution was prepared at 20 mg/mL in TE buffer, 0.2 μm filtered and stored in 2-mL aliquots at -30°C. The lysis B buffer consisted of 2.5 M NaCl, 100 mM EDTA, 10 mM Tris base in ddH_2O, adjusted to pH 10. Proteinase K at 1 mg/mL was added to the lysis buffer B immediately before use. The alkaline unwinding/electrophoresis buffer consisting of 300 mM NaOH, 0.1% 8-hydroxyquinoline, 10 mM EDTA, 2% DMSO in ddH_2O, was adjusted to pH 13.1 and protected from light. The ammonium acetate solution was prepared at 1 M in ddH_2O. The PBS solution consisted of 58 mM Na_2HPO_4, 17 mM $NaH_2PO_4 \cdot 2H_2O$ and 68 mM NaCl in ddH_2O to achieve a pH of 7.4. All agarose solutions were prepared in PBS pH 7.4 to 0.75% or 1% consistency (w/v). The gold nucleic acid dye staining solution was prepared by adding 5 μL of SYBRGold® to 50 mL of ddH_2O (1:10 000 dilution of the stock solution supplied by Molecular Probes) and the solution was stored at 4°C and protected from light. The bleaching solution contained 70% domestic bleach in water.

All drug-containing solutions along with their corresponding blank solutions were protected from light. A stock solution for each drug was prepared by mixing the dry drug with DMSO and subsequently taking a 100 μL aliquot and mixing with complete media to achieve the desired concentration. For example, 0.025 g of KP was added to 1 ml of DMSO, 100 μL of this solution was added to 9.9 mL of complete media to obtain a concentration of 1 mM. This method was used to avoid having to weigh very small amounts of the dry drug and to minimize the quantity of DMSO being added to

the cells. The stock solution was sterilized by passing it through a 0.2 μm filter. Most experiments were carried out using drug concentrations of 10 μM (physiological concentration) and 5 μM; therefore, solutions of 100 μM and 50 μM were prepared from the stock solution in complete media and were to be used for incubation of the cells in a 1:10 dilution. Drug solutions of 40 μM and 20 μM were prepared from the stock solution in complete media and were to be used in preparation of the drug-containing agarose solutions in a 1:4 dilution.

Drug-containing agarose solutions were prepared in order to prevent the drugs from leaching out of the cells when cast into the agarose. The volume of drug-containing agarose prepared depended on the volume needed to cast all the gels for a particular experiment. Generally, the drug solutions were mixed in a 1:4 dilution with 1% LMP agarose to obtain the desired drug concentrations in 0.75% LMP agarose. For example, in an experiment requiring 10 gels to be cast, 3 mL of drug-containing agarose was prepared since 270 μL of agarose is needed (mixing volume) for each gel; therefore, 0.750 μL of the drug solution was added to 2.25 mL 1% LMP agarose.

Blank drug solutions as well as blank drug-containing agarose solutions were prepared to act as controls. Blank solutions were prepared in the exact same fashion as drug-containing solutions, but without the drug, so as to achieve the best possible control solutions.

2.8.4 Cell Viability and Concentration Determination

To determine the cell concentration and viability, an aliquot of the cell suspension (50 μL) was taken and mixed with viability stain (50 μL) then dispensed onto a hemacytometer (refer to Appendix J for cell concentration determination technique) and

examined with a fluorescence microscope (Olympus BX-60, Olympus Optical Co., Japan) at 20X (UPlanAPO objective), fitted with a U-MNB (blue band) filter cube. Under these conditions, non-viable cells appeared red, while viable cells fluoresced green due to the conversion of fluorescein diacetate to fluorescein by membrane esterases in metabolically competent (viable) cells.[58] This method allowed for the concentration determination of the cells/mL.

2.8.5 HL60 Cell Line: Culture, Growth Curves and Freezing

HL60 cells were gently thawed from deep freeze conditions to 37°C in a water bath and added to 9 mL of complete media (pre-warmed to 37°C). Cells were grown in a 100 mm culture dish incubated at 37°C with a 5% carbon dioxide (CO_2) atmosphere, in excess humidity. Cell viability and concentration were determined daily to assure proper growth and cells were sub-cultured at 5 X 10^5 cells/mL confluence. Cell cultures were maintained under these conditions for as long as cells were needed for experiments. Experiments were conducted at confluences of *ca.* 1 X 10^5 cells/mL. If cells were contaminated or no longer needed, they were simply bleached in order to destroy all biological matter.

For the construction of growth curves, cells, at an initial confluence of 1 X 10^5 cells/mL, were subjected to the damaging agents and left to grow for 5 days while their viability and their concentration was determined daily. Damaging agents included: KP at concentrations of 1 μM, 10 μM and 100 μM and UVA radiation at doses of 771, 1052, 1541 or 2105 mJ/cm^2. Treated and untreated controls were also carried out; whereas treated controls for KP received the vehicle only (DMSO) and UVA radiation controls were put into the photoreactor chamber with the lamps off for the same time lapse as

the experiment, the untreated controls were left to grow without any manipulation whatsoever.

During the 3rd passage, one cell culture, that had reached 5 X 10^5 cells/mL confluence, was frozen for future culturing. The cell culture was centrifuged at 1500 rpm for 10 min. The supernatant was removed and 10 mL of freezing solution was added. The cell suspension was dispensed into 1 mL freezing vials and stored in a deep freezer at –86°C.

2.8.6 Isolation of Peripheral Blood Mononuclear Cells (PBMC)

All plasticware used during the isolation process was made of polypropylene and high binding plastics, such as polystyrene, were avoided as they bind cells to the centrifuge tube walls. A 10 mL human WB draw was collected into heparinized (10-20 U/mL) Vacutainer tubes (Becton Dickinson, NJ, USA). The WB was mixed with complete media in a 1:1 dilution then underlayed with 20 mL of Histopaque®-1077 and gradient-centrifuged for 60 min at 1500 rpm; both the complete media and Histopaque®-1077 should be brought to room temperature prior to isolation. The Histopaque®-1077 solution, consisting of polysucrose (5.7 g/dL) and sodium diatrizoate (9.0 g/dL) adjusted to a density of 1.077 ± 0.001 g/mL, is a medium that facilitates rapid recovery of viable mononuclear cells from small volumes of blood. During centrifugation, erythrocytes and granulocytes are aggregated by polysucrose and rapidly sediment; whereas, lymphocytes and other mononuclear cells remain at the plasma-Histopaque interface. The PBMC (Scheme 2.5) was carefully removed and transferred into a clean tube.

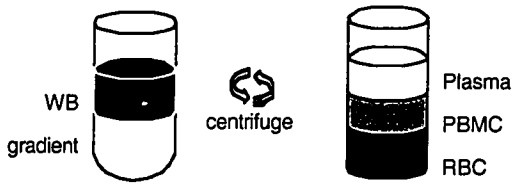

Scheme 2.5: Isolation of PBMC by centrifugation of WB through a gradient.

A cell count of the PBMC was carried out to determine the concentration in cells/mL. The PBMC was diluted 2:1 with complete media, to ease the centrifugation, separated into two tubes and centrifuged for 30 min at 1500 rpm. The supernatant was removed and both pellets were resuspended with 1 mL complete media and pooled into one of the tubes. The other tube was washed with 1 mL of complete media and added to the first tube (3 mL total). A cell count was carried out to determine concentration in cells/mL. The ideal cell suspension concentration for an experiment is 5 X 10^5 cells/mL; however, if the PBMC recovery was efficient (expected recovery of PBMC from WB is 30%), concentration to 1 X 10^6 cells/mL was carried out in order to reduce the volume of the cell suspension. A volume of 1 mL from the cell suspension was dispensed into as many 1.5 mL centrifuge tubes as there were drug concentrations in the experiment. For example, if 2 drugs were used at 2 different concentrations, then the cell suspension was dispensed into 6 centrifuge tubes; 2 for the first drug, 2 for the second drug and 2 for the blanks (control) of each drug. A volume of 110 µL (1:10 dilution) of the corresponding drug solution was added to each centrifuge tube and the tubes were incubated at 37°C with 5% CO_2 and in excess humidity for 1 h.

2.8.7 Casting onto Gelbond® Film

One major change made to the slide preparation technique developed by Olive *et. al.*[44] was the implementation of the casting of the cells, embedded in agarose, onto

Gelbond® films (agarose gel support medium from BioWhittaker Molecular Applications, Rockland, ME, USA) as opposed to the 'sandwich' procedure. The 'sandwich' technique required placing a layer of agarose onto a non-frosted slide, then applying a layer of the agarose-embedded cells and covering this with another layer of agarose; leaving the cells in the middle layer of the 'sandwich'. This technique had many problems, one of which was the inevitable occurrence of the 'sandwich' sliding off the slide; therefore, very careful manipulations were required. The use of Gelbond® film, a flexible support consisting of an agarose-coated polyester sheet, requires only a single layer of agarose-embedded cells to be permanently affixed to the Gelbond® film. This technique allows for the easy manipulation of the gels through the various buffers and for the creation of permanent slides.

Gelbond® films were cut in 6 cm X 10 cm dimension to accommodate up to 6 gels of 2 cm^2 each. Each experimental condition was cast in duplicate. Usually, three conditions were cast/Gelbond® film, one under the other, and the duplicates were side by side. A volume of 60 μL of the drug-incubated cell suspension was mixed with 540 μL of the corresponding drug-containing agarose solution, warmed to 42°C, (mixing volume of 600 μL; a 1:10 dilution of the cells). A volume of 120 μL of this solution was immediately dispersed into a 2 cm^2 casting chamber temporarily glued to the Gelbond® film, as previously described.[59] Once the gels were solidified, the casting chambers were carefully removed from the Gelbond® film and the samples of agarose-embedded cells, now attached to the Gelbond® film, were ready for irradiation.

2.8.8 Irradiation

UVA and UVB radiation experiments were carried out in a photoreactor (Luzchem Inc., Morin Heights, Québec, Canada), a 35 X 35 X 30 cm^3 box with aluminum chamber walls, equipped with an air extractor fan on the back wall and 8 horizontal light source sockets, 4 cm apart, on the ceiling of the box, 15 cm from the samples. For UVA radiation experiments in Sections 2.6.1 and 2.6.2, a combination of 4 and 8 RPR-3500 8 W lamps (Branford, CN, USA) were used in the 1, 3, 6 and 8, and 1-8 positions respectively, of the irradiation chamber (refer to Appendix D for the dose rate calculation). For UVA radiation experiments in Section 2.6.4, 5 RPR-3500 8 W lamps (Branford, CN, USA) emitting on average 1.34 mW/cm^2 were used in the 1, 3, 5, 6 and 8 positions of the irradiation chamber (refer to Appendix A for UVA lamps specifications). Irradiation doses were usually between 0-1156 mJ/cm^2. For UVB radiation experiments, 4 RPR-3000 4 W lamps (Branford, CN, USA) emitting on average 1.54 mW/cm^2 were used in the 1, 3, 6 and 8 position of the irradiation chamber (refer to Appendix B for UVB lamps specifications). Irradiation doses were usually between 0-92.4 mJ/cm^2.

A solar simulator, consisting of an ozone-free 300 W Xenon short arc lamp (Oriel, CN, USA) emitting 1.07 mW/cm^2 UVA radiation (320-400 nm) and 0.019 mW/cm^2 UVB radiation (290-320 nm) for a total dose rate of 1.09 mW/cm^2, was used for solar simulated irradiations. The radiation emitted from the solar simulator is comparable to the solar spectrum at 45° latitude at noon on the 21st of June (refer to Appendix C for SSR specifications).[60] Irradiation doses were usually between 0-1149 mJ/cm^2.

Irradiations were carried out on ice to prevent the sample from heating up as well as DNA repair in the cells. The individual Gelbond® films were placed onto a 150 mm ice-

filled petri dish which was placed in the center of the photoreactor floor, *ca.* 15 cm from the lamps.

2.8.9 The Neutral Comet Assay

The neutral version of the comet assay was conducted according to the method initially introduced by Ostling and Johanson,[41] subsequently enhanced by Olive *et. al.*[43] and modified by McNamee *et. al.*[61] Each of the buffers in the neutral comet assay was contained in 150 mm petri dishes. Immediately after irradiation and subsequent casting, the gels were submerged in 50 mL of lysis A buffer and left at 37°C for 1 h. After 60 min, the gels were removed from the lysing solution, rinsed with ddH_2O, submerged in 50 mL of neutral 1X TAE buffer and kept at room temperature for 30 min. Then, the gels were placed in a submarine gel electrophoresis chamber (Hoefer® HE33 Mini Horizontal Submarine Unit from Pharmacia Biotech Inc., San Francisco, CA, USA) filled with 220 mL of fresh 1X TAE buffer, and electrophoresis was performed at a constant 19 V, 300 mA/chamber, for 2 min at room temperature. After electrophoresis, the gels were rinsed with ddH_2O and covered with 50 mL of ethanol for 2 h, then removed and dried overnight before staining with the SYBRGold® staining solution.

2.8.10 The Alkaline Comet Assay

The alkaline comet assay was conducted according to the method introduced by Singh *et. al.*[57] and modified by McNamee *et. al.*[59] Each of the buffers in the alkaline comet assay was contained in 150 mm petri dishes. Immediately after irradiation, the gels were submerged in 50 mL of ice cold lysis A buffer and kept at 4°C overnight. After at least 14 h,[46] the gels were removed from the lysing solution, rinsed with ddH_2O,

submerged in 50 mL of alkaline unwinding buffer and kept in the dark at room temperature for 30 min. After the unwinding period, the gels were placed in a submarine gel electrophoresis chamber (Hoefer® HE33 Mini Horizontal Submarine Unit from Pharmacia Biotech Inc., San Francisco, CA, USA) filled with 220 mL of fresh alkaline unwinding buffer, and electrophoresis was performed at a constant 19 V, 300 mA/chamber, for 20 min at room temperature. After electrophoresis, the gels were rinsed with ddH_2O, submerged in 50 mL of a 1 M ammonium acetate solution and left for 30 min at room temperature. After 30 min, the gels were rinsed with ddH_2O and covered with 50 mL of ethanol for 2 h, then removed and dried overnight before staining with the SYBRGold® staining solution.

2.8.11 Statistical Measurement of DNA Damage

The samples were analyzed as previously described.[59] The dried agarose gels were cut in a way that only one experiment condition, along with its duplicate, would fit a microscope slide (75 mm X 25 mm). The gels were stained for *ca.* 5 min in a fresh solution of SYBRGold®, rinsed with ddH_2O, then mounted onto a glass slide. A 50 mm X 22 mm glass cover slip was gently but firmly applied onto the gels, removing excess water and forming a tight seal. Gold stained comets were visualized under a fluorescence microscope (Olympus BX-60F5, Olympus Optical Co., Japan) at 60X (UPlanFI oil objective), fitted with a U-MNB (blue band) filter cube. Comet images were captured with a Hitachi KP-D581U, CCD color digital camera (Hitachi Deushi Ltd, Japan) and the images were analyzed using the Alkomet v3.1 (Richard Branker Research Ltd, Ottawa, ON, Canada) image analysis system. Samples were blinded

and for each gel, a minimum of 50 cells were randomly selected and measured for tail ratio, tail moment, comet length and tail length.

2.9 References

(1) Diffey, B. L.; Brown, S., A Method for Predicting the Phototoxicity of Non-Steroidal Anti-Inflammatory Drugs, *Br. J. Pharmac.*, **1983**, 16, 633-638.

(2) Artuso, T.; Bernadou, J.; Meunier, B.; Paillous, N., DNA Strand Breaks Photosensitized by Benoxaprofen and Other Nonsteroidal Anti-Inflammatory Agents, *Biochem.Pharmacl.*, **1990**, 39, 407-413.

(3) Agapakis-Caussé, V.; Boscá, F.; Castell, J. V.; Hernández, D.; Marín, M. L.; Marrot, L.; Miranda, M. A., Tiaprofenic Acid-Photosensitized Damage to Nucleic Acids: A Mechanistic Study Using Complementary *in vitro* Approaches, *Photochem. Photobiol.*, **2000**, 71, 499-505.

(4) Boscá, F.; Marín, M. L.; Miranda, M. A., Photoreactivity of the Nonsteroidal Anti-Inflammatory 2-Arylpropionic Acids with Photosensitizing Side Effects, *Photochem.Photobiol.*, **2001**, 74, 637-655.

(5) Lu, X.; Fairbairn, D. W.; Bradshaw, W. S.; O'Neil, K. L.; Ewert, D. L.; Simmons, D. L., NSAID-Induced Apoptosis in Rous Sarcoma Virus-Transformed Chicken Embryo Fibroblasts is Dependent on v-src and c-myc and is Inhibited by bcl-2, *Prostaglandins*, **1997**, 54, 549-568.

(6) Cosa, G.; Martínez, L., J.; Scaiano, J. C., Influence of Solvent Polarity and Base Concentration on the Photochemistry of Ketoprofen: Independent Singlet and Triplet Pathways, *Phys.Chem.Chem.Phys.*, **1999**, 1, 3533-3537.

(7) Condorelli, G.; Costanzo, L. L.; De Guidi, G.; Giuffrida, S.; Miano, P.; Sortino, S.; Velardita, A., Photosensitization Induced by Non Steroidal Anti Inflammatory Drugs: An Overview of Molecular Mechanisms in Biological Systems, *Newsletter*, **1996**, 58, 66-77.

(8) Bezzant, J. L. www.medlib.med.utah.edu/kw/derm/melanoma/etio.htm, 1997.

(9) Hölzle, E.; Newmann, N.; Hausen, B.; Przybilla, B.; Schauder, S.; Hönigsmann, H.; Bircher, A.; PLewig, G., Photopatch Testing: The Five Year Experience of the German, Austrian and Swiss Photopatch Test Group., *J.Am.Acad.Dermatol.*, **1991**, 25, 59-68.

(10) Bagheri, H.; Lhiaubet, V.; Montastruc, J.; Chouinni-Lalanne, N., Photosensitivity to Ketoprofen, Mechanisms and Pharmacoepidemiological Data, *Drug Safety*, **2000**, 22, 339-349.

(11) de Jalón, E. G.; Josa, M.; Campanero, M. A.; Santoyo, S.; Ygartua, P., Determination by High-Performance Liquid Chromatography of Ketoprofen *in vitro* in Rat Skin Permeation Samples, *J. Chromatogr. A*, **2000**, 870, 143-149.

(12) Boscá, F.; Carganico, G.; Castell, J. V.; Gómez-Lechón, M. J.; Hernandez, D.; Mauleón, D.; Martínez, L. A.; Miranda, M. A., Evaluation of Ketoprofen (R, S and R/S) Phototoxicity by a Battery of *in vitro* Assays, *J. Photochem. Photobiol. B: Biol.*, **1995**, 31, 133-138.

(13) Mozzanica, N.; Pigato, P. D., Contact and Photocontact Allergy to Ketoprofen: Clinical and Experimental Study, *Contact Dermatitis*, **1990**, 23, 336-340.

(14) Ljunggren, B., Propionic Acid-Derived Non-Steroidal Anti-Inflammatory Drugs Are Phototoxic *in vitro*, *Photodermatology*, **1985**, 2, 3-9.

(15) Costanzo, L. L.; De Guidi, G.; Condorelli, G.; Cambria, A.; Fama, M., Molecular Mechanism of Drug Photosensitization - II. Photohemolysis Sensitized by Ketoprofen, *Photochem. Photobiol.*, **1989**, 50, 359-365.

(16) Boscá, F.; Miranda, M. A.; Carganico, G.; Mauleón, D., Photochemical and Photobiological Properties of Ketoprofen Associated with the Benzophenone Chromophore, *Photochem. Photbiol.*, **1994**, 60, 96-101.

(17) Chignell, C. F.; Sik, R. H., Magnetic Field Effects on the Photohemolysis of Human Erythrocytes by Ketoprofen and Protoporphyrin IX, *Photochem.Photobiol.*, **1996**, 62, 205-207.

(18) Hilleman, B., Health Effects of Electromagnetic Fields Remain Unsolved, *Chem.Eng.News*, **1993**, , 15-29.

(19) Moser, J.; Sarabia, Z.; Minter, H.; Lovell, W. W.; Beijersbergen van Henegouwen, G. M. J., Photobinding of Ketoprofen *in vitro and ex vivo*, *J.Photochem.Photobiol.B.: Biol.*, **2000**, 58, 37-45.

(20) Chuang, V. T. G.; Kuniyasu, A.; Nakayama, H.; Matsushita, Y.; Hirono, S.; Otagiri, M., Helix 6 of Subdomain III A of Human Serum Albumin is the Region Primarily Photolabeled by Ketoprofen, an Arylpropionic Acid NSAID Containing a Benzophenone Moiety, *Biochim.Biophys.M.*, **1999**, 1434, 18-30.

(21) Artuso, T.; Bernadou, J.; Meunier, B.; Piette, J.; Paillous, N., Mechanism of DNA Cleavage Mediated by Photexcited Non-Steroidal Antiinflammatory Drugs, *Photochem. Photobiol.*, **1991**, 54, 205-213.

(22) Chouinni-Lalanne, N.; Defais, M.; Paillous, N., Nonsteroidal Antiinflammatory Drug-Photosensitized Formation of Pyrimidine Dimer in DNA, *Biochem. Pharmacol.*, **1998**, 5, 441-446.

(23) De Guidi, G.; Giuffrida, S.; Condorelli, G.; Costanzo, L. L.; Miano, P.; Sortino, S., Molecular Mechanism of Drug Photosensitization. IX. Effect of Inorganic Ions on DNA Cleavage Photosensitized by Naproxen, *Photochem.Photobiol.*, **1996**, 63, 455-462.

(24) Martínez, L. J.; Scaiano, J. C., Characterization of the Transient Intermediates Generated from the Photoexcitation of Nabumetone: A Comparison with Naproxen, *Photochem. Photobiol.*, **1998**, 68, 646-651.

(25) Castell, J. V.; Gomez-Lechon, M. J.; Hernandez, D.; Martínez, L. A.; Miranda, M. A., Molecular Basis of Drug Phototoxicity: Photosensitized Cells Damage by the Major Photoproducts of Tiaprofenic Acid, *Photochem. Photobiol*, **1994**, 60, 586-590.

(26) Miranda, M. A.; Castell, J. V.; Hernandez, D.; Gomez-Lechon, M. J.; Bosca, F.; Morera, I. M.; Sarabia, Z., Drug-Photosensitized Protein Modification: Identification of the Reactive Sites and Elucidation of the Reaction Mechanism with Tiaprofenic Acid/Albumin as Model System, *Chem.Res.Toxicol.*, **1998**, 11, 172-177.

(27) Castell, J. V.; Hernandez, D.; Gomez-Lechon, M. J.; Lahoz, A.; Miranda, M. A.; Morera, D.; Perez-Prieto, J.; Sarabia, Z., Photobinding of Tiaprofenic Acid and Suprofen to Proteins and Cells. A Combined Study Using Radiolabeling, Antibodies and Laser Flash-Photolysis of Model Bichromophores, *Photochem.Photobiol.*, **1998**, 68, 660-665.

(28) De Vries, H.; Encinas, S.; Miranda, M. A.; Castell, J. V.; Vanhenegouwen, G. M. J. B., Photodegradation and Photobinding of Tiaprofenic Acid. *In-Vitro* Versus *In-Vivo*, *Photochem.Photobiol.*, **1997**, 66, 432-435.

(29) Lhiaubet, V.; Gutierrez, F.; Penaud-Berruyer, F.; Amouyal, E.; Daudey, J. P.; Poteau, R.; Chouini-Lalanne, N.; Paillous, N., Spectroscopic and Theoretical Studies of the Excited States of Fenofibric Acid and Ketoprofen in Relation with their Photosensitizing Properties, *New J.Chem.*, **2000**, 24, 403-410.

(30) Monti, S.; Sortino, S.; De Guidi, G.; Marconi, G., Photochemistry of 2-(3-benzoylphenyl)propionic Acid (Ketoprofen). Part I. A Picosecond and Nanosecond Time Resolved Study in Aqueous Solution, *J.Chem.Soc., Faraday Trans.*, **1997**, 93, 2269-2275.

(31) Martínez, L. J.; Scaiano, J. C., Transient Intermediates in the Laser Flash Photolysis of Ketoprofen in Aqueous Solutions: Unusual Photochemistry for the Benzopheneone Chromophore, *J.Am.Chem.Soc.*, **1997**, 119, 11066-11070.

(32) Encinas, S.; Miranda, M. A.; Marconi, G.; Monti, S., Triplet Photoreactivity of the Diaryl Ketone Tiaprofenic Acid and its Decarboxylated Photoproduct. Photobiological Implications, *Photochem. Photobiol.*, **1998**, 67, 420-425.

(33) Encinas, S.; Miranda, M. A.; Marconi, G.; Monti, S., Transient Species in the Photochemistry of Tiaprofenic Acid and its Decarboxylated Photoproduct, *Photochem. Photobiol.*, **1998**, 68, 633-639.

(34) Castell, J. V.; Gomez-Lechon, M. J.; Grassa, C.; Martínez, L. A.; Miranda, M. A.; Tarrega, P., Involvement of Drug-Derived Peroxides in the Phototoxicity of Naproxen and Tiaprofenic Acid, *Photochem.Photobiol.*, **1993**, 57, 486-490.

(35) Burrows, C. J.; Muller, J. G., Oxidative Nucleobase Modifications Leading to Strand Scission, *Chem. Res.*, **1998**, 98, 1109-1151.

(36) Chignell, C. F.; Sik, R. H., The Effect of Static Magetic Fields on the Photohemolysis of Human Erythrocytes by Ketoprofen, *Photochem. Photobiol.*, **1998**, 67, 591-595.

(37) De la Peña, D.; Marti, C.; Nonell, S.; Martínez, L. A.; Miranda, M. A., Time-Resolved Near Infrared Studies on Singlet Oxygen Production by the Photosensitizing 2-Aryl-Propionic Acids, *Photochem.Photobiol.*, **1998**, 65, 828-832.

(38) Lhiaubet, V.; Paillous, N.; Chouini-Lalanne, N., Comparison of DNA Damage Photo-Induced by Ketoprofen, Fenofibric Acid and Benzophenone *via* Electron and Energy Transfer, *Photochem.Photobiol.*, **2001**, 74, 670-678.

(39) Rojas, E.; Lopez, M. C.; Valverde, M., Single Cell Gel Electrophoresis Assay: Methodology and Applications, *J. Chromatog. B*, **1999**, 722, 225-254.

(40) Rydberg, B.; Johanson, K. J., *Estimation of Single Strand Breaks in Single Mammalian Cells*, In: DNA Repair Mechanisms, Hanawalt, P. C., Friedberg, E. C. and Fox, C. F., Academic Press, New York, 1978, 465.

(41) Ostling, O.; Johanson, K. J., Microelectrophoretic Study of Radiation-Induced DNA Damages in Individual Mammalian Cells, *Biochem.Biophys.Res.Commun.*, **1984**, 123, 291-298.

(42) Singh, N. P.; McCoy, M. T.; Tice, R. R.; Schneider, L. E., A Simple Technique for Quantitation of Low Levels of DNA Damage in Individual Cells, *Exp.Cell Res.*, **1988**, 175, 184-191.

(43) Olive, P. L.; Banáth, J. P.; Durand, P. E., Heterogeneity in Radiation-Induced DNA Damage, *Radiat.Res.*, **1990**, 122, 86.

(44) Olive, P. L.; Banáth, J. P.; Durand, P. E., Detection of Etoposide Resistance by Measuring DNA Damage in Individual Chinese Hamster Cells, *J.Natl.Cancer Inst.*, **1990**, 82, 779-783.

(45) Olive, O. L.; Durand, J., Detection of Hypoxic Cells in a Murine Tumor with the Use of the Comet Assay, *J.Natl.Cancer Inst.*, **1992**, 84, 707-711.

(46) Banáth, J. P.; Kim, A.; Olive, P. L., Overnight Lysis Improves the Efficiency of Detection of DNA Damage in the Alkaline Comet Assay, *Radiat. Res.*, **2001**, 155, 564-571.

(47) Rudy, A. C.; Liu, Y.; Brater, C.; Hall, S. D., Stereoselective Pharmacokinetics and Inversion of (R)-Ketoprofen in Healthy Volunteers, *J. Clin. Pharmacol.*, **1998**, 38, 3S-10S.

(48) Pourzand, C.; Tyrrell, R., M., Apoptosis, the Role of Oxidative Stress and the Example of Solar UV Radiation, *Photochem.Photobiol.*, **1999**, 70, 380-390.

(49) Banáth, J. P.; Wallace, S. S.; Thompson, J.; Olive, P. L., Radiation-Induced DNA Base Damage Detected in Individual Aerobic and Hypoxic Cells with Endonuclease III and Formamidopyrimidine-Glycosylase, *Radiat.Res.*, **1999**, 151, 550-558.

(50) Olive, P. L.; Banáth, J. P., Induction and Rejoining of Radiation-Induced DNA Single-Strand Breaks: "Tail Moment" as a Function of Position in the Cell Cycle, *Mutat. Res.*, **1993**, 294, 275-283.

(51) Alberts, B.; Bray, D.; Lewis, J.; Raff, M.; Roberts, K.; Watson, J. D., *Molecular Biology of the Cell*, 3rd, Garland Publshing Inc., New York, 1994.

(52) Peak, M. J.; Peak, J. G., *Photosensitized Reactions of DNA*, In: CRC Handbook of Organic Photochemistry and Photobiology, Horspool, W. M. and Song, P. S., CRC Press, Inc., Kentucky, 1995, 1318-1325.

(53) Deninger, M. J.; Schoenwald, R. D., Uptake of Ibuprofen, Indomethacin and Ketoprofen into Isolated Rabbit Parietal Cells, *J. Pharm. Pharmacol.*, **2000**, 52, 501-509.

(54) Li, L.; Bisht, K. S.; LaGoye, I.; Zhang, P.; Straube, W. L.; Moros, E. G.; Roti Roti, J. L., Measurement of DNA Damage in Mammalian Cells Exposed In Vitro to Radiofrequency Fields at SARs of 3-5 W/kg, *Radiat.Res.*, **2001**, 156, 328-332.

(55) Vijayalaxmi; Leal, B. Z.; Szilagyi, M.; Prihoda, T. J.; Meltz, M. L., Primary DNA Damage in Human Blood Lymphocytes Exposed In Vitro to 2450 MHz Radiofrequency Radiation, *Radiat.Res.*, **2000**, 153, 479-486.

(56) Franklin, W. A.; Lo, K. M.; Haseltine, W. A., Alkaline Lability of Fluorescent Photoproducts Produced in Ultraviolet Light-Irradiated DNA, *J.Biol.Chem*, **1982**, 257, 13535-13543.

(57) Singh, N. P.; Stephens, R. E.; Schneider, E. L., Modifications of Alkaline Microgel Electrophoresis for Sensitive Detection of DNA Damage, *Int. J. Rad. Biol.*, **1994**, 66, 23-28.

(58) Strauss, G. H., Non-Random Cell Killing in Cryopreservation for Performance of the Battery of Leukocyte Tests (BLT), I. Toxic and Immunotoxic Effects, *Mut.Res.*, **1991**, 252, 1-15.

(59) McNamee, J. P.; Bellier, P. V.; McLean, J. R. N.; Marro, L.; Gajda, G. B.; Thansandote, A., DNA Damage and Apoptosis in the Immature Mouse Cerebellum After Acute Exposure to a 1 mT, 60 Hz Magnetic Field, *Mut. Res.*, **2001**, 513, 121-133.

(60) Reinhardt-Poulin, P.; McLean, J. R.; Deslauriers, Y.; Gorman, W.; Cabat, S.; Rouabhia, M., The Use of Silver-Stained "Comets" to Visualize DNA Damage and Repair in Normal and *Xeroderma pigmentosum* Fibroblasts After Exposure to Simulated Solar Radiation, *Photochem.Photobiol.*, **2000**, 71, 422-425.

(61) McNamee, J. P.; Bellier, P. V.; McLean, J. R. N., Differential Rates of Cytokine Production and Apoptosis in Venipuncture and Finger-Stab Derived Blood Cultures, *Cytokine*, **2001**, 15, 274-280.

Chapter 3

Detection of DNA Damage Using a Novel Time-Resolved Fluorescence Measurement Technique

3.1 Introduction

In the last two decades, many techniques to assess DNA damage have been developed. Rydberg and Johanson were pioneers in this field, in being the first to directly quantitate DNA damage in individual cells.[1] The method they used to isolate, unwind and measure the DNA set the foundation for many of the techniques still being used today. The cells, embedded in agarose, were lysed and the DNA was unwound using mild alkaline conditions. Once neutralized, the DNA was stained with acridine orange and DNA damage was assessed by measuring the ratio of green (double-stranded DNA (dsDNA)) to red (single-stranded DNA (ssDNA)) fluorescence with a photometer.[1] The processes of DNA isolation from cells, DNA unwinding and measuring DNA damage by visualizing the fluorescence of the dye-DNA complex have evolved to some extent; nevertheless, they remain key steps in many recent techniques for measuring DNA damage. These techniques, among many others, include the ultrasensitive assay for DNA damage,[2] the fluorometric analysis of DNA unwinding (FADU) assay,[3,4] the single cell gel electrophoresis technique (SCGE or comet assay)[5-9] and the alkaline version of the pulsed-field gel electrophoresis.[10,11]

The goal of this project was to introduce a new technique to measure DNA damage based on the variation of fluorescence lifetimes of a DNA dye, PicoGreen® (PG), which depends on whether PG is complexed with ssDNA or dsDNA. Experiments were carried out using both calf thymus DNA (CT-DNA) as well as DNA isolated from sheep white blood cells (WBC). A simple protocol for isolating WBC from sheep whole blood (WB) was established. DNA was damaged following gamma radiation (γ radiation) with doses ranging from 0-100 Gray (Gy). This form of ionizing radiation is

known to generate hydroxyl radicals (HO•) which are responsible for the formation of *ca.* 1040 single-strand breaks (SSBs)/Gy in cellular DNA[12,13] (refer to Appendix I for calculation of SSBs/DNA base pairs). The key to this novel technique resides in the unwinding buffer concentration as well as the unwinding time (along with the pre-established advantage of using PG) and contributes to its ability to differentiate between various doses of γ radiation. This concept is based on the notion that DNA damaged by radiation will experience an increased rate of unwinding which can be used as a sensitive measure of SSBs.[14-18] Therefore, various unwinding buffer concentrations as well as different unwinding times were explored in order to establish a possible field of application for this technique.

This chapter is concerned with the development of a simple method for measuring DNA damage, on DNA isolated from WBC, using a time-resolved fluorescence technique, which includes finding the right conditions for sample preparation, cell lysis, DNA unwinding times and buffers as well as sample measurements. This was accomplished through collaborations with Dr. J.R.N. McLean from Health Canada, and Dr. G. Cosa from professor J.C. Scaiano's research group at the University of Ottawa. Although some details concerning the spectroscopic and fluorescence kinetics aspects of this project appear here, a more detailed discussion can be found in the Ph. D. thesis of Dr. G. Cosa.

3.1.1 Previous Work Contributions

Many components of this technique were made possible only through the recognition of certain key principles from earlier investigations. The first of which led to the selection of PG as the most appropriate DNA dye to use with this technique. Cosa and co-

workers tested 9 different commercially available DNA dyes for their ability to differentiate between ssDNA and dsDNA given by the fluorescence lifetime variation of the dye-DNA complexes.[19] PG exhibited an increase in fluorescence lifetime of *ca.* 2.5[20] when complexed with dsDNA compared to ssDNA, the most of all the dyes tested. This phenomenon is attributed to the structure of PG, based on that of recently patented unsymmetric cyanine dyes,[21,22] which exhibit a 1000-fold increase in their fluorescence quantum yields when bound to dsDNA compared to free in solution. The high sensitivity of PG to dsDNA can be explained by considering the energy dissipation pathways adopted by photoexcited PG when complexed to DNA compared to that of free PG in solution (Figure 3.1).

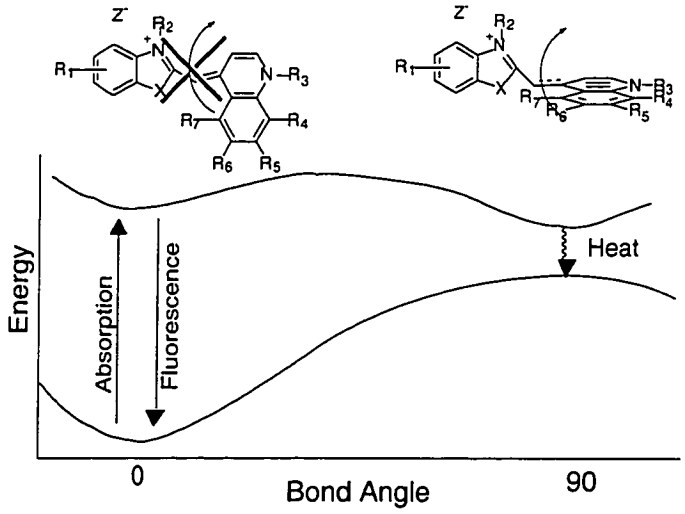

Figure 3.1: Energy dissipation pathways of PG in the singlet excited state.

When free in solution, ground state PG is in the *trans* form. Upon absorption of a photon, the excited *trans*-singlet state is formed and rotation along the central methine bridge converts PG into an excited perpendicular singlet state which decays non-radiatively, through internal conversion, to the perpendicular ground state.[23,24]

However, upon intercalation into DNA base pairs, this rotation along the methine bridge is restricted and PG is forced to dissipate its energy predominantly through emission *via* fluorescence.

This property was exploited *via* time-resolved fluorescence measurements of PG-DNA complexes which revealed a virtually pure monoexponential decay for PG-dsDNA and a biexponential decay for PG-ssDNA.[20] A triexponential decay is therefore expected with this system given that both the PG-ssDNA and the PG-dsDNA complexes decay independently.[20] From these results, an analytical technique was developed that could simultaneously measure ssDNA as well as dsDNA in solution. A one parameter fit was reported (Equation 3.1), that could fit the decay traces obtained from PG-DNA complexes using different ssDNA:dsDNA ratios (Figure 3.2A).[20]

$$I = a_{ds}e^{-0.22t} + \frac{(1 - a_{ds})}{2}(e^{-0.86t} + e^{-0.32t})$$

Equation 3.1: Determination of the pre-exponential factor for dsDNA.

In Equation 3.1, I is the fluorescence intensity, a_{ds} is the pre-exponential factor for dsDNA and t is the time in ns. When the pre-exponential factors obtained from Equation 3.1 are plotted as a function of the fraction of dsDNA actually contained in the sample (Figure 3.2B), the experimental slope obtained strays from the expected theoretical slope of one due to the background noise contribution during the time-resolved measurements.

$$\% \text{ dsDNA} = 100\left(\frac{a_{ds} - 0.048}{0.80}\right)$$

Equation 3.2: Percentage of dsDNA determination.

To compensate for this discrepancy, which is specific to the instrument used to measure the fluorescence lifetimes of PG-DNA complexes, percentages of dsDNA are calculated with Equation 3.2, using the a_{ds} obtained with Equation 3.1.[20]

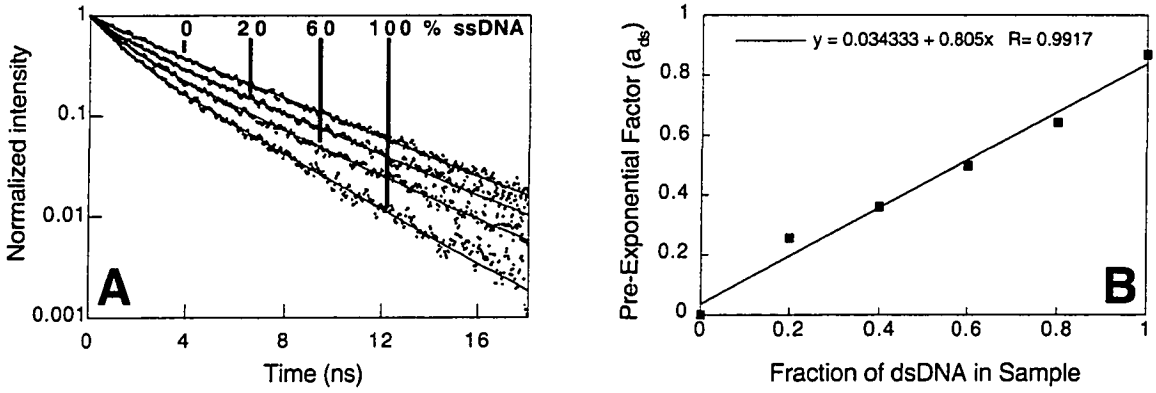

Figure 3.2: (A) Normalized fluorescence decay profiles of air equilibrated solutions containing various percentages of CT-dsDNA in Tris buffer pH 7.4 following 355 nm laser excitation. (B) Pre-exponential factor of dsDNA as a function of the dsDNA in solutions containing various percentages of CT-dsDNA.[20]

The fluorescence properties of PG have been employed in techniques such as, the temperature fluorescence assay[25] and various DNA unwinding techniques;[26] however, steady-state as opposed to time-resolved measurements were performed. Using fluorescence lifetimes foregoes the need to use blanks since it is not dependent on the amount of fluorophore and is unique for a given dye under specific conditions. However, previous investigations by Cosa and co-workers, revealed that dye:DNA ratios higher than 1:10 invite the possibility of intermolecular interactions between two dye molecules leading to deviations from the kinetic laws employed in the fluorescence lifetime fitting; therefore, fixing the DNA concentration (base pairs molarity) of a given sample to 10-fold that of PG.[20] In developing this analytical method with a simple system, which involves establishing necessary parameters using lifetime decay

equations in order to correlate pre-exponential factors with ssDNA and dsDNA, its future application to more complex systems is feasible.

Agarose is the most commonly employed solid support material used with techniques that require the isolation of DNA from the cellular nucleus.[4,27-29] It allows for easy sample manipulation and provides a practical medium for DNA analysis. Since agarose was also considered for use as a solid support material with this technique, it was necessary to evaluate the effect it might have on the fluorescence lifetime of the PG-DNA complexes as well as the possible contribution to background noise. Cosa and co-workers measured the fluorescence lifetimes of both PG-ssDNA and PG-dsDNA embedded in agarose using CT-DNA, and compared them to those obtained with PG-ssDNA and PG-dsDNA in phosphate buffered saline (PBS) (Figure 3.3).[20]

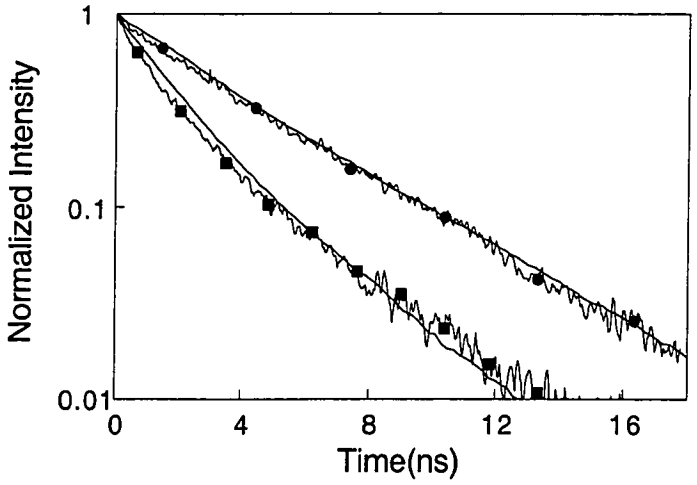

Figure 3.3: Fluorescence decay profiles of PG-dsDNA (●) and PG-ssDNA (■) complexes suspended in 0.75% agarose. Overlaid are the smoothed traces of PG-dsDNA (top trace) and PG-ssDNA (bottom trace) in PBS buffer from Figure 3.2A, 0% and 100% ssDNA respectively; measurements were conducted with CT-DNA. The smoothed traces are not a fit of the fluorescence decay profiles, they are two separate measurements.

In both cases, the decay traces obtained with PG-DNA embedded in agarose closely match those obtained with PG-DNA in PBS, rendering agarose an appropriate solid support material to be used with this fluorescence lifetime measurement technique.

3.1.2 Relevance of DNA Damage Detection

Great importance is placed on establishing the DNA damage detection limits of this technique as it will determine the most appropriate field of application for this technique. The radiation doses used with this technique include 0, 1, 2, 3, 4, 5, 10, 25, 50 and 100 Gy of γ radiation. These radiation doses are relevant when compared to other fields where γ radiation has been the source of DNA damage, such as radiotherapy treatments (~2 Gy),[26] food irradiation (> 1000 Gy)[30-32] and interestingly, survivors of the Chernobyl accident (1986) who were exposed to radiation doses ranging from 2.1-9 Gy.[33] While being able to differentiate between various γ radiation doses would be considered the greatest asset for this technique, possible applications could include determining whether DNA, from virtually any source, has been damaged or not.

3.2 Results and Discussion

Given the fact that this is a new time-resolved fluorescence technique, many obstacles were encountered during the process of constructing a reliable protocol for detecting DNA damage. Initial experiments were carried out very differently from the protocol stipulated in Section 3.4; therefore, variations on that protocol will be explicitly noted. These variations include: the trial of numerous methods to isolate sheep WBC from sheep WB, the elucidation of a practical technique to cast, lyse and unwind the DNA while using appropriate support material, discovering the proper cell lysis times and buffers, and finding suitable unwinding times and buffer concentrations in order to maximize the detection limits of this technique. The results are presented as the percentage of ssDNA (100 - %dsDNA) as the purpose of this technique is to determine the amount of ssDNA produced under certain specific experimental conditions. Unless otherwise stated, each experimental condition was carried out in triplicate for all experiments; therefore, the percentages of ssDNA values correspond to the average of three independent measurements.

3.2.1 Sheep White Blood Cell (WBC) Isolation

Human WBC are easily isolated from WB due to the large difference in size between red blood cells (RBC) and WBC; human RBC are *ca.* 8 μm in diameter while human WBC are 15-20 μm in diameter.[34] Therefore, the use of a gradient is effective in separating the WBC as the RBC, due to their smaller size, will sediment during centrifugation, while the WBC will be trapped within the gradient. Sheep RBC and WBC are similar in size and are three times smaller than human blood cells which makes

the use of any size of gradient inefficient in separating the two types of blood cells.[34] Nevertheless, both Histopaque-1077 and Histopaque-1119 gradients were tested separately as well as combined (one overlayed onto the other), and resulted in a very low recovery of sheep WBC, too little to be useful as the isolation technique.

The next option was removing the RBC altogether by means of cell lysis. This can be accomplished by exposing the cells to either a hypertonic or hypotonic environment. When the cells are exposed to a hypertonic environment, the solute concentration outside of the cell is higher than inside, causing the cell to expulse their cytoplasmic content to the point of implosion.[35] On the other hand, if the cells are exposed to a hypotonic environment, the solute concentration outside of the cell is lower than that inside forcing water to enter the cell to the point of explosion.[35] RBC are lysed at a higher rate compared to WBC since WBC are able to actively pump out water reducing the occurrence of explosion. The lysis of the RBC was attempted using various solutions (osmotic environments).

Ammonium chloride, a salt solution (hypertonic environment), was the first solution chosen for the RBC lysis. A solution of ammonium chloride was added (2:1) to sheep WB previously diluted (1:1) with complete media, and kept on ice for 45 min. The solution was centrifuged for 20 min at 1500 revolutions per minute (rpm) and the resulting pellet was resuspended in 30 mL of ammonium chloride buffer. This procedure was repeated until all of the RBC had been lysed. This method proved to be too gentle (*i.e.* not effective); therefore, too time consuming and, in the end, it did not completely remove all of the RBC.

A glycerol solution was employed in another attempt at RBC lysis. Glycerol rapidly penetrates the cell membranes (since it is polar and the cell does not have a mechanism

to pump this solute back out) and quickly creates a hypotonic environment which consequently forces water inside the cell resulting in its explosion.[35] Sheep WB was mixed with a glycerol solution (1:3) and kept at room temperature for 5 min, then centrifuged for 10 min at 3000 rpm. It became clear that the glycerol solution was effective as the quantity of RBC decreased rapidly with every repetition of the process; however, this method was still too gentle and time consuming.

Water is another solution that can be used for cell lysis; however, it is considered quite harsh and WBC may be sacrificed in the process. To a cell, water is considered to be a very dilute solution and in its attempt to restore osmotic equilibrium, it will succumb to osmotic fragility.[35] Water presents an extremely hypotonic environment to the cell and will cause large amounts of water to enter it, resulting in explosion. Since this process is fairly rapid and can harm the WBC, the amount of time that the cells are exposed to the water solution must be limited. A saline rescue solution is therefore necessary in order to reestablish an isotonic environment for the WBC. In this case a 2X saline rescue solution was employed to immediately interrupt the cell lysis as well as to compensate for the water dilution.

The first attempt with the water lysis proved very successful. Sheep WB was diluted (1:1) with complete media, then, sterile distilled and deionized water (ddH_2O) was added (1:2) and the solution was gently mixed for less than 30 sec. The 2X saline rescue solution was immediately added after 30 sec to stop the lysis. The solution was centrifuged for 30 min at 1500 rpm and the supernatant was discarded. A very small quantity of RBC still remained after this treatment. Therefore, it was thought that a combination of the water lysis followed by a glycerol treatment might help in removing the remaining RBC. A volume of 5 mL of ice cold glycerol solution was added to the

pellet obtained from the previous centrifugation, and kept on ice for 30 min. The solution was then centrifuged for 5 min at 1500 rpm and the pellet was washed twice with Hank's balanced salt solution (HBSS) (washes involve mixing the pellet with fresh solution and subsequent centrifugation). All traces of RBC were successfully removed by this treatment.

This WBC isolation method was employed for many of the following experiments; however, the presence of very small amounts of RBC frequently occurred. This was easily overcome by repeating the glycerol treatment; however, the isolation time was consequently increased by 2 h.

Finally, to reduce the isolation time, the water lysis was repeated twice. The second water lysis was performed by adding 5 mL of sterile ddH_2O to the pellet obtained from the centrifugation, followed by adding 5 mL of 2X saline rescue solution after 30 sec of gentle mixing. The solution was centrifuged for 5 min at 1500 rpm and the pellet was washed twice with HBSS. This method was infallible at removing all of the RBC and consumed very little time.

In order to confirm that the WBC had not been harmed during the isolation manipulations, a viability test as well as a Giemsa stain test were performed on the WBC before continuing with the rest of the experiment. The viability test indicated that the number of non-viable cells was always below 10%. The Giemsa stain test is a quick method to determine whether the cellular membranes have suffered any damage. When the cells were examined for such damage, they displayed evidence of good cell morphology (*i.e.,* cell membranes were intact) every time. Both of these tests confirmed that the isolation manipulations did not harm the WBC. If on any given day either of these tests revealed less than favorable results (*i.e.,* high concentration of non-

viable cells or poor cell membrane morphology), the WBC were not processed through the rest of the experiment.

3.2.2 DNA Support Material

Initially, it was thought that CT-DNA or WBC isolated from WB could be mixed with agarose and cast onto a Gelbond® film (refer to Section 3.4.9 for a description), in a similar fashion as that of the comet assay (*vide supra*), and that the samples would be measured directly from the solid support. However, closer consideration of the photophysical properties of the Gelbond® film indicated that its fluorescence spectrum overlapped with that of PG between 475 and 575 nm (spectra not shown). The fluoresecence decay profile of the Gelbond® film compared to that of PG-ssDNA and PG-dsDNA complexes (Figure 3.4) indicates that its fluorescence lifetime would interfere with the measurements of PG-DNA samples. Therefore, due to the nature of this technique, Gelbond® film is not considered to be an appropriate support material.

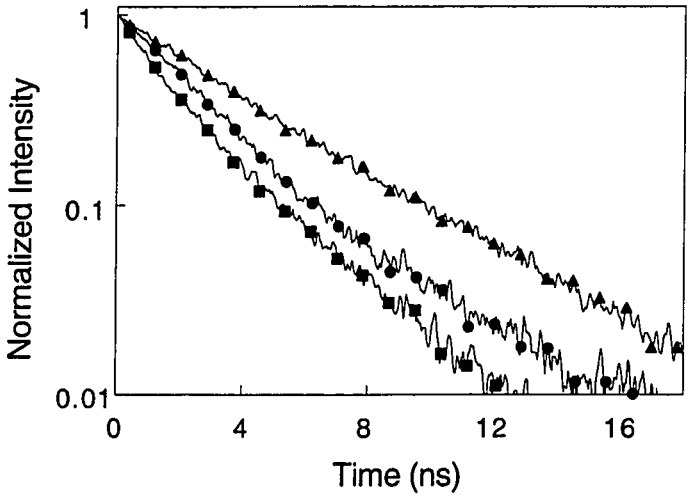

Figure 3.4: Fluorescence decay profiles of a Gelbond® film (●) compared to PG-ssDNA (■) and PG-dsDNA (▲) complexes.

The volume of sample being irradiated by the laser during measurements is described as a cylinder of *ca.* 4 mm in length and 4 mm in diameter. The gels cast onto a Gelbond® film are 2 X 2 X 0.1 cm^3; therefore, they make inefficient use of the PG-DNA complex by preventing much of the sample area from receiving laser irradiation (*i.e.,* not contributing to the fluorescence lifetimes). Therefore, proper support material incorporating a smaller sample area needed to be established.

In an attempt to reduce the sample size, a CT-DNA/cell-agarose suspension was dispensed as a bead onto a parafilm surface, then allowed to solidify. However, the bead still remained too large for the laser to completely irradiate in one measurement due to the lateral spreading of the agarose before solidification. Bead volumes from 230 μL to 100 μL were also tested to no avail.

A breakthrough came when it was decided to dispense the CT-DNA/cell-agarose suspension into the wells of a 96-well microplate. The wells are cylinders of 1 cm in length and 7 mm in diameter; therefore, the volume of the gels can be adjusted to just over 4 mm in length for accurate sample measurement.

The samples could not be measured directly while still in the wells because, like the Gelbond® film, the microplate displayed intense fluorescence properties which interfered with the sample measurement (data not shown). Therefore, the gels were removed with the tip of a glass NMR tube, which fits perfectly into the microplate wells, and the latter was used as the sample holder. This technique proved to be very efficient since the laser beam was aligned with the glass NMR tube before measuring the first sample, and need not be realigned for subsequent sample measurements. Sample manipulation became relatively easy with this method; the lysis and unwinding solutions were added and removed while the gels remained in the wells, the gels

remained hydrated until being measured and the microplate was ideal for sample transportation.

Although samples could be processed much faster with this method, serious reproducibility issues arose which could not be overcome even when CT-DNA was used instead of WBC isolated from WB (*vide infra*). With these results, indicating that using DNA isolated from blood cells was not the cause of the irreproducibility, it was recognized that the method still needed to be modified. Many attempts to overcome irreproducibility were carried out by repeating experiments while following the same protocol; however, results were never consistent. In examining the results (irreproducible results not shown), it appeared that duplicates of the same experiment displayed smaller differences among the lifetime decay values when the gels had been subjected to the unwinding buffer for longer unwinding times; hence, shorter unwinding times showed the greatest difference among duplicates. Irreproducibility was greater with samples exposed to shorter unwinding times. It was proposed that diffusion of the unwinding buffer through the gels was inconsistent; the unwinding buffer was able to diffuse adequately through the gels during longer unwinding times, while for shorter unwinding times, the unwinding buffer was only able to penetrate a small portion of the gel's surface.

This problem was overcome by adopting the current method (refer to Section 3.4 for more explicit details), based on the comet assay's sample manipulation. Briefly, the CT-DNA/cell-agarose suspension was dispensed as beads with a volume of 100 μL onto a Gelbond® film and the gels, once solidified, were submerged into 50 mL of the lysing and/or unwinding buffers contained in 150 mm petri dishes. The thin gels allowed for more efficient diffusion of the buffers throughout the gel's increased surface and the

ease of sample manipulation had not been compromised. To measure the samples, the gels were carefully inserted into the tip of a glass NMR tube and measured as described above and in Section 3.4. The results obtained from following this method displayed little differences in fluorescence lifetimes between the duplicates, as will be evidenced by the error bars displayed within the plots of the discussions to follow.

3.2.3 White Blood Cell (WBC) Lysis

In order to isolate the DNA from WBC, cellular and nuclear membranes must be removed. This is accomplished by subjecting the agarose-embedded WBC to lysing solutions. Two different lysis buffers were tested in order to establish their ability to remove sheep WBC cellular membranes; namely a urea buffer (hypotonic solution) as well as the lysis A buffer (hypertonic solution) (*vide supra*). Sheep WBC were isolated from sheep WB, irradiated with various γ radiation doses and, while fixed in the agarose gel, exposed to one of the lysis buffers, using one of three different protocols, to test their efficiency.

The first protocol consisted of exposing the cells to the urea buffer for at least 14 h at 4°C.[36] After which, the isolated DNA was subjected to a 1M KOH unwinding buffer and unwound for 0, 30 and 60 min. In this case the cells had been irradiated with 0, 1 and 2 Gy of γ radiation. In looking at the fluorescence decay profiles for these conditions (Figure 3.5A), there is no differentiation between radiation doses or unwinding times. This indicates that the urea buffer is too weak to properly remove all of the cellular membranes, even after long exposure, since there is no significant difference between the weakest (no radiation and no unwinding) and the strongest (2 Gy of γ radiation and 60 min unwinding time) conditions.

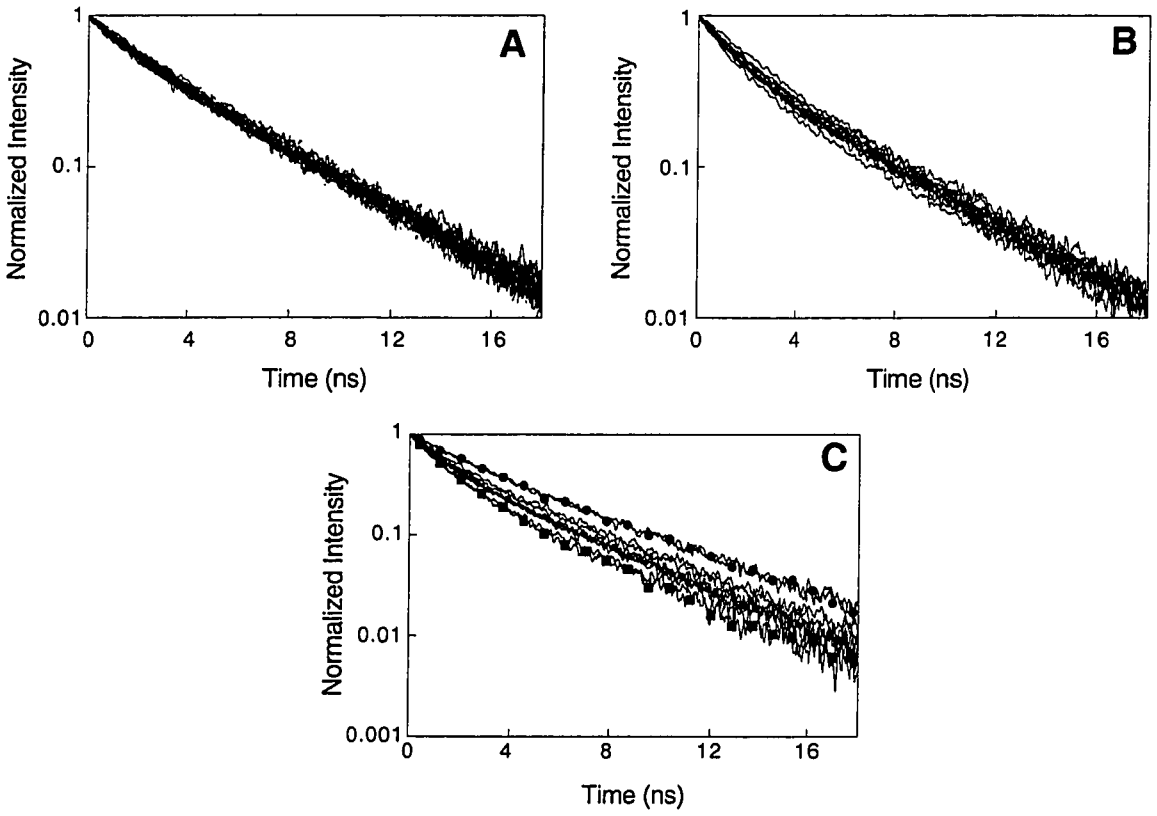

Figure 3.5: **(A) Fluorescence decay profile of PG-DNA complexes using DNA isolated from sheep WBC following 0, 1 and 2 Gy of γ radiation, overnight cell lysis using a urea buffer and 0, 30 and 60 min unwinding time with a 1 M KOH unwinding buffer. (B) Fluorescence decay profile of PG-DNA complexes using DNA isolated from sheep WBC following 0 and 5 Gy of γ radiation, 1 h cell lysis using lysis A buffer and 0, 10, 15, 20 and 60 min unwinding time with a 1 M KOH unwinding buffer. (C) Same as B with overnight cell lysis using lysis A buffer. No labels have been applied for A and B since they are used as evidence of no differentiation between experimental conditions and for C, only the top (●) and bottom (■) profiles are of interest (refer to text).**

If the cellular membranes have not been properly removed, no unwinding of the DNA will occur regardless of the strength of the unwinding buffer or the amount of time the DNA is exposed to it. Therefore, the urea buffer was not considered adequate for the lysis of the sheep WBC.

The second lysing protocol consisted of exposing the cells to the lysis A buffer for 1 h at 4°C. Then, the isolated DNA was subjected to a 1M KOH unwinding buffer and unwound for 0, 10, 15, 20 and 30 min. In this case the cells had been irradiated with 0 and 5 Gy of γ radiation. In looking at the fluorescence decay profiles for these conditions (Figure 3.5B), there still is no differentiation between radiation doses or unwinding times. And there is still no significant difference between the weakest (no radiation and no unwinding) and the strongest (5 Gy of γ radiation and 60 min unwinding time) conditions. Since lysis A is the buffer that is used for cell lysis in the comet assay and produces satisfying results, it was thought that a 1 h lysis with the lysis A buffer was not long enough to obtain good lysing conditions with sheep WBC. The lysis protocol was, therefore, repeated with the lysis A buffer, but the lysis time was extended to at least 14 h,[36] similar to the comet assay protocol. The fluorescence decay profiles for this experiment (Figure 3.5C), showed significant differentiation between the weakest (no radiation and no unwinding, top profile) and the strongest (5 Gy of γ radiation and 60 min unwinding time, bottom profile) conditions, with all the other conditions in between. It was therefore established that the lysis A buffer would be used to lyse the sheep WBC and the lysing time would be at least 14 h.[36]

3.2.4 Unwinding Buffer Concentration and Unwinding Times

The unwinding buffer concentration along with the amount of time the DNA is exposed to it are crucial in determining proper differentiation between ssDNA and dsDNA. DNA that is damaged will unwind faster than non-damaged DNA, under the same unwinding conditions.[14-18] Consequently, the amount of ssDNA formed is directly proportional to the unwinding time used and eventually, all the DNA will become single-stranded if left

to unwind long enough. As a result, the amount of unwound DNA corresponds to the amount of ssDNA found in the sample (*vide supra*). The concentration and unwinding times are interrelated in that, a high concentrated buffer used for a short unwinding time can accomplish the same amount of unwinding as a low concentration buffer with a high unwinding time. This phenomenon was exploited in order to determine the ideal conditions for differentiating between DNA that was damaged to various degrees.

Initial experiments were conducted with WBC isolated from sheep WB using different concentrations of unwinding buffers as well as various unwinding times.

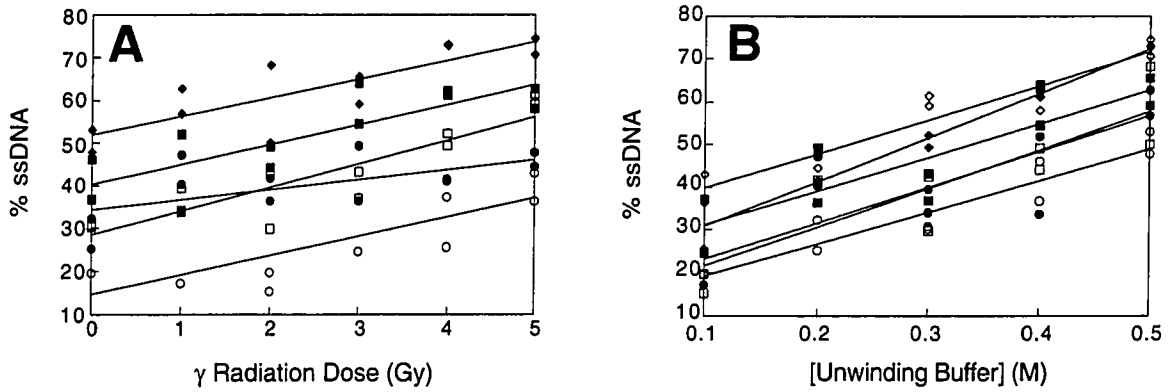

Figure 3.6: (A) Percentage of ssDNA as a function of the γ radiation dose using DNA isolated from sheep WBC following 15 min unwinding time with a 0.1 (○), 0.2 (●), 0.3 (□), 0.4 (■) and 0.5 (◆) M KOH unwinding buffer. (B) Percentage of ssDNA as a function of the KOH unwinding buffer concentration using DNA isolated from sheep WBC following 15 min unwinding time and γ radiation doses of 0 (○), 1 (●), 2 (□), 3 (■), 4 (◆) and 5 (◊) Gy.

The results obtained from sheep WBC following 0, 1, 2, 3, 4 and 5 Gy of γ radiation doses and 15 min unwinding with a 0.1, 0.2, 0.3, 0.4 and 0.5 M KOH unwinding buffer (Figure 3.6), proved to be very informative. The results were plotted using the γ radiation dose (Figure 3.6A) and the unwinding buffer concentration (Figure 3.6B) for a clearer demonstration of the effect from the various conditions. The results indicate an

increase in ssDNA with increasing γ radiation dose with all the unwinding buffer concentrations. For each γ radiation dose, the greatest differentiation occurs between the 0.1 and 0.5 M KOH unwinding buffers. The 0.2, 0.3 and 0.4 M KOH unwinding buffers do not have the ability to significantly differentiate between the different γ radiation dose. Since only one unwinding time (15 min) had been used, it was thought that better differentiation could be obtained using various unwinding times while keeping the buffer concentration constant.

A 0.4 M KOH unwinding buffer concentration was chosen to conduct an experiment with sheep WBC where the γ radiation doses were increased to include 0, 5 and 10 Gy (Figure 3.7).

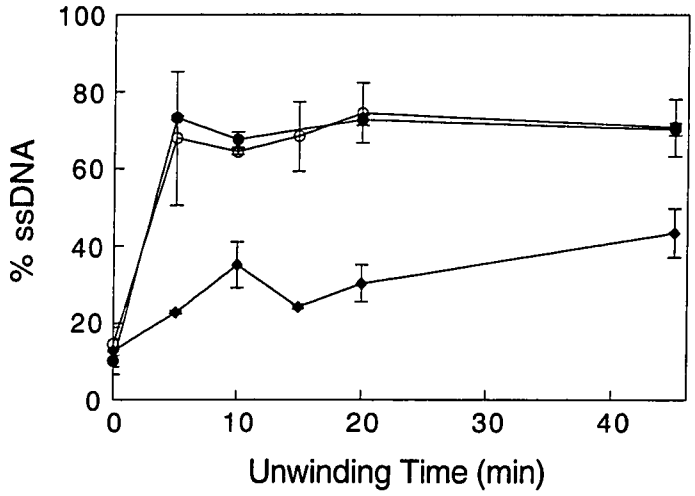

Figure 3.7: Percentage of ssDNA using DNA isolated from sheep WBC following 0 (◆), 5 (O) and 10 (●) Gy of γ radiation using various unwinding times and a 0.4 M KOH unwinding buffer.

The results show great differentiation between 0 and 5 Gy of γ radiation; however; the unwinding buffer was unable to differentiate between 5 and 10 Gy of γ radiation. Initially, it was thought that the buffer was too strong since it had unwound DNA that was

damaged with 5 Gy of γ radiation to the same degree as DNA damaged with 10 Gy of γ radiation; yet 100% unwinding (100% ssDNA) had not occurred for either of those conditions.

In light of this fact, it was decided that experiments would be conducted with CT-DNA until the proper conditions were established. The first experiment was kept simple since the range of experimental conditions had yet to be established. CT-DNA was subjected to 5 min unwinding with a 0.1 M KOH unwinding buffer without γ radiation (Figure 3.8).

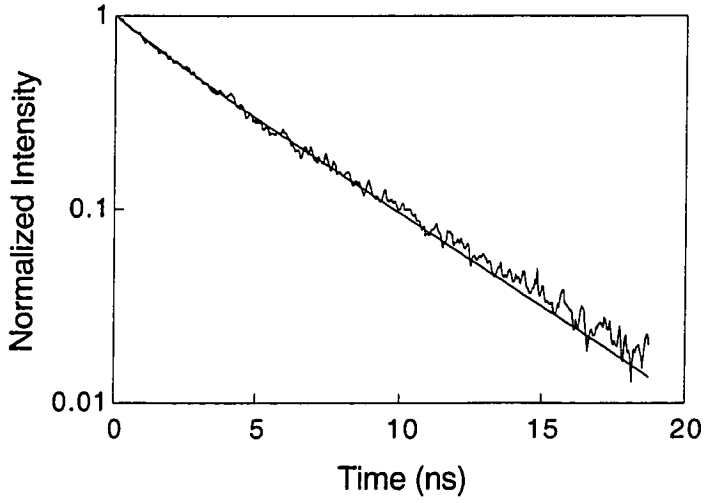

Figure 3.8: Fluorescence decay profiles of PG-DNA complexes using CT-DNA with no γ radiation following no unwinding (top profile) and 5 min unwinding with a 0.1 M KOH unwinding buffer (bottom profile).

The fluorescence decay profile clearly shows the differentiation between the experimental condition and the control (no γ radiation and no unwinding). Since a 0.1 M KOH unwinding buffer was able to unwind undamaged DNA after only 5 min, this meant that with damaged DNA, lower concentrations of unwinding buffer or shorter unwinding times should be used.

In order to incorporate longer unwinding times (> 5 min), concentrations lower than 0.1 M of KOH unwinding buffers were used with CT-DNA without γ radiation (Figure 3.9). Under these conditions, a 0.01 and 0.005 M KOH buffer were unable to produce any ssDNA even after 45 min of unwinding. Despite their weakness with undamaged DNA, these buffers might prove useful during experiments when DNA has been damaged. The 0.1 and 0.05 M KOH buffers showed great differences in their unwinding abilities even after 5 min. As the percentage of ssDNA approaches 100% with the 0.1 M KOH unwinding buffer, it becomes clear that, if these unwinding times are to be adopted, the concentration of the unwinding buffer will have to be lower than 0.1 M when using damaged DNA.

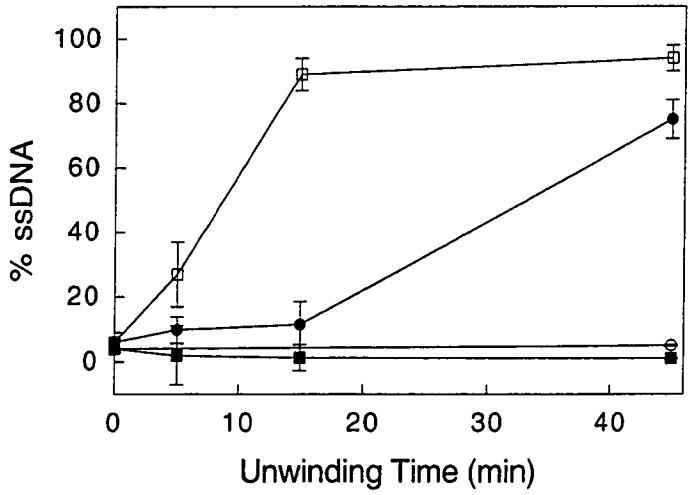

Figure 3.9: Percentage of ssDNA obtained with CT-DNA following no γ irradiation using various unwinding times and KOH buffers of 0.1 (□), 0.05 (●), 0.01 (■) and 0.005 (○) M.

Proof of this is shown in Figure 3.10, where CT-DNA is completely unwound after only 5 min unwinding with a 0.1 M KOH unwinding buffer, following 0, 5 and 10 Gy of γ radiation. It is important to notice that at 0 Gy of γ radiation, 100% ssDNA is reached during this experiment while in the previous experiment, ssDNA was *ca.* 30%. This

result demonstrated the lack of robustness and sensitivity of this technique at these γ radiation doses.

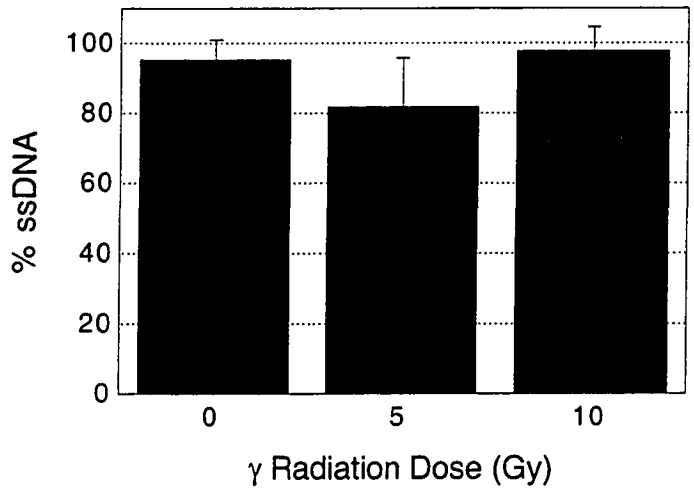

Figure 3.10: Percentage of ssDNA obtained with CT-DNA following 0, 5 and 10 Gy of γ radiation and 5 min unwinding time with a 0.1 M KOH unwinding buffer.

To address these issues, (i) that an unwinding buffer of *ca.* 0.05 M KOH should produce more ssDNA with damaged DNA compared to non-damaged DNA and (ii) %ssDNA greatly varies between experiments using the same conditions, another experiment was carried out based on the results of the previous two experiments. A 0.06 M KOH unwinding buffer was used and DNA was subjected to 0, 5 and 10 Gy of γ radiation. Although ssDNA increases with increasing unwinding time (Figure 3.11) and ssDNA values are greater than those obtained with the 0.05 M KOH unwinding buffer (Figure 3.9), the 0.06 M KOH unwinding buffer was not able to show significant differentiation between the γ radiation doses, even after 30 min unwinding time. Furthermore, in comparing the amount of ssDNA obtained with a 0.05 M KOH unwinding buffer following no γ radiation (Figure 3.9) to that obtained with a 0.06 M KOH unwinding buffer following no γ radiation (Figure 3.11), there is nearly a 4-fold

increase in %ssDNA with the 0.06 M KOH unwinding buffer after 15 min unwinding, and even after 30 min, there is still a 2-fold increase. If the %ssDNA between the 0.05 M and 0.06 M KOH unwinding buffers had been more similar (as anticipated), the results with the 0.06 M KOH unwinding buffer would have displayed better differentiation between 0 and 5 or 10 Gy of γ radiation.

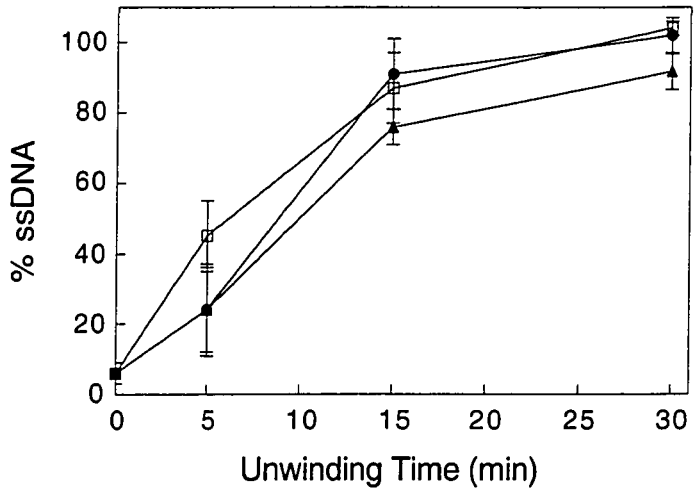

Figure 3.11: Percentage of ssDNA obtained with CT-DNA following 0 (▲), 5 (●) and 10 (□) Gy of γ radiation using various unwinding times and 0.06 M KOH unwinding buffer.

During the course of the many experiments carried out using different unwinding buffer concentrations and various unwinding times, two conclusions were drawn concerning this technique. The first, this technique is very sensitive to the unwinding buffer concentration when using low doses of γ radiation. This sensitivity; however, contributes to this technique's lack of robustness since slight differences in unwinding buffer concentration (encountered during solution preparation) can vary the degree of DNA unwinding that will be detected during the fluorescence lifetime measurements. This phenomenon is mainly due to the similar unwinding rates of damaged DNA using low γ radiation doses. A slight variation in the unwinding buffer concentration will cause the already similar

unwinding rates to overlap, making differentiation virtually impossible with this technique. However, as a second conclusion, this technique is clearly able to detect whether DNA has been damaged or not. As evidenced by the many variations of the unwinding buffer concentration and the unwinding times, this technique could be fine tuned to detect even relatively low DNA damage (1 Gy of γ radiation), if necessary.

In order to establish a general field of application for this technique, and to bypass the sensitivity issue, further experiments were conducted using γ radiation doses of up to 100 Gy of γ radiation. The next experiments were carried out using sheep WBC as the previous experiments with CT-DNA had already established the range of unwinding conditions needed to obtain proper differentiation between experimental conditions. The results obtained from DNA isolated from sheep WBC following 0, 25, 50 and 100 Gy of γ radiation doses and various unwinding conditions (Figure 3.12), revealed the ability for this technique to detect DNA damage. When DNA was unwound for 20 min with a 0.01 M KOH unwinding buffer (Figures 3.12A and B), the differentiation between the γ radiation doses are not significant. When the unwinding buffer concentration is increased to 0.05 M KOH (Figures 3.12C and D), a considerable increase in ssDNA is observed and significant differentiation is obtained between the γ radiation doses, even after only 5 min unwinding time. It is interesting to note that under these conditions, a 2-fold increase in the unwinding buffer concentration can increase the amount of ssDNA almost 3-fold in a quarter of the time.

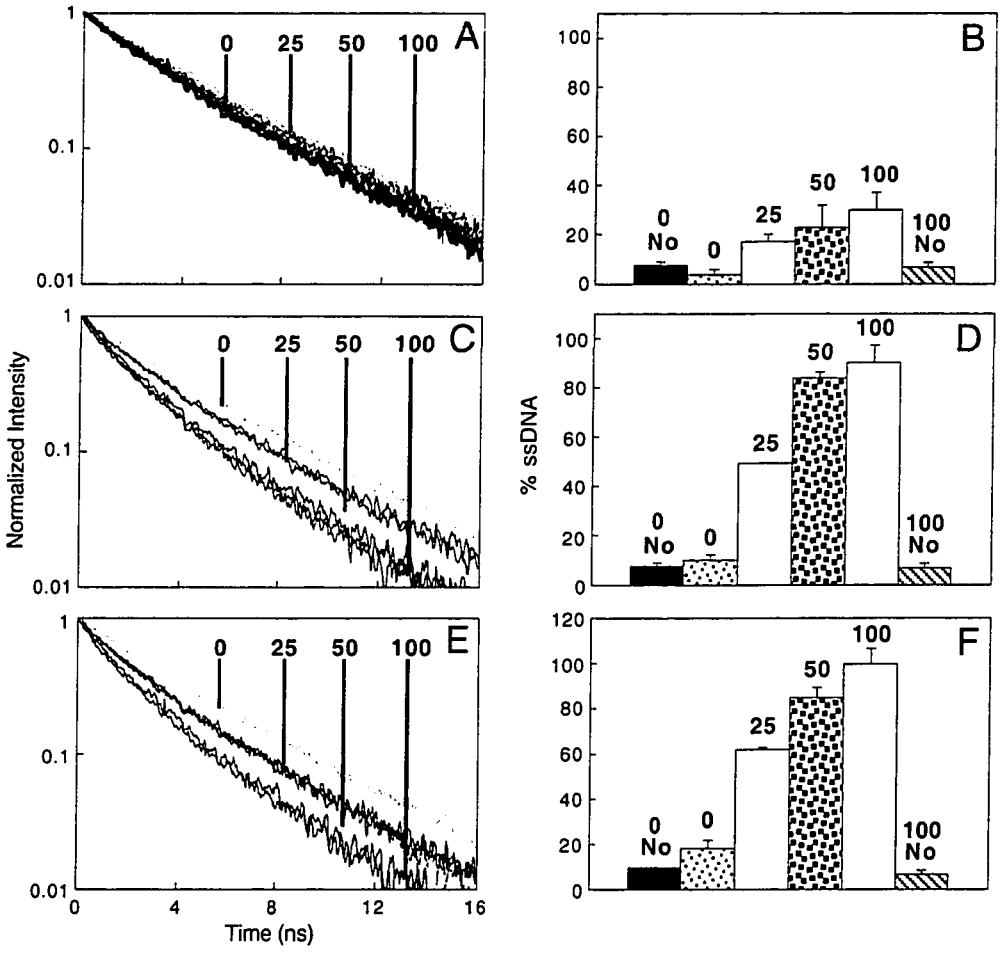

Figure 3.12: A, C and E are the fluorescence decay profiles obtained for PG-DNA complexes using DNA isolated from sheep WBC following 0, 25, 50 and 100 Gy of γ radiation. B, D and F represent the percentage of ssDNA obtained with DNA isolated from sheep WBC following 0 (light speckle), 25 (white), 50 (dark speckle) and 100 (gray) Gy of γ radiation (obtained from the respective fluorescence decay traces in A, C and E). A and B represent 20 min unwinding with a 0.01 M KOH unwinding buffer. C and D represent 5 min unwinding with a 0.05 M KOH unwinding buffer. E and F represent 10 min unwinding with a 0.05 M KOH unwinding buffer. For B, D and F, the black bars represent samples that have not been irradiated and were not unwound; and the diagonal bars represent samples that received 100 Gy of γ radiation and were not unwound.

If the unwinding time is increased by 5 min using a 0.05 M KOH unwinding buffer (Figures 3.12E and F), there is little increase in the amount of ssDNA for any of the γ radiation doses. These results suggest the limitations of the unwinding buffers as well as to what degree damaged DNA is able to unwind (the plateau indicates complete conversion to ssDNA). This is further evidenced by the trivial amount of ssDNA obtained following 100 Gy of γ radiation not subjected to any unwinding conditions; these are comparable to the amount of ssDNA obtained from undamaged DNA without unwinding.

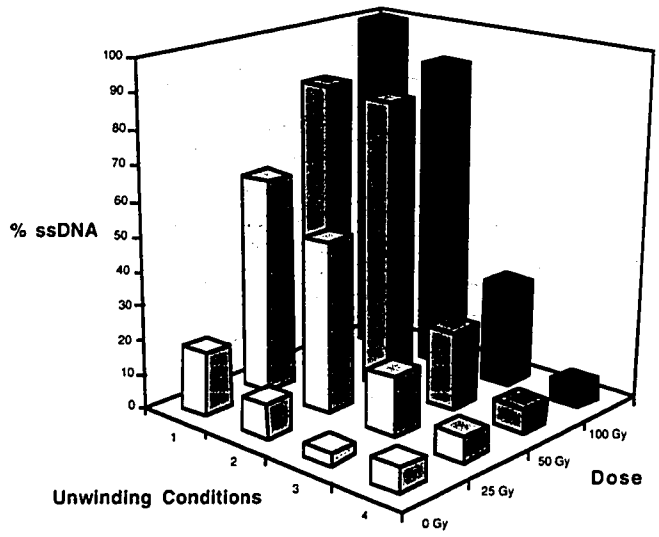

Figure 3.13: Percentage of ssDNA obtained with DNA isolated from sheep WBC as a function of both γ radiation doses and unwinding conditions of (1) 10 min unwinding time using a 0.05 M KOH unwinding buffer, (2) 5 min unwinding time using a 0.05 M KOH unwinding buffer, (3) 20 min unwinding time using a 0.01 M KOH unwinding buffer and (4) no unwinding.

As these results revealed the possible application of detecting DNA damage in the 0-100 Gy of γ radiation dose range, the data was plotted to better visualize the effect that

the unwinding buffer and the γ radiation doses have on the amount of ssDNA produced (Figure 3.13). This chart could be a useful tool in determining the proper experimental conditions needed in order to obtain satisfactory results when using this technique.

At this point, the experimental protocol for this technique is simple and well established, and the experimental conditions for detecting DNA damage in the 0-100 Gy of γ radiation range have been determined. Therefore, a final experiment, using DNA isolated from sheep WBC and including γ radiation doses as low as 5 Gy, was carried out using a 0.05 M KOH unwinding buffer and 10 min unwinding time (Figure 3.14).

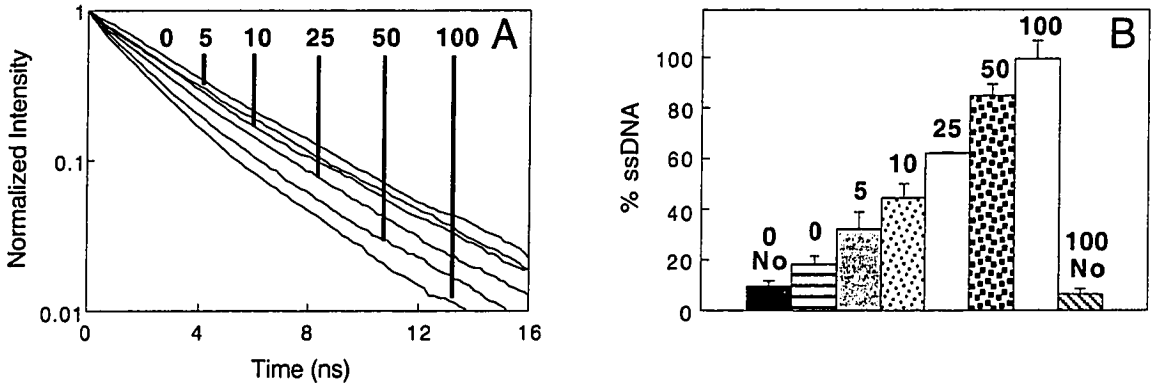

Figure 3.14: (A) Smoothed fits of fluorescence decay profiles of PG-DNA complexes using DNA isolated from sheep WBC following 0, 5, 10, 25, 50 and 100 Gy of γ radiation and unwound for 10 min with a 0.05 M KOH unwinding buffer. (B) Percentage of ssDNA obtained with DNA isolated from sheep WBC following 0 (horizontal), 5 (dark gray), 10 (light speckle), 25 (white), 50 (dark speckle) and 100 (light gray) Gy of γ radiation (obtained from the respective fluorescence decay traces in A). The black bar represents a sample that has not been irradiated and was not unwound; and the diagonal bar represents a sample that received 100 Gy of γ radiation and was not unwound.

Under these conditions, excellent differentiation between all of the different γ radiation doses was obtained. The percentage of ssDNA increases with increasing γ radiation

dose. The samples that received 5 and 10 Gy of γ radiation, are the average of six independent measurements while the samples that received 25, 50 and 100 Gy of γ radiation, are the average of three independent measurements. It is interesting to note, however, that the standard deviation is *ca.* 5 in %ssDNA and that the values obtained for the γ radiation doses of 25, 50 and 100 Gy, closely matched those obtained in the previous experiment.

Table 3.1 identifies the main steps of the final protocol developed to produce samples that were fit to measure DNA damage with this time-resolved fluorescence technique.

Step	Manipulation	Purpose
1. WBC Isolation	Subject whole blood to a water treatment and subsequent 2X saline rescue solution and repeat	Removal of RBC
2. Viability and Concentration	Add viability staining solution to cell suspension, count number of viable and non-viable cells and determine cell concentration	Assess % of non-viable cells and determine number of isolated cells
3. DNA Concentration Determination	Add PG to a predetermined cell suspension concentration, measure fluorescence intensity and compare with standard curve	Calculate exact DNA concentration of cell suspension
4. Irradiation	Subject cell suspension to γ radiation	Cause DNA damage
5. Casting	Mix cell suspension with agarose and dispense as a bead onto a Gelbond® film	Provide a solid DNA support and environment for consistent lysing and unwinding
6. Cell Lysis	Subject agarose-embedded cells to a high salt buffer for at least 14 h	DNA isolation by removal of all cellular membranes and components
7. DNA Unwinding	Subject agarose-embedded DNA to alkaline unwinding buffer	Convert damaged DNA into ssDNA
8. Staining	Add PG solution to agarose-embedded DNA samples without exceeding the dye:DNA ratio of 1:10	Form dye-DNA complexes
9. Measurements	Perform time-resolved fluorescence measurements using the third harmonic (355 nm) pulse from a Continuum PY-61 Nd:YAG laser (35 ps, ≤4 mJ/pulse) as the excitation source.	Determine the fluorescence lifetime of PG-DNA complexes in order to determine the amount of ssDNA produced.

Table 3.1: Final protocol used in the preparation of samples fit to measure DNA damage using a time-resolved fluorescence technique. Refer to Section 3.4 for more detailed descriptions of each step.

3.3 Conclusion

Results from a new technique for measuring DNA damage based on the time-resolved fluorescence decay measurements of dye-DNA complexes have been presented. This technique, which incorporates key concepts such as alkaline unwinding buffers and higher unwinding rates of damaged DNA compared to non-damaged DNA, was able to reproducibly measure and differentiate DNA damage between 0 and up to 100 Gy of γ radiation. New protocols for isolating sheep WBC from sheep WB and for isolating DNA from the WBC *via* membrane lysis were also established. Although this technique exhibits a high sensitivity to minute variations in unwinding buffer concentration at low γ radiation doses (0-5 Gy), it demonstrated potential in being adapted to differentiate between damaged and non-damaged DNA under these conditions. The results presented included experiments carried out using CT-DNA as well as DNA isolated from sheep WBC, suggesting its potential for use with isolated DNA from virtually any eukaryotic cell. The fact that this novel technique is devoid of subjectivity, can detect useful signals using as little as 6000 cells for one sample (36 ng of DNA) and its only requirement is not exceeding the dye:DNA ratio of 1:10,[20] are only a few of its many advantages. Since detecting whether DNA has been damaged or not is this technique's greatest strength, it could find a potential application as a diagnostic tool for measuring radiation exposure in humans and in food products.

3.4 Experimental

3.4.1 Introduction

The protocol described hereafter reflects the development of a simple method for sample preparation, fit to analyze DNA damage using a time-resolved fluorescence measurement technique. The initial stages in the development of this protocol are explicitly detailed in section 3.2. The experiments in their entirety were performed under reduced lighting. The units used to define DNA concentration or dye:DNA ratios are base pairs of nucleotides, unless otherwise stated.

3.4.2 Materials

Sheep blood was obtained from the Animal Diseases Research Institute at Agriculture Canada (Ottawa, Ontario, Canada). PicoGreen® nucleic acid stain (PG) was obtained from Molecular Probes (Eugene, OR, USA) and kept at -20°C until use. Hank's balanced salt solution without phenol red, 0.1 μm filtered (HBSS) was from Gibco BRL Life Technologies (Grand Island, NY, USA). Phosphate buffered sodium heparin at 500 units/mL, Histopaque®-1077, Histopaque®-1119, fluorescein, fluorescein diacetate, ethidium bromide (EtBr), sodium hydroxide (NaOH), sodium dodecyl sulfate (SDS) and N-lauroyl sarcosine sodium salt (SLS) were obtained from Sigma Chemical Company (St-Louis, MO, USA). Agarose high strength, analytical grade, ultra pure DNA grade (low-melting point agarose) was obtained from Bio-Rad Laboratories (Hercules, CA, USA). Calf thymus DNA (Type I)(CT-DNA), Trizma preset crystals (reagent grade, pH 7.4) and disodium ethylene diamine tetraacetate (Na_2EDTA) were from Sigma-Aldrich Canada (Oakville, ON, Canada). Sodium chloride (optical grade)

(NaCl) was from Alfa Aesar (Ward Hill, MA, USA). Dimethyl sulfoxide (DMSO), trishydroxymethylaminomethane (Tris base), acetone, ammonium chloride (NH_4Cl), urea, potassium bicarbonate (K_2CO_3), sodium tetra ethylene diamine tetraacetate (EDTA), methanol, sodium phosphate monobasic ($NaH_2PO_4 \cdot 2H_2O$) and sodium phosphate dibasic (Na_2HPO_4) were obtained from Fischer Scientific (Fairlawn, NJ, USA). Iso-octylphenoxypolyethoxy-ethanol (Triton X-100), sodium chloride (NaCl), glycerol and potassium hydroxide (KOH) were from BDH (Toronto, ON, Canada). The TAE buffer (0.4 M Tris acetate, 0.2 M glacial acetic acid, 0.1 M EDTA), 10X pH 8.4 was from Roche Diagnostics (Manheim, Germany). Wright-Giemsa Stain was obtained from EM Science (Gibbstown, NJ, USA). All solvents and chemicals were used without further purification.

3.4.3 Preparation of Solutions

All solutions were prepared with 18 MΩ water (ddH_2O) (Milli-Q plus PF unit, Millipore Corp., Bedford, MA, USA). ddH_2O for RBC lysis was sterilized by passing it through a 0.2 μm filter (Acrodisc, low protein binding, Gelman Sciences, Ann Arbor, MI, USA). The PBS solution consisted of 58 mM Na_2HPO_4, 17 mM $NaH_2PO_4 \cdot 2H_2O$ and 68 mM NaCl in ddH_2O to achieve a pH of 7.4. The ammonium chloride solution consisting of 0.83% NH_4Cl, 7 mM K_2CO_3, 89 μM EDTA in ddH_2O; the glycerol solution consisting of 4% glycerol in PBS pH 7.4 and the 2X saline rescue solution consisting of 1.8% NaCl in ddH_2O were all sterilized in the same way as the ddH_2O for RBC lysis. Fluorescein diacetate was prepared at 5 mg/mL in acetone. The EtBr solution was prepared at 200 μg/mL in HBSS. The working viability stain was prepared by adding 50 μL of the EtBr solution and 7.5 μL of the fluorescein diacetate solution to 1.2 mL of HBSS. The

agarose solution was prepared in PBS pH 7.4 to 0.75% consistency (w/v). The urea lysis buffer consisted of 10 M urea, 0.1% SDS, 2.5 mM EDTA and 10 mM KOH in ddH_2O. The lysis A buffer consisted of 2.5 M NaCl, 100 mM EDTA, 10 mM Tris base, 1% SLS in ddH_2O, adjusted to pH 10, 1% Triton X-100 and 10% DMSO were added to the lysing solution immediately before use, to assist in the removal of cellular proteins. The Tris buffer consisted of 10 mM Trizma pre-set crystals, 1 mM Na_2EDTA and 100 mM NaCl (optical grade) in ddH_2O to achieve a pH of 7.4. Various concentrations of the unwinding buffer were prepared in ddH_2O, ranging from 0.005-1 M KOH. The Giemsa stain was prepared by adding 5 mL of the Giemsa solution to 100 mL of ddH_2O. The 1X TAE buffer was prepared by making a 1:10 dilution of the 10X TAE stock solution. The PG staining solution was prepared by adding 196 μL of PG to 10 mL of Tris buffer (1:50 dilution of the stock solution supplied by Molecular Probes to obtain a 5.9 μM solution) and the solution was stored at 4°C and protected from light.

3.4.4 Experiments with DNA in Buffered Solution

CT-DNA suspensions were prepared in a Tris buffer at pH 7 (1 mM stock solution). The ssDNA was obtained after boiling a dsDNA solution for 30 min followed by immediate immersion into an ice bath. Complete denaturation was confirmed by comparing the absorption ratio at 260 nm for the heated (ssDNA) and non-heated (dsDNA) samples. A value of 1.32 was obtained, in good agreement with the literature value.[37] DNA sample concentrations were from 70-150 μM during measurements of percentages of dsDNA and the PG staining solution concentration was 11 μM in all cases. For measurements of CT-DNA embedded in agarose, a volume of 20 μL of

the CT-DNA stock solution was mixed with 20 μL of the PG staining solution (100 μM) then added to 360 μL of 0.75% agarose.

3.4.5 Isolation of White Blood Cells (WBC) from Sheep Whole Blood (WB) (Step 1)

All plasticware used during the isolation process was made of polypropylene and high binding plastics, such as polystyrene, were avoided as they bind cells to the centrifuge tube walls. A volume of 100 mL of sheep WB was collected in a culture flask containing 10 mL of phosphate buffered sodium heparin. The sheep WB was dispensed into centrifuge tubes (15 mL of WB X 8 centrifuge tubes) and kept on ice for 30 min. RBC were lysed with 15 mL of ice cold ddH_2O for no longer than 30 sec, then 15 mL of ice cold 2X saline solution was added to stop the RBC lysis and restore the cellular osmotic pressure. The mixtures were centrifuged for 1 h at 1500 rpm. The supernatants were decanted and the RBC lysis was repeated (5 mL of ddH_2O and 5 mL of 2X saline solution) to remove the remaining RBC. The WBC were collected by centrifugation for 15 min at 1500 rpm. The supernatants were decanted and the WBC pellets were resuspended in 2.5 mL HBSS and pooled.

3.4.6 Cell Viability and Concentration Determination (Step 2)

To determine the cell concentration and viability, an aliquot of the cell suspension (50 μL) was taken and mixed with viability stain (50 μL) then dispensed onto a hemacytometer and examined with a fluorescence microscope (Olympus BX-60, Olympus Optical Co., Japan) at 20X (UPlanAPO objective), fitted with a U-MNB (blue band) filter cube. Under these conditions, non-viable cells appeared red while viable cells fluoresced green due to the conversion of fluorescein diacetate to fluorescein by

membrane esterases in metabolically competent (viable) cells.[38] This method allowed for the concentration determination in cells/mL (refer to Appendix J for cell concentration calculation).

To determine whether the cells had been harmed during isolation manipulations, a Giemsa stain test was performed. A drop of the cell suspension was dispensed onto a 75 mm X 25 mm microscope slide and allowed to dry. The slide was then submerged into the Giemsa staining solution for 5-10 min, then removed and allowed to dry. Once dried, the slide was submerged into methanol for 5-10 min, removed and allowed to dry. The dried slide was examined by brightfield microscopy (Nikon LABOPHOT, Nikon Canada Inc., Mississauga, ON, Canada) at 60X (PlanApo objective).

3.4.7 DNA Concentration Determination (Step 3)

In order to verify the actual concentration of the WBC suspension isolated from sheep WB, a DNA standard curve was constructed against which a sample of the cell suspension was analyzed. The DNA standard curve was constructed following a protocol detailed by Molecular Probes using their PG dsDNA quantitation reagents and kits.[39] All solutions were prepared using polypropylene plasticware.

Briefly, the absorbance of a 0.95 mg/mL CT-DNA solution in 1X TAE buffer was measured at 260 nm (Bausch & Lomb Spectronic®2000 spectrophotometer system, USA) and its exact concentration was calculated (refer to Appendix K). The DNA solution was diluted to 2 μg/mL in 1X TAE buffer and from this solution, 1 mL DNA solutions were prepared in the 0-1000 ng/mL range. A volume of 1 mL of the PG working solution (a 200-fold dilution of the PG reagent in 1X TAE buffer *i.e.,* 100 μL PG added to 19.9 mL 1X TAE buffer) was added to all the DNA solutions and they were

allowed to equilibrate for 5 min. Fluorescein was used as a standard for the DNA determination curve and was measured for fluorescence along with the DNA solutions. The fluorescein solution was prepared in 0.1 M NaOH and its absorbance was matched with that of the PG working solution at 485 nm. A 200 μL aliquot from each the DNA solution and the fluorescein solution, was dispensed in triplicate into the wells of a 96-well plate and measured for fluorescence (excitation at 485 nm; emission at 538 nm) (*f*max fluorescence microplate reader, Molecular Devices, Sunnyvale, CA, USA)(Figure 3.15). The values were averaged and the blank was subtracted.

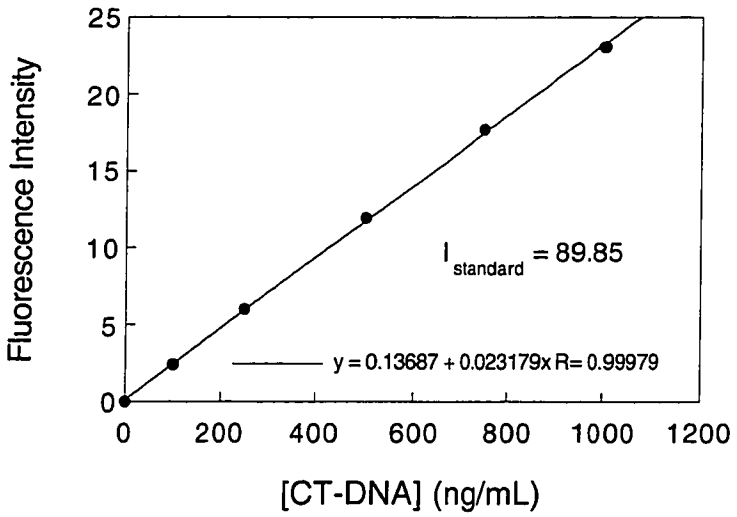

Figure 3.15: CT-DNA standard curve in the 0-1000 ng/mL range used to determine the DNA concentration of the sheep WBC suspension. $I_{standard}$ is the value of the fluorescein standard measured on the same day the curve was measured.

A 2 μg/mL DNA solution in 1X TAE buffer was prepared from the WBC suspension (1X TAE buffer was added to 55 μL cell suspension to fill a 10 mL volumetric flask), assumed to contain 60 million cells/mL as confirmed by the concentration determination (*vide supra*). A 1 mL DNA solution of 800 ng/mL in 1X TAE buffer was prepared from the 2 μg/mL DNA solution and 1 mL of the PG working solution was added. After 5

min, an aliquot of 200 μL of each the DNA solution, the 1X TAE buffer and the fluorescein solution were dispensed in triplicate into the wells of a 96-well plate and measured for fluorescence (excitation at 485 nm, emission at 538 nm). The DNA concentration of the WBC suspension was calculated (ng/mL) using Equation 3.3, where the fluorescence intensity values were averaged and the blank was subtracted beforehand.

$$[DNA] = \frac{I_{DNA\ sample}}{I_{new\ standard}} \times \frac{I_{standard}}{slope}$$

Equation 3.3: DNA concentration determination.

The exact concentration of the WBC suspension (cells/mL) was calculated by backtracking to the initially inferred concentration of 60 million cells/mL (refer to Appendix L).

3.4.8 Irradiation (Step 4)

The WBC suspension was centrifuged for 30 min at 1500 rpm. The supernatant was discarded and the pellet was resuspended in HBSS to obtain a cell concentration of 60 X 10^6 cells/mL. The WBC suspension was divided and dispensed into glass vials (as many vials as there are γ radiation doses), and put on ice. For γ radiation doses of 1-10 Gy, irradiations were carried out using a Gammacell®40 (Atomic Energy of Canada Ltd., Radiochemical Company) ^{137}Cesium source with a dose rate of 0.955 Gy/min. For γ radiation doses of 25, 50 and 100 Gy, irradiations were carried out using a Gammacell®220 (Atomic Energy of Canada Ltd., Radiochemical Company) ^{60}Cobalt source with a dose rate of 38.462 Gy/min. All irradiations were performed with the glass vials, containing the cell suspension, on ice.

3.4.9 Casting (Step 5)

Figure 3.16 illustrates the next steps of the protocol which include casting, lysing, unwinding, staining as well as the time-resolved fluorescence measurements of the sample.

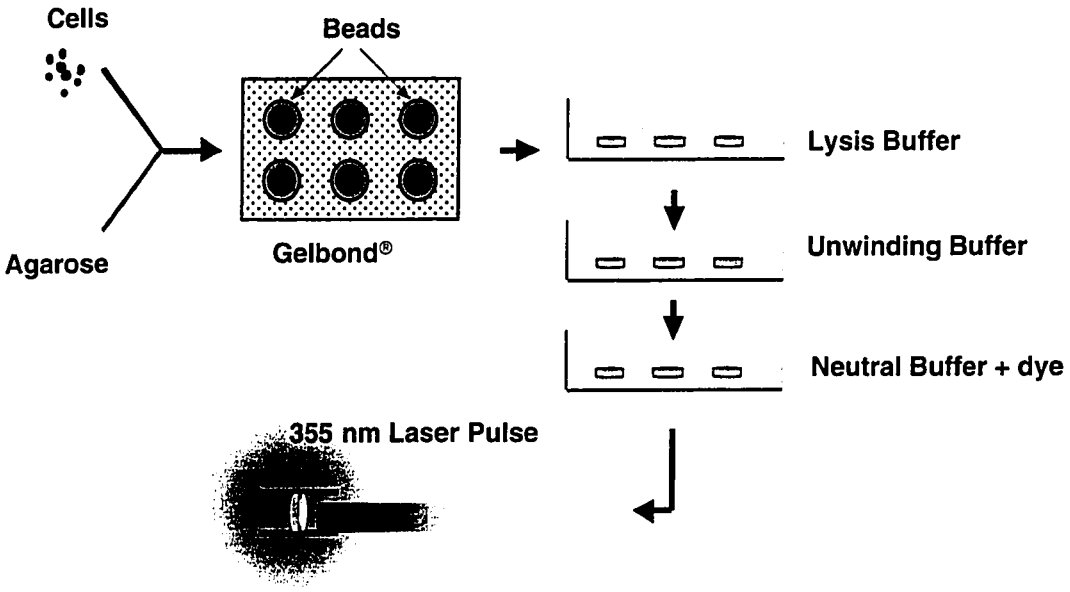

Figure 3.16: Stages of the protocol for time-resolved fluorescence measurements using DNA isolated from living cells following damage from γ radiation.

Gelbond® film (agarose gel support medium from BioWhittaker Molecular Applications, Rockland, ME, USA) is a flexible support consisting of an agarose-coated polyester sheet. Films were cut in 6 cm X 10 cm dimension. For each dose of γ radiation, a volume of 50 μL of WBC suspension was mixed with 125 μL of 0.75% agarose. An aliquot of 150 μL of the cell suspension (containing at least 1 million cells) was dispensed as a bead onto a Gelbond® film (6 beads/film *i.e.,* 3 radiation doses in duplicate).

3.4.10 Lysing and Unwinding (Step 6 and 7)

Once the gels had solidified, they were submerged into a 150 mm pertri dish containing 50 mL of ice cold lysis A buffer and kept at 4°C overnight. After at least 14 h,[36] the lysing solution was removed and the gels were rinsed with ice cold HBSS. The gels were then submerged into a 150 mm petri dish containing 50 mL of ice cold unwinding buffer and kept at 4°C for 0-45 min (depending on the experiment). Once the unwinding time had lapsed, the gels were rinsed with ice cold HBSS then 50 mL of fresh ice cold HBSS was dispensed onto the gels and they were kept at 4°C until staining.

3.4.11 Staining (Step 8)

Each gel was carefully peeled off of the Gelbond® film with a spatula and placed into a well of a 24-well culture plate. The gels were stained by adding 150 μL of the PG staining solution and kept at 4°C overnight (*ca.* 8.7×10^{-10} moles of PG were added to each gel). The gels contained 6 μg of DNA (equivalent to 9.5 nmoles of base pairs) and were exposed to *ca.* 0.87 nmole of PG resulting in a dye:DNA ratio of 1:10.

3.4.12 Measurements (Step 9)

Each gel was carefully placed into the tip of a glass NMR tube, ready to be measured. Fluorescence time-resolved measurements for short-lived singlet states were carried out using the third harmonic (355 nm) pulse from a Continuum PY-61 Nd:YAG laser (35 ps, ≤4 mJ/pulse) as the excitation source. A Hamamatsu C4334 streak camera was used for time resolved fluorescence detection and data acquisition.[40] The instrument response is *ca.* 80 ps.

3.5 References

(1) Rydberg, B.; Johanson, K. J., *Estimation of Single Strand Breaks in Single Mammalian Cells*, In: DNA Repair Mechanisms, Hanawalt, P. C., Friedberg, E. C. and Fox, C. F., Academic Press, New York, 1978, 465.

(2) Le, X. C.; Xing, J. Z.; Lee, J.; Leadon, S. A.; Weinfeld, M., Inducible Repair of Thymine Glycol Detected by Ultrasensitive Assay for DNA Damage, *Science*, **1998,** 280, 1066-1069.

(3) Birnboim, H. C.; Jevcak, J. J., Fluorometric Method for Rapid Detection of DNA Strand Breaks in Human White Blood Cells Produced by Low Doses of Radiation, *Cancer Res.*, **1981,** 41, 1889-1892.

(4) Baumstark-Khan, C.; Hentschel, U.; Nikandrova, Y.; Krug, J.; Horneck, G., Fluorometric Analysis of DNA Unwinding (FADU) as a Method for Detecting Repair-Induced DNA Strand Breaks in UV-Irradiated Mammalian Cells, *Photochem. Photobiol.*, **2000,** 72, 477-484.

(5) Ostling, O.; Johanson, K. J., Microelectrophoretic Study of Radiation-Induced DNA Damages in Individual Mammalian Cells, *Biochem.Biophys.Res.Commun.*, **1984,** 123, 291-298.

(6) Singh, N. P.; McCoy, M. T.; Tice, R. R.; Schneider, L. E., A Simple Technique for Quantitation of Low Levels of DNA Damage in Individual Cells, *Exp.Cell Res.*, **1988,** 175, 184-191.

(7) Olive, P. L.; Banáth, J. P.; Durand, P. E., Detection of Etoposide Resistance by Measuring DNA Damage in Individual Chinese Hamster Cells, *J.Natl.Cancer Inst.*, **1990,** 82, 779-783.

(8) Olive, P. L.; Banáth, J. P.; Durand, P. E., Heterogeneity in Radiation-Induced DNA Damage, *Radiat.Res.*, **1990,** 122, 86.

(9) McNamee, J. P.; Bellier, P. V.; McLean, J. R. N.; Marro, L.; Gajda, G. B.; Thansandote, A., DNA Damage and Apoptosis in the Immature Mouse Cerebellum After Acute Exposure to a 1 mT, 60 Hz Magnetic Field, *Mut. Res.*, **2001,** 513, 121-133.

(10) Schwartz, D. C.; Cantor, D. R., Separation of Yeast Chromosome-Sized DNAs by Pulsed Field Gradient Gel Electrophoresis, *Cell*, **1984,** 37, 67-75.

(11) Carle, G. F.; Frank, M.; Olson, M. V., Electrophoretic Separations of Large DNA Molecules by Periodic Inversion of the Electric Field, *Science*, **1986,** 232, 65-68.

(12) Ward, J. F., *DNA Damage Produced by Ionizing Radiation in Mammalian Cells: Identities, Mechanisms of Formation, and Reparability*, In: Nucleic Acid Research and Molecular Biology, Academic Press Inc., New York, 1988, Vol. 35, 95-125.

(13) Goodhead, D. T., Initial Events in the Cellular Effects of Ionizing Radiations: Clustered Damage in DNA, *Int.J.Radiat.Biol*, **1994,** 65, 7-17.

(14) Ahnström, G.; Erixon, K., Radiation Induced Strand Breakage in DNA From Mammalian Cells. Strand Separation in Alkaline Solution, *Int.J.Radiat.Biol.Relat.Stud.Phys.Chem.Med.*, **1973,** 23, 285-289.

(15) Kohn, K. W.; Erickson, L. C.; Ewig, A. G.; Friedman, C. A., Fractionation of DNA From Mammalian Cells by Alkaline Elution, *Biochemistry*, **1976,** 15, 4629-4637.

(16) Kohn, K. W.; Ewig, R. A. G., Alkaline Elution Analysis, a New Approach to the Study of DNA Single-Stranded Interruptions in Cells, *Cancer Res.*, **1973,** 33, 1849-1853.

(17) Rydberg, B., The Rate of Strand Separation in Alkali of DNA of Irradiated Mammalian Cells, *Radiat.Res.*, **1975,** 61, 274-287.

(18) Sheridan, R. B.; Huang, P. C., Single Strand Breakage and Repair in Eukaryotic DNA as Assayed by S1 Nuclease, *Nucleic Acids Res.*, **1977,** 4, 299-318.

(19) Cosa, G.; Focsaneanu, K.-S.; McLean, J. R. N.; McNamee, J. P.; Scaiano, J. C., Photophysical Properties of Fluorescent DNA Dyes Bound to Single- and Double-Stranded DNA in Aqueous Buffered Solution, *Photochem.Photobiol.*, **2001,** 73, 585-599.

(20) Cosa, G.; Focsaneanu, K.-S.; McLean, J. R. N.; Scaiano, J. C., Direct Determination of Single to Double Stranded DNA Ratio in Solution Applying Time-Resolved Fluorescence Measurements of Dye-DNA Comlexes, *Chem.Commun.*, **2000,** , 689-690.

(21) Haughland, R. P.; Yue, S. T.; Millard, P. J.; Roth, B. L. *Cyclic Substituted Unsymmetrical Cyanine Dyes*, US5436134: United States Patent Office, 1995.

(22) Yue, S. T.; Singer, V. L.; Roth, B. L.; Mozer, T. J.; Millard, P. J.; Jones, L. J.; Xiaokui, J.; Haughland, R. P. *Substituted Unsymmetrical Cyanine Dyes with Selected Permeability*, WO96/13552, 1996.

(23) Saltiel, J., The Role of Phantom States in the *cis-trans* Isomerizations of Stylbene, *J.Am.Chem.Soc.*, **1967,** 89, 1036-1037.

(24) Gilbert, A.; Baggott, J., *Essential of Molecular Photochemistry*, Blackwell Scientific Publications, Oxford, 1991.

(25) Rogers, K. R.; Apostol, A.; Madsen, S. J.; Spenser, C. W., Detection of Low Dose Radiation Induced DNA Damage Using Temperature Differential Fluorescence Assay, *Anal.Chem.*, **1999,** 71, 4423-4426.

(26) Elmendorff-Dreikorn, K.; Chauvin, C.; Slor, H.; Kutzner, J.; Batel, R.; Müller, W. E. G.; Schröder, H. C., Assessment of DNA Damage and Repair in Human Peripheral Blood Mononuclear Cells Using a Novel DNA Unwinding Technique, *Cell. Mol. Biol.*, **1999,** 45, 211-218.

(27) Reinhardt-Poulin, P.; McLean, J. R.; Deslauriers, Y.; Gorman, W.; Cabat, S.; Rouabhia, M., The Use of Silver-Stained "Comets" to Visualize DNA Damage and Repair in Normal and *Xeroderma pigmentosum* Fibroblasts After Exposure to Simulated Solar Radiation, *Photochem.Photobiol.*, **2000,** 71, 422-425.

(28) Olive, P., DNA Damage and Repair in Individual Cells: Applications of the Comet Assay in Radiobiology, *Int. J. Radiat. Biol.*, **1999,** 75, 395-405.

(29) McNamee, J. P.; McLean, J. R. N.; Ferrarotto, C. L.; Bellier, P. V., Comet Assay: Rapid Processing of Multiple Samples, *Mut. Res.*, **2000,** 466, 63-69.

(30) Beaulieu, M.; Béliveau, M.; D'Aprano, G.; Lacroix, M., Dose Rate Effect of Gamma Irradiation of Phenolic Compounds, Phenol Oxidase and Browning Mushrooms (*Agaricus Bisporus*), *J.Agric.Food.Chem.*, **1999,** 47, 2537-2543.

(31) Zareena, A. V.; Variyar, P. S.; Gholap, A. S.; Bongirwar, D. R., Chemical Investigation of Gamma-Irradiated Saffron (*Crocus Sativus L.*), *J.Agric.Food.Chem.*, **2001,** 49, 687-691.

(32) Fan, X.; Gates, R. A., Degradation of Monoterpenes in Orange Juice by Gamma Radiation, *J.Agric.Food.Chem.*, **2001,** 49, .

(33) Gottlöber, P.; Steinert, M.; Weiss, M.; Bebeshko, V.; Belyi, D.; Nadejina, N.; Stefani, F. H.; Wagemaker, G.; Fliedner, T. M.; Peter, R. U., The Outcome of Local Radiation Injuries: 14 Years of Follow-Up After the Chernobyl Accident, *Radiat. Res.*, **2001,** 155, 409-416.

(34) Alberts, B.; Bray, D.; Lewis, J.; Raff, M.; Roberts, K.; Watson, J. D., *Molecular Biology of the Cell*, 3rd, Garland Publshing Inc., New York, 1994.

(35) Rhoades, R.; Pflanzer, R., *Human Physiology*, Second Edition, Saunders College Publishing, Fort Worth, 1992.

(36) Banáth, J. P.; Kim, A.; Olive, P. L., Overnight Lysis Improves the Efficiency of Detection of DNA Damage in the Alkaline Comet Assay, *Radiat. Res.*, **2001,** 155, 564-571.

(37) Gallagher, S. R., *Quantitiation of DNA and RNA with Absorption and Fluorescence Specttroscopy*, In: Current Protocols in Molecular Biology, Ausubel, F. M., Brent, R., Kingston, R. E., Moore, D. D., Seidman, J. G., Smith, J. A. and Struhl, K., Greene Pub. Associates and Wiley-Interscience, New York, 1994, Vol. 3, A.3D.1-A.3D.8.

(38) Strauss, G. H., Non-Random Cell Killing in Cryopreservation for Performance of the Battery of Leukocyte Tests (BLT), I. Toxic and Immunotoxic Effects, *Mut.Res.*, **1991,** 252, 1-15.

(39) Molecular Probes PicoGreen® dsDNA Quantitation Reagents and Kits, www.probes.com, 2001.

(40) Mohtat, N.; Cozens, F. L.; Scaiano, J. C., Multistage Exit of Excited Xanthone from Micelles, *J.Phys.Chem.: B*, **1998,** 102, 7557.

Chapter 4

Claims to Original Research and Future Directions

4.1 Claims to Original Research

Most of the work presented in this thesis marks the first attempt at such experiments. Consequently, all of the results have contributed to the knowledge of the photochemical and photobiologial aspects of DNA damage in living cells.

i) A protocol for the preparation of samples suitable for the measurement of NSAID photo-induced DNA damage in living cells was established.

ii) The tolerance of HL60 cells to various concentrations of KP as well as different doses of UVA radiation was determined.

iii) The lethal concentration of KP and the lethal dose of UVA radiation to HL60 cells were established.

iv) KP photo-induced DNA damage did not lead to apoptosis in HL60 cells as determined by the neutral version of the comet assay.

v) Using the alkaline comet assay and PBMC, a dose-response of DNA damage was observed with repair times as well as SSR doses.

vi) Using the alkaline comet assay and a low SSR dose (230 mJ/cm^2), a dose-response of KP photo-induced DNA damage with increasing KP concentration was observed and was further increased with 60 min repair time.

vii) Prompt TP photo-induced DNA damage as well as delayed KP photo-induced DNA damage was observed with all radiation sources using the alkaline comet assay; TP photo-induced DNA damage was repeatedly higher than that observed with KP photo-induced DNA damage.

viii) An efficient method for isolating WBC from sheep WB was developed.

ix) A protocol for the preparation of samples suitable for the measurement of DNA damage using a time-resolved fluorescence technique in WBC isolated from sheep WB was established.

x) DNA damage assessment using the time-resolved fluorescence technique was presented; using the difference in lifetimes between PG-ssDNA and PG-dsDNA, significant differentiation of damage in DNA isolated from sheep WBC caused between γ radiation doses was possible.

4.2 Future Directions

4.2.1 The Comet Assay and Measuring NSAID Photo-Induced DNA Damage

Now that a proper protocol has been established, tested and deemed suitable to measure NSAID photo-induced DNA damage in living cells with the comet assay, a series of possible experiments have emerged. First, in order to complete the results presented in this thesis, NSAID photo-induced DNA damage could be measured using the alkaline comet assay with higher SSR doses (up to 1 MED (minimal erythemal dose)). Subsequently, other NSAIDs could be measured for their ability to photo-induce DNA damage in living cells using the alkaline as well as the neutral version of the comet assay. In order to provide more evidence that the delayed KP photo-induced DNA damage is due to the lack of immediate generation of noxious species, similar experiments could be conducted with the major photoproduct (3-ethylbenzophenone) which should not give a delayed reaction. It would also be interesting to assess the ability of the cells to repair NSAID photo-induced DNA damage, by conducting experiments where the cells are assayed at various timepoints until complete repair has occurred. Valuable information could be obtained by analyzing the mixture of photoproducts generated by HPLC/MS in order to determine which one(s) is(are) responsible for the DNA damage at specific NSAID concentrations and radiation doses. As the reactivity of many NSAIDs towards DNA has already been determined in solution, the results of such experiments could provide vital knowledge on the actual manifestation of their phototoxicity on biological molecules, namely DNA.

4.2.2 The Time-Resolved Fluorescence Measurement Technique and the Detection of DNA Damage

As this time-resolved fluorescence measurement technique was newly developed and experiments were basically conducted to establish the proper functioning conditions, many variations of the protocol could broaden the field of application for this technique. Since this technique can detect whether DNA has been damaged or not using γ radiation doses of 25-100 Gy, higher γ radiation doses (> 1000) could potentially elicit the same results. Presently, certain foods entering Canada are irradiated with γ radiation in the kGy range to inactivate food pathogens, to eradicate pests and to extend their shelf-life;[1] therefore, this technique could see useful applications in the food industry. As successful experiments were conducted on CT-DNA in solution as well as WBC isolated form sheep WB, this technique could potentially be used with virtually any eukaryotic cell. With this in mind, this technique could see potential applications in the medical field. It could be used to estimate the level of radiation individuals received from radiation therapy, X-rays, exposure from radioactive spills or other DNA damaging sources. As experiments with the final protocol were mostly conducted using higher γ radiation doses, further work to establish reliable conditions for the detection and efficient differentiation of DNA damage from lower doses of γ radiation (< 5 Gy) would be useful. In addition to the results obtained with this technique, the alkaline comet assay could be carried out alongside experiments in order to quantify the amount of DNA damage detected by this novel time-resolved fluorescence measurement technique.

4.3 References

(1) Cerda, H.; Delincee, H.; Haine, H.; Rupp, H., The DNA 'Comet Assay' as a Rapid Screening Technique to Control Irradiated Food, *Mutat.Res.*, **1997**, 375, 167-181.

4.4 Publications

4.4.1 Publications Resulting from Research Presented in This Thesis

(1) Vinette, A.L.; McLean, J.R.N.; McNamee, J.; Bellier, P.; Scaiano, J.C. Prompt and Delayed NSAID Photo-Induced DNA Damage in Living Cells Measured by the Comet Assay. *Manuscript in Preparation.*

(2) Cosa, G.; Vinette, A.L.; McLean, J.R.N.; Scaiano, J.C. A Novel DNA Damage Detection Technique Applying Time-Resolved Fluorescence Measurements. *Manuscript in Preparation.*

4.4.2 Other Publication

(1) Vinette, A.L.; Hahn, P.; King, M.C.; Fernãndez, M.P.; Avila, D.V.; Schmidt, J.A.; McGarry, P.; Scaiano, J.C. The Photoyellowing Inhibition of Paper. *Manuscript in Preparation.*

Chapter 5

Appendix

Appendix A - UVA Lamps Specifications

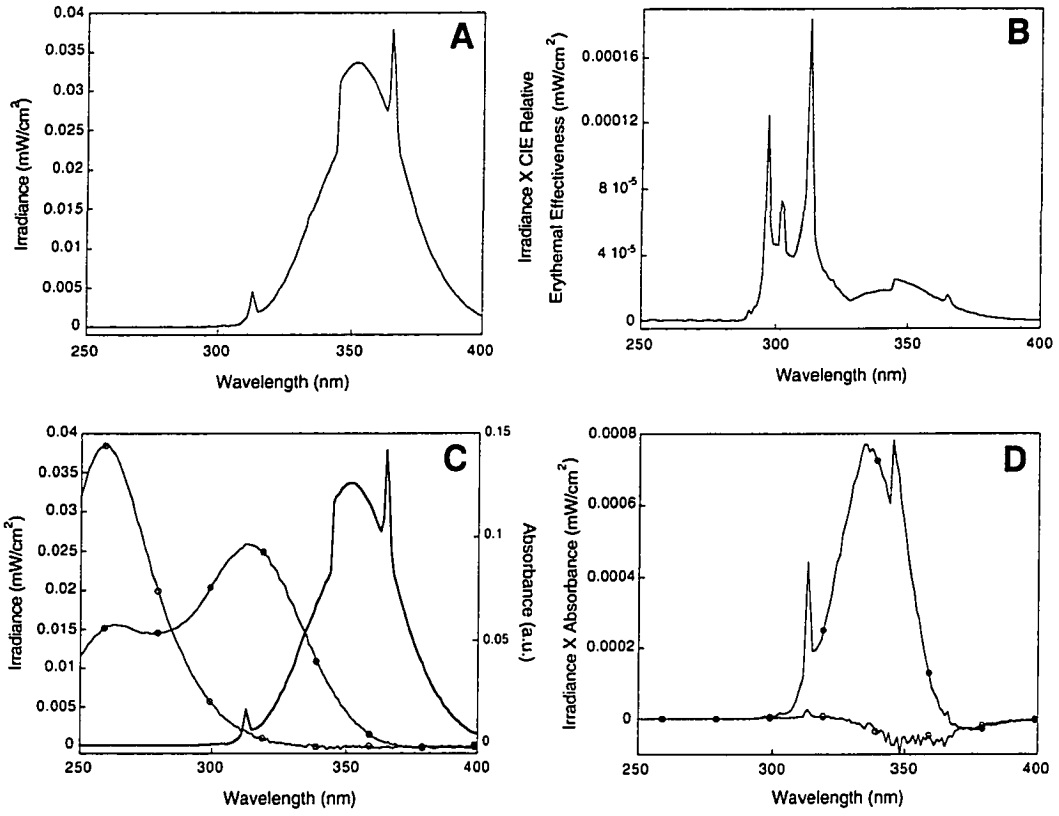

Figure A.1: **(A) Irradiance spectrum of 5 UVA lamps measured in positions 1, 3, 5, 6 and 8 of the photoreactor. Total actual irradiance (dose rate) of UVA lamps between 290-400 nm = 1.34 mW/cm². (B) Irradiance spectrum of UVA lamps multiplied by the CIE Relative Erythemal Effectiveness spectrum.[1] Represents area where human skin cells are most susceptible to harm from radiation emitted from UVA lamps. Total weighted irradiance (dose rate) of UVA lamps between 290-400 nm = 2.55 μW/cm². (C) Irradiance spectrum of UVA lamps (-) compared to the absorbance spectra of 10 μM KP (O) and 10 μM TP (●). (D) Irradiance spectrum of UVA lamps multiplied by the absorbance spectra of 10 μM KP (O) and 10 μM TP (●). Represents the amount of radiation emitted by the UVA lamps absorbed by the drug.**

Appendix B - UVB Lamps Specifications

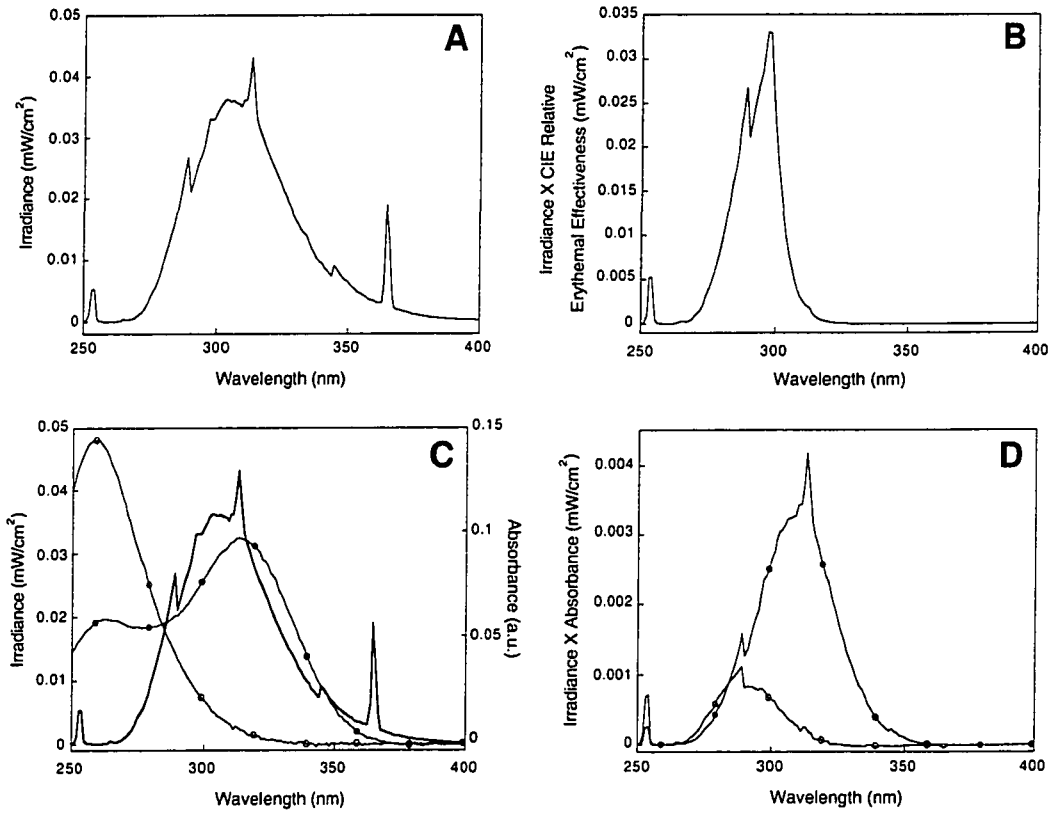

Figure A.2: (A) Irradiance spectrum of 4 UVB lamps measured in positions 1, 3, 6 and 8 of the photoreactor. Total actual irradiance (dose rate) of UVB lamps between 290-400 nm = 1.54 mW/cm^2. (B) Irradiance spectrum of UVB lamps multiplied by the CIE Relative Erythemal Effectiveness spectrum.[1] Represents area where human skin cells are most susceptible to harm from radiation emitted from UVB lamps. Total weighted irradiance (dose rate) of UVB lamps between 290-400 nm = 0.39 mW/cm^2. (C) Irradiance spectrum of UVB lamps (-) compared to the absorbance spectra of 10 μM KP (O) and 10 μM TP (●). (D) Irradiance spectrum of UVB lamps multiplied by the absorbance spectra of 10 μM KP (O) and 10 μM TP (●). Represents the amount of radiation emitted by the UVB lamps absorbed by the drug.

Appendix C - SSR Lamp Specifications

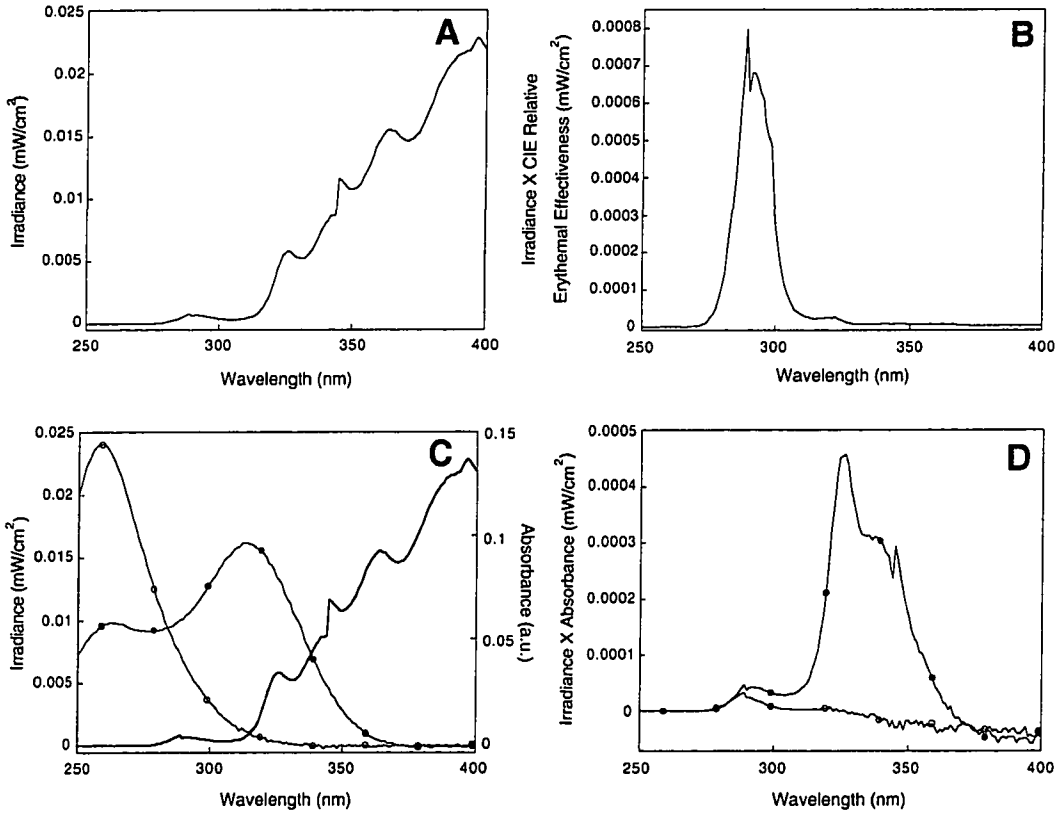

Figure A.3: (A) Irradiance spectrum of the 300 W Xenon lamp used for SSR. Total actual irradiance (dose rate) of SSR lamp between 290-400 nm = 1.09 mW/cm^2. (B) Irradiance spectrum of SSR lamp multiplied by the CIE Relative Erythemal Effectiveness spectrum.[1] Represents area where human skin cells are most susceptible to harm from radiation emitted from the SSR lamp. Total weighted irradiance (dose rate) of SSR lamp between 290-400 nm = 7.69 μW/cm^2. (C) Irradiance spectrum of the SSR lamp (-) compared to the absorbance spectra of 10 μM KP (O) and 10 μM TP (●). (D) Irradiance spectrum of the SSR lamp multiplied by the absorbance spectra of 10 μM KP (O) and 10 μM TP (●). Represents the amount of radiation emitted by the SSR lamp absorbed by the drug.

Appendix D - Calibration Curve for UVA Lamps

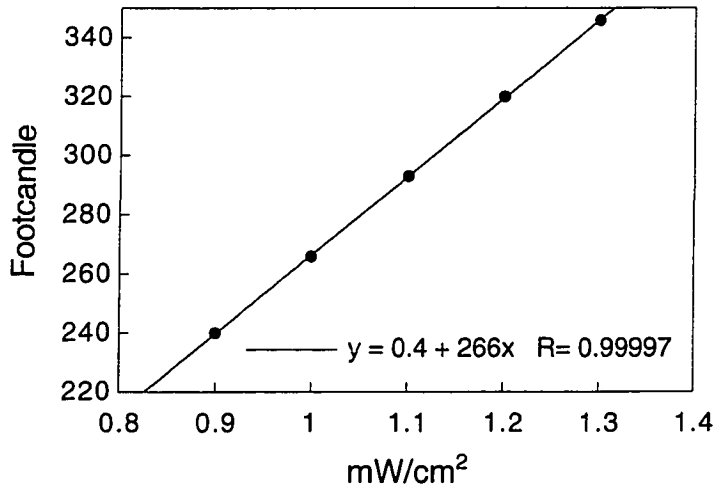

Figure A.4: Calibration curve for the UVA lamps; irradiance in Footcandle (FC) as a function of the dose rate (mW/cm^2).

This calibration curve was constructed by comparing the irradiance of the UVA lamps in the photoreactor measured with a lightmeter (A.W. Sperry SLM-110 digital lightmeter, N.C.E #23), given in Footcandle (FC), with that measured with a powermeter (OAT 306 UV powermeter), given in dose rate (mW/cm^2). The dose rate, for Sections 2.6.1 and 2.6.2, was calculated using the generated line fit equation (inset of plot) with the value obtained from the lightmeter, in FC, to obtain a value in mW/cm^2.

Appendix E - CIE Erythemal Effectiveness Spectrum[1]

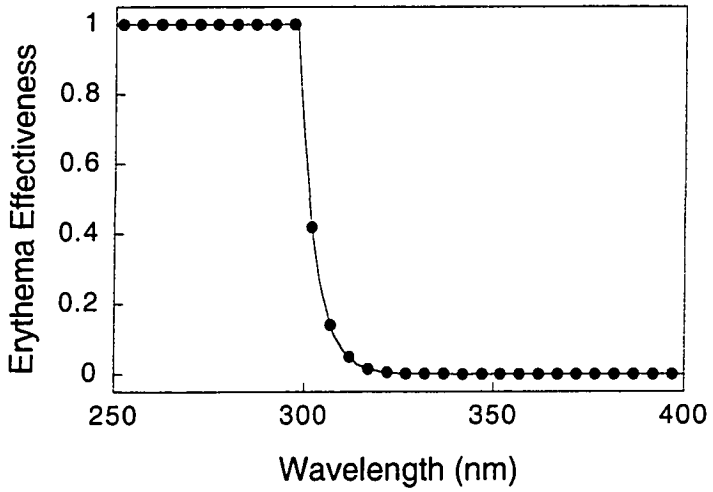

Figure A.5: Proposed erythemal effectiveness spectrum for human skin cells by La Commission International de l'Éclairage (CIE); to be used only as a guide to evaluate the susceptibility of human skin cells to UVB radiation damage.

This effectiveness spectrum was multiplied by the irradiance spectra of the UVA, UVB and SSR lamps (Appendix A, B and C respectively) in order to obtain the area in the UV spectrum where human skin cells are most susceptible to harm from UVB radiation (290-400 nm) emitted from the specific lamps. From this spectrum, the weighted UVA, UVB as well as the total irradiance values can be determined. These values are used in the calculation of 1 MED (Appendix F) and the determination of irradiation time to obtain 1 MED for each radiation source (Appendix G).

Appendix F - Calculation of 1 MED

The weighted irradiance values (dose rate) obtained from the irradiance spectrum (specific to each radiation source) multiplied by the CIE erythemal effectiveness spectrum (Appendix E) are used to calculate the MED. In the calculation example below, the values obtained for the SSR lamp are used. Fred Urbach designated 30 mJ/cm^2 to be equal to 1 MED for skin type II corresponding to the total UVB radiation contribution of a specific radiation source.[2]

300 W Xenon lamp emits a total weighted irradiance of SSR of 7.69 $\mu W/cm^2$ (290-400 nm)

where 7.11 $\mu W/cm^2$ is the total UVB contribution (290-319 nm)

and 0.578 $\mu W/cm^2$ is the total UVA contribution (320-400 nm)

With a total weighted irradiance of 7.69 $\mu W/cm^2$, 92.47% of that total irradiance is from UVB

↑

(% UVB = 7.11 / 7.69 = 0.9247 X 100)

Therefore 30 mJ/cm^2 = 92.47%

(30 / 92.47 X 100)

↓

And 1 MED for this radiation source = 32.44 mJ/cm^2

Appendix G - Relevant Values for Radiation Sources

		UVA	UVB	SSR
Actual Irradiance (mW/cm^2)	UVA	1.31	0.57	1.07
	UVB	0.03	0.97	0.02
	Total	1.34	1.54	1.09
Weighted Irradiance (mW/cm^2)	UVA	$9.37X10^{-4}$	$1.22X10^{-3}$	$5.78X10^{-4}$
	UVB	$1.61X10^{-3}$	0.39	$7.11X10^{-3}$
	Total	$2.55X10^{-3}$	0.39	$7.69X10^{-3}$
% UVB (%)	Actual	1.98	63.51	1.83
	Weighted	63.14	99.74	92.47
MED (mJ/cm^2)	Actual	1515.15	47.33	1634.88
	Weighted	47.51	30.08	32.44
Time to get 1 MED (min)	Actual	18.85	0.5	25
	Weighted	310	1.3	70

Appendix H - Drug:Base Pairs Molar Ratio Calculation

1 cell = 6×10^{-12} g DNA = 9.324×10^{-15} moles of base pairs

(6×10^{-12} g DNA / 643.5 g/mol bp)

Mm_{AT} = 643 g/mol
Mm_{GC} = 644 g/mol
} average = 643.5 g/mol

Samples contained on average 1 million cells per mL = 9.324×10^{-9} moles of base pairs

(1×10^{6} cells X 9.324×10^{-15} moles of base pairs)

The drug concentration was 1×10^{-5} M = 1×10^{-8} moles of drug

In 1 mL there are 9.324×10^{-9} moles of base pairs and 1×10^{-8} moles of drug

Therefore, the drug to base pair molar ratio is: $1 \times 10^{-8} / 9.324 \times 10^{-9} = 1.07$

Appendix I - DNA Strand Breaks Calculation

1 Gy will deliver 1000 SSBs and 40 DSBs per cell = 1040 breaks per cell

1 cell = 6×10^{-12} g DNA = 9.324×10^{-15} moles of base pairs = 5.615×10^{9} base pairs

(6×10^{-12} g DNA / 643.5 g/mol bp) (9.324×10^{-15} mole bp $\times$ 6.022×10^{23} mol^{-1})

Therefore: 1040 breaks / 5.615×10^{9} = 1.852×10^{-7} breaks per base pair

OR

1 break every ~ 5.4 M base pairs

Appendix J - Hemacytometer Calculations

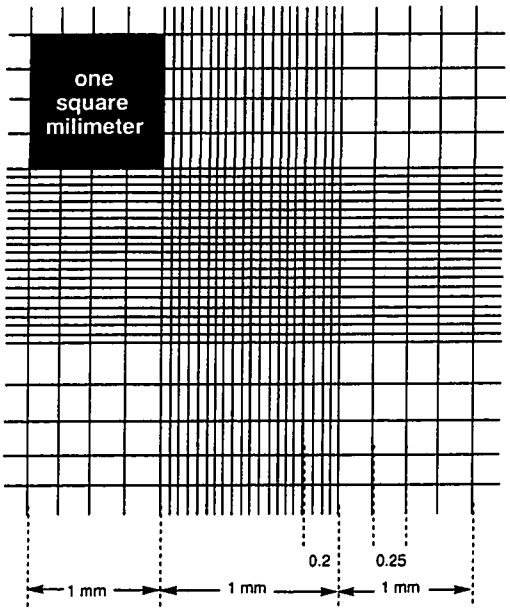

The middle square of the grid has a volume of 0.1 mm^3. The cell suspension is diluted 1:1 with the working viability stain and carefully dispensed onto the hemacytometer (using both counting plates), then visualized through a fluorescence microcope. The green cells are counted as viable and the red cells as non-viable. If there are 30 viable cells in the middle square of both counting plates, the concentration is determined by adding the number of cells from plate 1 to the number of cells from plate 2 and multiplying by 10 000 to obtain cells/mL. If there are less than 30 viable cells in the middle square of either counting plates, then all nine squares of both counting plates are counted. The concentration in cells/mL is then determined by adding the total number of cells from both counting plates, dividing by 9 and multiplying by 10 000.

Appendix K - DNA Concentration Determination From Absorbance Measurements

A 1:20 and a 1:100 dilution of the CT-DNA solution was made ([DNA] = 0.95 mg/mL in 1X TAE)

The absorbance of both solutions was measured at 260 nm

For the 1:20 dilution: $A_{260} = 0.894$

$$[\text{ssDNA}] = \frac{A_{260}}{0.27} = \frac{0.894}{0.27} = 3.3111\ \mu g/mL$$

+

$$[\text{dsDNA}] = \frac{A_{260}}{0.02} = \frac{0.894}{0.02} = \frac{44.7\ \mu g/mL}{48.0111\ \mu g/mL}$$

X 20 = 960.222 µg/mL = 0.960222 mg/mL

For the 1:100 dilution: $A_{260} = 0.176$

$$[\text{ssDNA}] = \frac{A_{260}}{0.27} = \frac{0.176}{0.27} = 0.65185\ \mu g/mL$$

+

$$[\text{dsDNA}] = \frac{A_{260}}{0.02} = \frac{0.176}{0.02} = \frac{8.8\ \mu g/mL}{9.45185\ \mu g/mL}$$

X 100 = 945.185 µg/mL = 0.945185 mg/mL

$$\text{Average [DNA]} = \frac{0.960222 + 0.945185}{2} = 0.9527035\ mg/mL$$

Appendix L - DNA Concentration Determination From Standard Curve

$$[DNA] = \frac{I_{DNA\ sample}}{I_{new\ standard}} \times \frac{I_{standard}}{slope}$$

($I_{DNA\ sample} - I_{blank} = 7.02 - 0.213 = 6.0807$) $I_{DNA\ sample}$ = *fluorescence intensity of sample*

($I_{new\ standard} - I_{blank} = 96.037 - 0.213 = 95.824$) $I_{new\ standard}$ = fluorescence intensity of standard

($I_{standard}$ = initial fluorescence intensity of the fluorescein standard = 89.8497)

(slope = obtained from the DNA standard curve = 0.023179)

[DNA] = (6.0807 / 95.824) X (89.8497 / 0.023179) = 275.362 ng/mL

[cell] = 0.275362 μg/mL X 2000 μL / 800 μL = 0.6884 μL

This solution was originally thought to have been 2 μg/mL

[cell] = 0.6884 μg/mL X 10 000 μL / 55 μL = 125.164 μg/mL

This solution was originally thought to have been 360 μg/mL

Since 360 μg/mL corresponds to the amount of DNA in 60 X 10^6 cells (6 pg DNA per cell)

[cell] = 125.164 μg/mL X 60 X10^6 cells/mL / 360 μg/mL = 20.86 X 10^6 cell/mL

Since an aliquot of 50 μL of cell suspension was mixed with 125 μL of agarose, therefore:

20.86 X 10^6 cell/mL X (50/175) = 5.96 X 10^6 cells/mL

And 150 μL were didpensed per gel, resulting in:

(5.96 X 10^6 cells X 150 μL) / 1000 μL = 8.94 X 10^5 cells/gel

5.1 References for Appendices

(1) McKinley, A. F.; Diffey, B. L., *Human Exposure to Ultraviolet Radiation - Risks and Regulations*, Passchier, W. F. and Bosnjakovic, B.F.M., Elsevier Science Publisher, New York, 1987.

(2) Parrish, J. A.; Anderson, R. R.; Urbach, F.; Pitts, D., Biological Effects of Ultraviolet Radiation With Emphasis on Human Responses to Longwave Radiation, Plenum Press, New York, 1978.